Construction of Hydrogen-Bonded Organic Frameworks Based on Nitrogen-Containing π-Conjugated Molecular Systems

(窒素含有π共役分子系に基づく水素結合性有機フレームワークの構築)

北海道大学大学院環境科学院

JI QIN

令和 3 年度　博士論文

Construction of Hydrogen-Bonded Organic Frameworks Based on Nitrogen-Containing π-Conjugated Molecular Systems

（窒素含有π共役分子系に基づく水素結合性有機フレームワークの構築）

北海道大学大学院　　環境科学院

環境物質科学専攻　光電子科学コース

JI QIN

2021.08

Acknowledge

This doctorate thesis has been completed under the guidance of Professor Ichiro Hisaki (Osaka University), under the supervision of Professor Takayoshi Nakamura from October 2018 to July 2021 at Graduate School of Environment Science, Hokkaido University.

The author would like to express her sincere gratitude to Professor Ichiro Hisaki for his careful guidance, valuable suggestions and encouragement during the course of this work. The author would like to thank him for teaching her to do experiments hand in hand at the beginning, teaching me a lot of methods and tricks of organic synthesis, and helping me to revise her paper word by word. Prof. Hisaki's active academic thinking, profound theoretical foundation, rich experimental experience, diligent and selfless work attitude and conscientious academic attitude have deeply influenced and inspired her. At present, her academic achievements may still be less than his painstaking cultivation, but she still wants to say that being able to learn from Prof. Hisaki is one of the luckiest things in her life.

The author would like to deeply appreciate that he admitted her as a doctor student and take kind care of her life throughout the PhD period. And also express her greatest gratitude to Professor Takayoshi Nakamura for his kind suggestions and warm encouragements. Prof. Nakamura is academically rigorous, knowledgeable and approachable and it is a great honor for her to do research under his guide.

The author would like to give her greatest appreciation to Assistant Professor Kiyonori Takahashi for his timely help to order reagents and helping her solve various experimental difficulties. Without his help, her work cannot be completed so smoothly.

The author is thankful to Associate Professor Kenta Kokado for his help and teaching the operation of all kinds of experimental equipment with his patience.

The author is thankful to Professor Shin-ichiro Noro for his kind suggestions and their equipment for gas absorption.

The author is thankful to Associate Professor Yoshimitsu Sagara (Tokyo Institute of Technology) for preparative HPLC experiments. The author is thankful to Associate

Professor Yusuke Ishigaki and his student Mr. Takashi Harimoto for UV-vis and fluorescence spectroscopy, CV measuerments. The author is thankful to Associate Professor Takahiro Suzuki for amination reaction. The author is thankful to Spring-8.

The author is thankful to Assistant Professors Ruikang Huang and Chen Xue, Dr. Xin Zheng, Dr. Simin Li, Miss. Xin Chen, Miss. Jiao Chen, Miss. Dongfang Wu, Mr. Jiabing Wu, Mr. ZhuXi Yang, Mr. Zijian Diao, Mr. Chao Wang and Mr. Masato Haneda. The author is thankful to Mrs. Yumie Fujiwara, Ms. Hiroko Yonemori and Ms. Mariko Kato for their secretarial works and warm encouragements. And all other members of Professor Nakamura's laboratory and Professor Noro's laboratory for their friendship and encouragements.

Finally, the author would like to expresse her deep appreciation to her parents, Mr. Zhaojin Ji and Mrs. Changxiu Zhu for constant financial supports and affectionate encouragements. And the author also thanks her friends, Mrs. Jingjing Zhong, Miss. Yating Yang, and Mr. Jun Sun for their steadfast concern and support.

JI QIN

Graduate School of Environment Science

Hokkaido University

June 2021

Contents

Chapter 1

General Introduction

Crystalline porous materials can be divided into pure inorganic crystalline porous materials and crystalline porous materials containing organic components, the former mainly includes zeolite and molecular sieves, while the latter includes metal-organic frameworks (MOFs)[1,2] or porous coordination polymers (PCPs)[3], covalent organic frameworks (COFs)[4], and hydrogen-bonded organic frameworks (HOFs)[5]. Compared with the pure inorganic crystalline porous materials, the crystalline porous materials containing organic components have the characteristics of richer structure, easier adjustment of channel shape and size, and easier modification of channel surface. In the past few decades, scientists have successfully developed wide range of porous MOFs / COFs materials with special functions such as gas adsorption and separation, catalysis, sensing, fluorescence and proton conduction using a variety of organic compounds. HOFs are a family of porous molecular crystals, in which building block molecules are networked through hydrogen bonds and π–π stacking interaction, which have emerged recently as new porous materials.

1-1. Hydrogen Bond

Hydrogen bonding is a unique form of bonding that exists in structural chemistry and biology. [6] It plays an important role in the process of molecular association and its functional importance comes from both thermodynamic and kinetic aspects. In supramolecular chemistry, hydrogen bonds have sufficient strength and directionality to control and direct the assembly of molecules. This control is reliable and repeatable, and researchers have now expanded it to the most subtle architectures.

Hydrogen bonds, commonly referred to as weak hydrogen bonds, can be defined as interactions between X–H•••A. The hydrogen atoms form a bond between two structural units X and A, both of which can be of medium to low electronegativity.[7] The term “weak hydrogen bond” seems to be an oxyparadox. Normally we think of bonds as being strong, but since they pass through X–H•••A, so the hydrogen bond is not particularly strong. At the same time, it is because of this electrostatic interaction that the force is relatively weak that hydrogen bonds can retain their unique inherent

properties. It should be noted that hydrogen bonds are defined on a phenomenological basis, not on an energy basis[8]. Hydrogen bonding also plays a role in improving the stability of the structure, especially when there are multiple hydrogen bonds in the system and there are synergistic interactions between each other, this effect will be very significant. It is precisely because of these properties that hydrogen bonds, known as "universal role in supramolecular", play a vital role in the construction of multidimensional supramolecular network structure.

Hydrogen bonds can be either intermolecular or intramolecular. The bond energies range from 1 to 170 kJ/mol, which is lower than those for coordination bonds (90~350 kJ/mol) and covalent bonds (300~600 kJ/mol). As a result, the rigidity and directionality of hydrogen bonds are lower than the similar properties of coordination and covalent bonds, which makes the rational design of hydrogen-bonded organic frameworks more challenging. According to some evaluation criteria and based on the bond energy of hydrogen bonds, hydrogen bonds are classified into three types: weak hydrogen bonds, moderate hydrogen bonds and strong hydrogen bonds. [9-11] (Table 1.1 and Table 1.2)

Table 1.1 Strong, moderate, and weak hydrogen bonds following the classification of Jeffrey.[10]

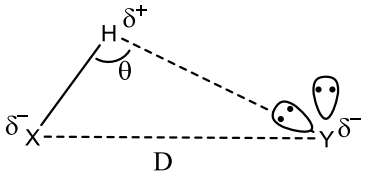

	Strong	Moderate	Weak
Interaction type	Strongly covalent	Mostly electrostatic	electrostat. / disper
D / Å	2.2–2.5	2.5–3.2	>3.2
H•••Y / Å	1.2–1.5	1.5–2.2	>2.2
θ / °	170–180	>130	>90
X-H vs. H•••Y	X-H ~ H•••Y	X-H > H•••Y	X-H >> H•••Y
Bond energy / kJ mol^{-1}	63–167	17–63	<17

Table 1.2 Different types of hydrogen bonds. [10]

	Dimer	Bond energy / kJ mol^{-1}
Strong	$[F{-}H{-}F]^-$	163
	$[H_2O{-}H{-}OH_2]^+$	138
	$[H_3N{-}H{-}NH_3]^+$	100
	$[HO{-}H{-}OH]^-$	96
	$NH_4^+{\bullet\bullet\bullet}OH_2$	79
	$NH_4^+{\bullet\bullet\bullet}Bz$	71
Moderate	$HOH{\bullet\bullet\bullet}Cl^-$	56
	$O{=}C{-}OH{\bullet\bullet\bullet}O{=}C{-}OH$	31
	$HOH{\bullet\bullet\bullet}OH_2$	20–21
Weak	$N{\equiv}C{-}H{\bullet\bullet\bullet}OH_2$	16
	$HOH{\bullet\bullet\bullet}Bz$	13
	$F_3C{-}H{\bullet\bullet\bullet}OH_2$	13
	$Me{-}OH{\bullet\bullet\bullet}Bz$	12
	$F_2HC{-}H{\bullet\bullet\bullet}OH_2$	9–10
	$NH_3{\bullet\bullet\bullet}Bz$	9
	$HC{\equiv}CH{\bullet\bullet\bullet}OH_2$	9
	$CH_4{\bullet\bullet\bullet}Bz$	6
	$FH_2C{-}H{\bullet\bullet\bullet}OH_2$	5
	$HC{\equiv}CH{\bullet\bullet\bullet}C{\equiv}CH^-$	5
	$HSH{\bullet\bullet\bullet}SH_2$	5
	$H_2C{=}CH_2{\bullet\bullet\bullet}OH_2$	4
	$CH_4{\bullet\bullet\bullet}OH_2$	1–3
	$C{=}CH_2{\bullet\bullet\bullet}C{=}C$	2
	$CH_4{\bullet\bullet\bullet}F{-}CH_3$	1

1-2. π-π Stacking Interaction

π–π stacking interaction is a kind of weak interaction, which usually occurs between one electron-rich aromatic ring and the other electron-deficient aromatic ring[12]. Compared with other strong interaction, π–π stacking interaction has only weakly intensity and orientation, so it is difficult to control and predict the interaction. But such interactions are also extremely important for some systems, such as aromatic guest complexes in stable solutions.[13,14]

1-3. Hydrogen-Bonded Organic Frameworks (HOFs)

1-3-1. The concept of HOFs

Hydrogen-bonded organic frameworks (HOFs), as a class of crystalline porous materials[15-17], is composed of organic or metal-organic building units connected by hydrogen bonds, π-π interactions and other non-covalent interactions (Figure 1.1). Due to the great degree of freedom of hydrogen bond, the organic structural units can form different hydrogen-bonded models under different solvent or temperature conditions, and then obtain HOFs with different structures. Therefore, HOFs have a very high sensitivity to the solvent[18]. In addition, π–π stacking interaction, CH•••π interaction and van der Waals forces can further enhance the stability of frameworks and obtain HOFs with excellent stability. According to the classification of the organic structure elements of HOFs, they can be divided into single-component organic structure elements and two-component organic structure elements, of which the single-component organic structure elements include 1) polydentate carboxylic acid structure elements; [19-29] 2) nitrogenous structure elements; [30-37] and 3) other structural elements.[38]

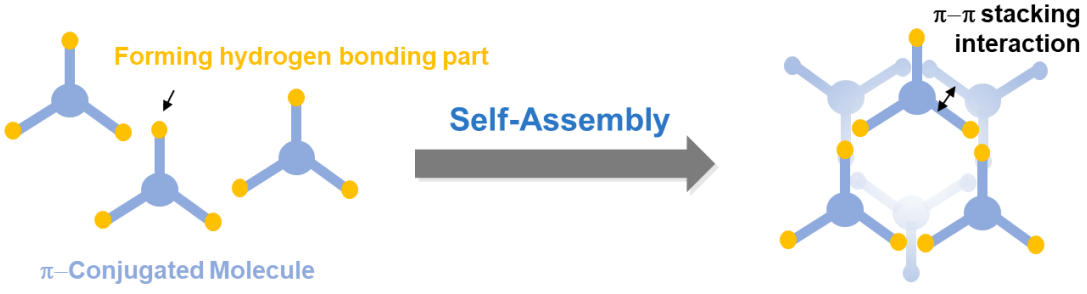

Figure 1.1 The simulation diagram of the self-assembly HOFs

1-3-2. The development of carboxylic acid-based HOFs

A carboxy group is the simplest functional group for making molecular assemblies. The carboxy dimer has been used to construct exotic molecular assemblies in natural products and in organic chemistry.[39] Because of its facile synthesis and high directionality of H-bond formation, the carboxy dimer is a suitable supramolecular synthon for design of tectons and HOFs.

In 1969, Marsh and Duchamp[19] had reported the first crystalline compound with a hexagonal honeycomb HOF using trimesic acid (**1**) as a building block, as shown in Figure 1.2b and d. The framework constructed by six trimesic acid molecules formed a two-dimensional plane, with three layers interpenetrating each other. Although the concept of using hydrogen bonds to construct HOFs materials and using coordination bonds to construct MOFs materials was put forward almost in parallel at the same time, the development of HOFs was much slower than that of MOFs, and the early preparation of HOFs basically did not receive too much attention, which is mainly due to the weak force, strong flexibility and poor directionality of hydrogen bonds, so the target HOFs structure is not only difficult to be synthesized accurately, but also the stability of the framework is generally much worse than the corresponding MOFs. In the following decades, the development of HOFs is basically at a standstill. In 2000, Kobayashi and coworkers demonstrated that hexakis(4-carboxyphenyl)benzene (**2**) also gave hexagonally-networked 2D sheets, which accumulate layer-by-layer without interpenetration (Figure 1.2e).[20] In fact, the framework of early synthetic HOFs often collapsed when the solvents filled in the pores were removed, and early scientists did not pay much attention to the porosity of HOFs, so the development of HOFs as a porous material was very slow. The porosity of HOFs began to be gradually known[21] until about 2015.

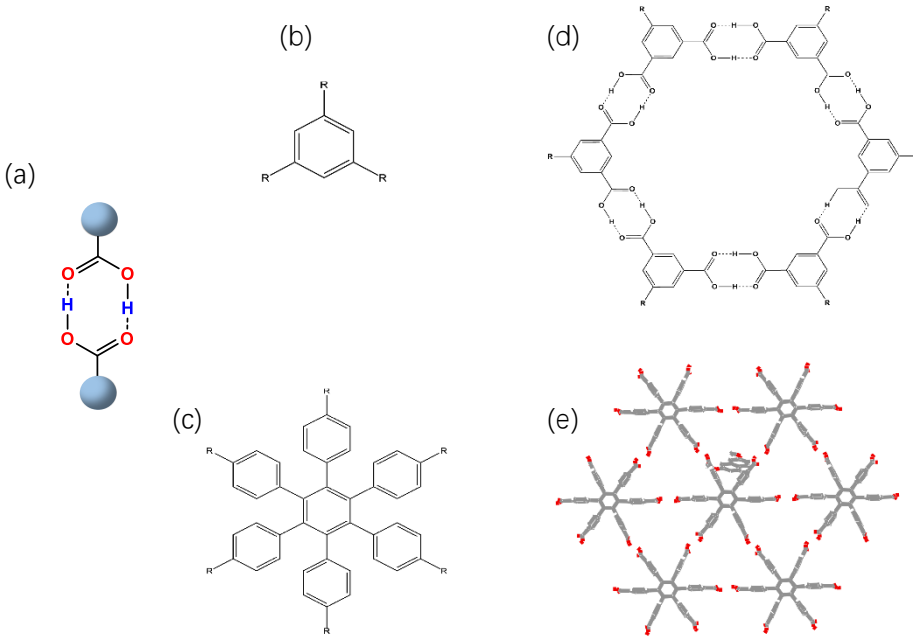

Figure 1.2 (a) H-bonding ways of carboxy groups. b) Chemical structures of **1**. c) Chemical structures of **2.** d) Honeycomb network of **1**.[20] e) Hexagonal (trigonal) network of **2**.[21]

In 2015, Cassandra A. Zentner and co-workers[21] prepared two kinds of HOFs with different structures based on 1,3,5-tris(4-carboxyphenyl)benzene (TCPB) by dissolving TCPB in different alcohol solutions and then volatilizing the solvents. It assembles into an intricate 8-fold polycatenated assembly of (6,3) hexagonal nets. After that, the research group of Kwang. S. Kim[22] applied HOF-BTB based on TCPB to the selective separation of C_2 gases and methane, and showed excellent performance. In 2016, Ramanathan Vaidhyanathan's group[23] took TCTP as the ligand and added the ligand to acetic acid to obtain a stable hydrogen-bonded organic framework IISERP-HOF1, which has a one-dimensional channel of 9.4 Å × 9.1 Å in *a* axis direction and the void ratio is about 34%. In addition, IISERP-HOF1 has extremely high thermal and water stability. It retains crystallinity well above 280 ℃ and maintains structural integrity in 3 mol L^{-1} of hydrochloric acid solution. And it shows preferential adsorption of CO_2 over N_2 with very high selectivity. In the same year, Ichiro Hisaki's group obtained a series of HOFs by solvothermal method using compounds with C_3-symmetric π-conjugated planar molecules as ligands [24], which are two-dimensional robust hydrogen-bonded hexagonal networks (H-HexNets) with dual or triple pores, with porosity of 45–

59% and excellent thermal stability. It is the first time that large conjugated molecules with C_3 symmetry are considered to be excellent organic building units. Later, Ichiro Hisaki also published a series of X-shaped π-conjugated system to provide a new structural insight into porous 2D COFs.[25] In 2017, Mao-Chun Hong's research group obtained a HOF-TCBP with high thermal stability[26]. The material has a one-dimensional channel with a diameter of 18.25 Å and a porosity of 56% in *a* axis direction. The N_2 sorption isotherm of the material measured at 77 K shows atypical Type I isotherm with saturation uptake of 535 $cm^3\ g^{-1}$, and the material has a high BET surface area of 2066 $m^2\ g^{-1}$, which has excellent ability of selective adsorption and separation of light hydrocarbon. In 2018, Rong Cao's group designed and synthesized the first example of HOF materials for multiple therapeutics for cancer based on 1,3,6,8-tetrakis (*p*-benzoic acid) pyrene (H_4TBAPy) [27] with high specific surface area, thermal stability, and excellent chemical stability which maintained the framework after soaking in concentrated hydrochloric acid for 117 days. In 2019, J. Fraser Stoddart's research group used H_6PET as ligand to effectively control the interpenetration of materials in the process of self-assembly by adjusting the synthesis conditions, and obtained two kinds of HOFs with interpenetration isomerism, **PETHOF-1** and **PETHOF-2**, [28] with the same topology and different interpenetrated structures. Among them, **PETHOF-1** has a large guest-accessible volume of about 80%, because two separate network structures form an intersecting structure by reversing symmetry. In 2020, Bang-Lin Chen's group reported a three-dimensional microporous organic framework composed of hydrogen bonds synthesized by 5-(2,6-bis(4-carboxyphenyl)pyridin-4-yl)isophthalic acid (H_4BCPIA)[29] as a hydrogen bond between the elements. The activated HOF-20a has a moderately high BET surface area of 1323 $m^2\ g^{-1}$ and excellent stability in water and HCl aqueous solution. In addition, the recognition of aniline molecules by HOF-20 could restrict the rotation of the aromatic rings in H_4BCPIA linkers, reducing the nonradiative decay pathways upon photoexcitation and subsequently enhancing the fluorescence intensity.

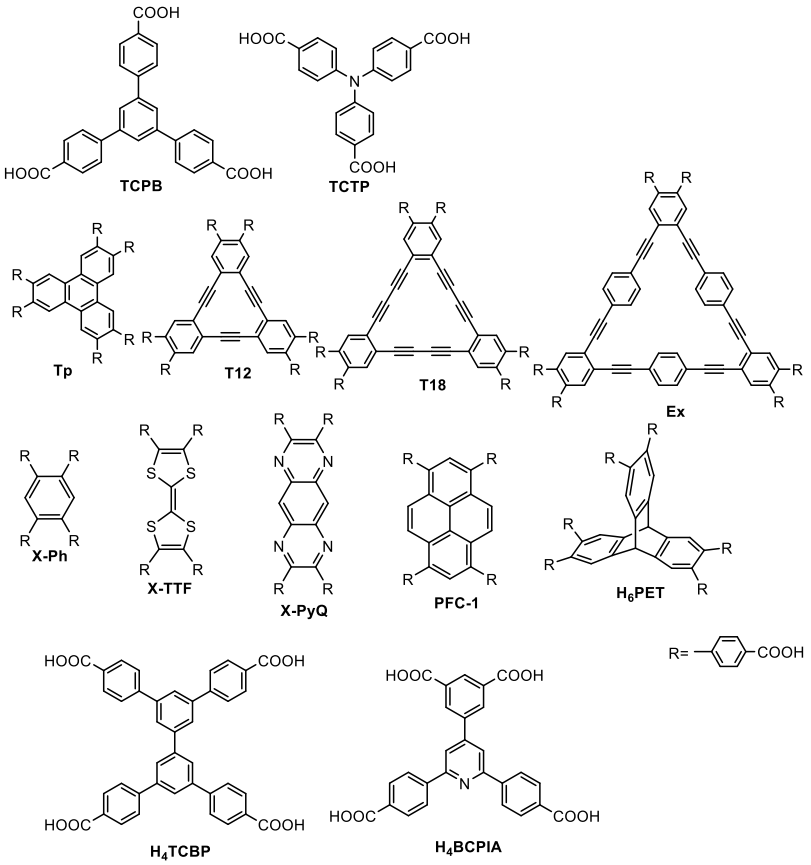

Figure 1.3 Examples of carboxylic acid derivatives providing stable 2D- or 3D-networked frameworks reported from other groups. Names of the HOFs constructed from the corresponding molecules are shown in parentheses.

1-3-3. The application of HOFs

As a new kind of porous crystalline material, HOF has the characteristics of high specific surface area, orderly pore structure, and pore modification and functionalization, etc. Therefore, these materials have great application potential in the fields of greenhouse gas adsorption and separation, energy gas storage, fluorescent probes, molecular devices, molecular magnetism, proton conduction, molecular recognition, host and guest assembly, etc..[40]

Gas storage and separation

Porous HOF materials can be modified according to the pore size and shape of the skeleton material and are widely used in selective adsorption and separation of gases.

The selectivity and adsorption capacity of HOFs for ethylene, acetylene and carbon dioxide depend on the structural characteristics of the adsorbed gas and the porous material itself. The adsorption of gas molecules is mainly due to the interaction between the adsorbate and the internal surface and pore structure of the HOF.

Carbon dioxide capture. In general, the interaction force between the HOFs and CO_2 is stronger than the interaction force between the HOFs and N_2, so most of the HOFs has excellent performance of selective adsorption of CO_2/N_2. Cao Rong's group constructed SOF-7a[41] using multiple hydrogen bond receptors containing nitrogen groups and hydrogen bond donors containing carboxylic acid. The adsorption capacity of SOF-7a on carbon dioxide reached 156 $cm^3\ g^{-1}$ at 273 K, which has good performance of CO_2 capture.

Hydrogen storage. Hydrogen is a clean energy and the most promising alternative to fossil fuels in the future. The safe and efficient storage of hydrogen is a prerequisite for hydrogen energy utilization on a large scale. In order to develop porous adsorption materials with high efficiency and high capacity of hydrogen, increasing the specific surface area of the adsorbent is an effective method to improve the gas adsorption and storage performance. And it is important to increase the interaction between Hydrogen and adsorbents at room temperature. For example, Mastalerz et al.[42] reported an ultra-high surface area HOF based on triptycene trisbenzimidazolone (TTBI), which adsorbs 243 $cm^3\ g^{-1}$ of H_2 at 77 K and 1 bar, it is used for adsorption storage of H_2.

The molecular recognition of HOFs

The molecular recognition of HOFs has been studied extensively, many of which have been applied to the detection of radioactive elements and toxic organic small molecules. For example, Di Chang Zhong's research group constructed the hydrogen-bonded organic framework HOF-8, which has a good recognition effect for organic small molecule benzene.[43] They believe that the material recognizes benzene because of the very strong interaction (π-π stacking) between the benzene ring and pyridine in the molecules, while the interaction between small organic molecules such as ethane

and propane and HOF-8 is too weak to recognize it.

Photochemical property of HOFs

To construct HOFs with permanent porosity, their building blocks are usually designed to be highly rigid molecules featuring aromatic moieties of a large π-conjugated system, which usually are excellent fluorescent and phosphorescent dyes, highlighting HOFs as very promising luminescent materials. Depending on the degree of π-conjugation, the emission wavelengths of these organic molecules can distribute over a wide range, facilitating the rational design of luminescent HOF materials with tunable colors. Furthermore, the highly crystalline nature of HOFs indicates the highly ordered arrangement of organic chromophores, giving significantly different emission behavious as compared to their solution states, such as aggregation induced emission (AIE). For example, Ichiro Hisaki and co-workers constructed an acid-responsive HOF, **CPHATN-1a**.[44] which exhibits a rich photochemistry due to intramolecular charge-transfer and interunit proton-transfer reactions.

1-4. HOFs composed of π-conjugated hydrocarbons

Under the premise of keeping the carboxylic acid dimer as the construction element, the conjugate degree of scaffold can be expanded as far as possible. HOFs usually contain large π-conjugate aromatic groups. Introduction of large π-conjugate aromatic moieties as building skeleton enhances the chemical resistance for organic solvents, acids, and bases substantially, owing to their inert reactivity. Likewise, strong noncovalent π–π interactions can endow the supramolecular frameworks superior thermoelasticity, flexibility, and self-healing ability, as well as high fragile resistance when the crystals suffer touch, movement, or solvent cleansing. For example, Cao Rong and coworkers selected a planar pyrene ring as the core center and prepared a non-interpenetrating HOF using H_4TBAPy (PFC-1, Fig. 1.3b)[27]. In the structure of **PFC-1**, four neighboring molecules through carboxylic acid dimer form a two-dimensional layer, which is stacked by means of AA stacking to form a three-dimensional open framework. Due to the accumulation of AA, the **PFC-1** structure has a very strong π-π

interaction between pyrene and pyrene and between benzene rings. According to the strategy of network chemistry, Chen Banglin et al.[45] further successfully prepared HOF isomorphic to **PFC-1** by substituting H_4TBAPy with H_4PTTNA ligand with a larger conjugated system (**HOF-14**, Fig. 1.4c). As the π-π interaction between benzene rings in **PFC-1** is replaced by the stronger π-π interaction between naphthalene rings and naphthalene rings, the π-π interaction between layers is further enhanced. Omar K. Farha and co-workers[46] also synthesized HOF-100 (Figure 1.4a), HOF-101 (Figure 1.4b) and HOF-102 (Figure 1.4c) using H_4TCPy, H_4TBAPy and H_4PTTNA, respectively.

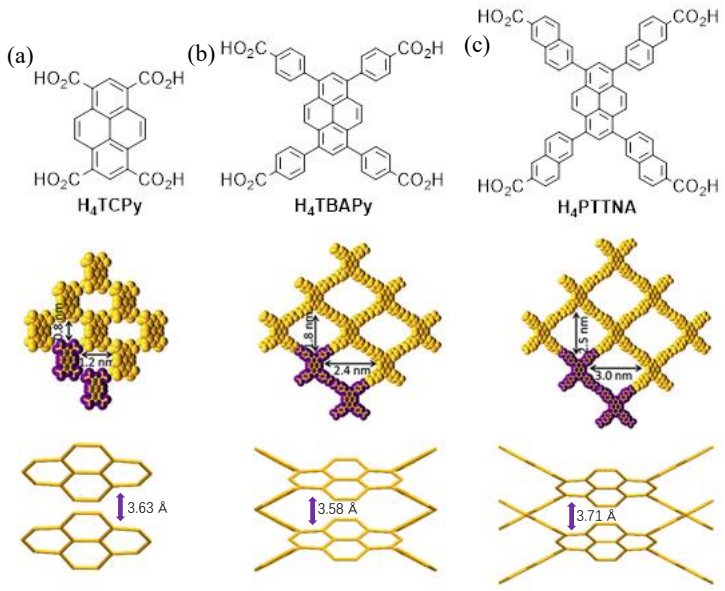

Figure 1.4 Construction of (a) HOF-100, (b) PFC-1/HOF-101, and (c) HOF-14/HOF-102 by H_4TCPy, H_4TBAPy and H_4PTTNA building blocks respectively.[46]

1-5. Nitrogen-Containing π-Conjugated Hydrocarbons

1-5-1. Polycyclic aromatic hydrocarbons

The polycyclic aromatic hydrocarbons (PAHs) are generally composed of hydrocarbons with more than two benzene rings and have a large delocalized π-conjugated structure.[47] Typical organic PAHs are conjugated small molecules such as naphthalene, anthracene, phenanthrene and pyrene. (Figure 1. 5)

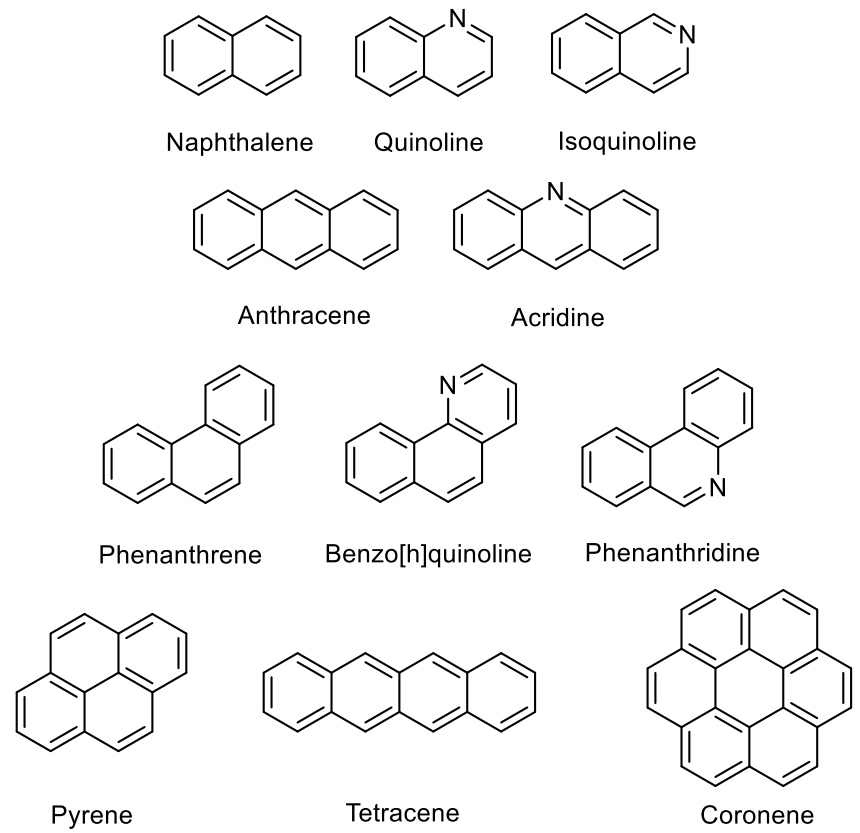

Figure 1.5 Typical organic PAHs and N-PAHs

1-5-2. Influence on physical and chemical properties of nitrogen-containing PAHs (N-PAHs)

Variation of the edge structures of PAHs molecules and enlargement of their aromatic π-system result in adjusted electronic properties. Further tailoring of the HOMO and LUMO energy levels can be achieved through doping with heteroatoms, resulting in heteroaromatics.[48] One of the most important dopants used to tune the optic and electronic properties and to alter the HOMO-LUMO gap of PAH molecules is nitrogen. The atomic radii of nitrogen and carbon are similar, and therefore the nitrogen atom fits well into the carbon framework. The overlap of the nitrogen and the carbon bonding orbitals is good, resulting in strong bonding.[49] N-PAH molecules are achieved through a formal replacement of a carbon atom with a nitrogen atom. As shown in Figure 1.5, the nitrogen atom can either be positioned at the periphery, resulting in externally pyridine derived molecules, or at the interior of the carbon framework,

leading to internally, pyridine derived molecules.[50-52] For externally N-containing molecules, a positive charge can be introduced through alkylation, arylation, or protonation at the nitrogen atom. A positive charge can also be introduced via the placement of the nitrogen atom at a ring junction.[53,54] Natural occurrences of N-doped PAH molecules are mainly biological materials, such as nucleic acids, pigments, and vitamins.[55]

The reactivities of PAH and N-PAH cations with H atom are equivalent within experimental precision, when comparing N-PAH cations of the same size and geometry (Figure 1.6). The exothermicities of the reaction for association at the nitrogen and the most exothermic carbon are listed in Table 1.3.[56]

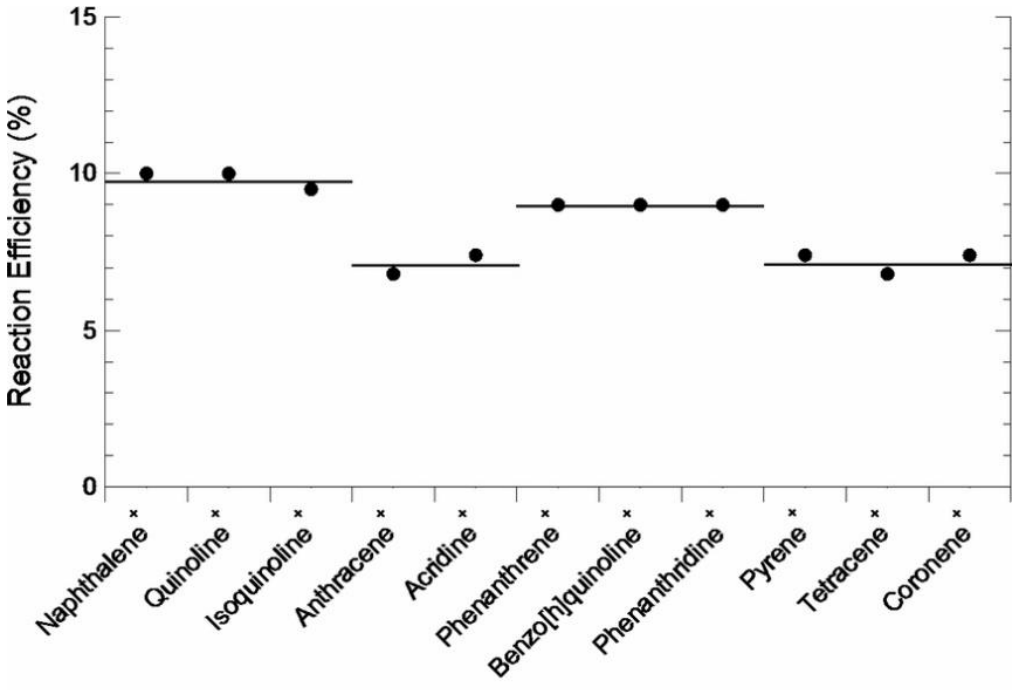

Figure 1.6 Plot of the reaction efficiency for the reaction of N-PAHs cations with H atom. The solid horizontal lines have been added to indicate that the encompassed data points are equivalent within experimental precision. Reaction efficiencies are reported as k_{exp}/k_{col}, where kcol is the collision rate constant determined by Langevin theory. [56]

Table 1.3 N-PAHs Cation/H Atom Association Reactions. [56]

M^+	k_{exp}[a] (10^{-9} cm^3 s^{-1})	Efficiency[b]	$-\Delta H_{exp}$[c] (kcal mol^{-1})	Association at N $-\Delta H_{theor}$[d] (kcal mol^{-1})	Association at C $-\Delta H_{theor}$[d,e] (kcal mol^{-1})
Naphthalene	0.19[f]	0.10	66.1	...	64.5
Quinoline	0.19	0.10	113.2	109.7	72.0
Isoquinoline	0.18	0.095	110.6	108.4	67.0
Anthracene	0.13	0.068	67.7	...	63.2
Acridine	0.14	0.074	98.8	97.5	61.9
Phenanthrene	0.17	0.090	65.7	...	61.6
Benzo[h]quinoline	0.17	0.090	...	96.7	65.1
Phenanthridine	0.17	0.090	...	104.6	68.6
Pyrene	0.14[g]	0.074	65.4	...	62.8
Tetracene	0.13	0.068	63.6	...	59.9
Coronene	0.14[h]	0.074	60.4	...	57.8

1-5-3. Applications of N-PAHs

N-PAHs have attracted much attention regarding application for organic semiconducting materials, sensors, and so on. Compared with their carbon analogues, the introduction of heteroatoms results in the disruption of the carbon sp^2 hybridization, which promotes intramolecular charge transport. At the same time, the introduced heteroatoms can effectively regulate the molecular orbital energy levels and the interactions between molecules. Therefore, heteroatom-doped polycyclic aromatic hydrocarbons have a broad application prospect in the field of organic electrons. Among many heteroatoms, nitrogen atom is a good alternative to a carbon atom in the construction of functional PAHs due to its size matching and electronegativity. From an application point of view, the substitution of carbon atoms with electronegative nitrogen atoms can also produce positive effects, such as in the application of organic light-emitting diodes[57], where electronegative atomic energy improves the charge transfer characteristics of the system. Introducing nitrogen atoms to replace part of carbon atoms in polycyclic compounds forms nitrogen-containing conjugated system molecules, which can significantly improve the stability and assembly performance of the materials, so as to significantly improve the photoelectric properties and multifunctionality of organic photoelectric materials.[58] At the same time, the multi-functional modification of N-PAHs is also an important means to give the regulation and diversity of organic photoelectric molecules.

N-PAHs include linear azaacenes,[59-61] star-shaped azatriphenylene,[62] discotic azabenzocoronene,[63] and bowl-shaped aza-PAHs[64] such as azacorannulene[65] and azasumanene.[66] Some scientists have systematically studied molecular properties, aggregate structures, and solid-state properties were conducted from theoretical and experimental aspects. Davide Bonifazi and co-workers reported a series of co-crystals based on aza-PAHs and boronic acids via hydrogen-bonding.[67] Bunz, Dreuw, Himmel, and co-workers reported precise spectroscopic analyses of tetracene analogues with N-substituted members of the tetracene family in solid noble-gas matrices.[68] Alex K.-Y. Jen and co-works reported a series of hexaazatrinaphthylene derivatives as efficient electron-transporting materials.[69]

1-6. Scope of This Thesis

N-PAHs have been systematically studied, as a class of compounds with a wide variety of molecular sizes and structural forms, which in turn due to a diversity of chemical and physical properties. However, effects of nitrogen atoms in N-PAHs on their molecular arrangements in hydrogen-bonded organic frameworks (HOFs) with permanent porosity have not fully been developed. HOFs, one of families of porous materials, are generally constructed by self-assembly of organic molecules through directional H-bonds, and have shown the advantages of high crystallinity, solution processability, easy healing and purification, due to the reversible and flexible nature of H-bonding connections. Therefore, the author has been interested in constructing N-PAHs-based HOFs (**Nπ-HOFs**) with permanent porosity.

The main purpose of this thesis is to construct external stimuli-responsive Nπ-HOFs with multiple active sites based on new building block molecules possessing highly-symmetric N-PAH cores and peripheral carboxyphenyl groups and expect to show interesting physical properties due to its symmetry and topology.

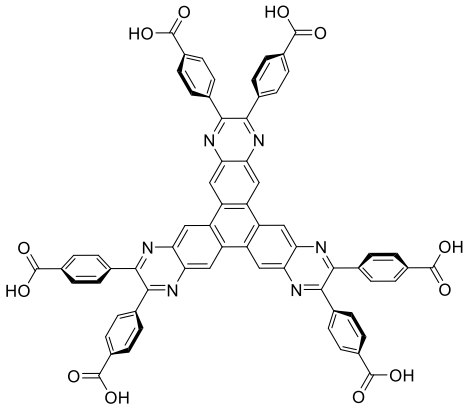

CPBTQ

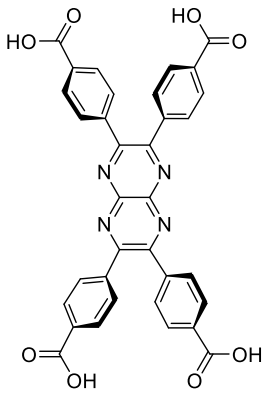

CP-PP

In this paper, I obtained two kinds of Nπ-HOFs. One of them is a HOF with hexagonally-networked structure composed of a C_3-symmetric benzotriquinoxaline derivative. Another is a HOF with rhombic networked structure composed of a C_2-symmetic pyrazinopyrazine derivative. In the process of crystal synthesis, we explored different synthesis methods, used different solvents, and studied the influence of these changes on crystal growth, so as to optimize a final synthesis method with simple synthesis method, little pollution and high purity. Most of the crystal synthesis methods we finally choose are recrystallization methods, because the synthesis method is simple and easy to operate, and the selection of solvent is mainly mixed solvent. After obtaining the crystal materials, we studied their structural characteristics and hydrogen bond patterns, as well as the thermal stability of the frame structure by single crystal structure diffraction, Powder X-Ray Diffraction (PXRD), thermogravimetric analysis and variable temperature PXRD. I investigated positional effects of annulated pyrazine-rings on structure and stability of Nπ-HOFs to establish design principle of Nπ-HOFs. The gas adsorption performance of activated **CPBTQ** with pore structure was also studied. **CP-PP** has essential structural motifs of highly N-content polycyclic aromatic hydrocarbons. And describes spectroscopic and electronic properties of **CP-PP** and its ester precursor.

References

1. G. Férey, et al., A chromium terephthalate-based solid with unusually large pore volumes and surface area. *Science*, **2005**, *309*, 2040.

2. X. Meng, et al., Proton-conducting crystalline porous materials. *Chem. Soc. Rev.*, **2017**, *46*, 464.

3. S. Kitagawa, et al., Functional porous coordination polymers. *Angew. Chem. Int. Ed.*, **2004**, *43*, 2334.

4. A. P. Côté, et al., Porous, crystalline, covalent organic frameworks. *Science*, **2005**, *310*, 1166.

5. Y. He, et al., A microporous hydrogen-bonded organic framework for highly selective C_2H_2/C_2H_4 separation at ambient temperature. *J. Am. Chem. Soc.*, **2011**, *133*, 14570.

6. G. C. Pimentel, et al., The hydrogen bond. *W. H. Freeman and Company: San Fransisco, CA, USA*. **1960**. 475.

7. E. Arunan, et al., Definition of the hydrogen bond (IUPAC Recommendations 2011). *Pure Appl. Chem.*, **2011**, *83*, 1637.

8. G. R. Desiraju, Reflections on the hydrogen bond in crystal engineering. *Cryst. Growth Des*. **2011**, *11*, 896.

9. T. Steiner, The hydrogen bond in the solid state. *Angew. Chem. Int. Ed*. **2002**, *41*, 48.

10. G. A. Jeffrey, An introduction to hydrogen bonding. *Oxford University Press*. **1997**.

11. R. B. Lin, et al., Multifunctional porous hydrogen-bonded organic framework materials. *Chem. Soc. Rev.* **2019**, *48*, 1362.

12. E. A Meyer, et al., Interactions with aromatic rings in chemical and biological

recognition. *Angew Chem Int Ed*., **2003**, *42(35)*, 4120.

13. S. V. Shishkina, et al., Hydrogen bonding vs. stacking interaction in the crystals of the simplest coumarin derivatives: a study from the energetic viewpoint. *CrystEngComm*, **2019**, *21*, 6945.

14. L. M. Salonen, et al., Aromatic rings in chemical and biological recognition: Energetics and Structures. *Angew. Chem. Int. Ed.* **2011**, 50, 4808.

15. J. Luo, et al., Hydrogen-bonded organic frameworks: design, structures and potential applications. *CrystEngComm*, **2018**, *20*, 5884.

16. I. Hisaki, et al., Designing hydrogen-bonded organic frameworks (HOFs) with permanent porosity. *Angew. Chem. Int. Ed*., **2019**, *58*, 11160.

17. J. Yang, et al., Porous hydrogen-bonded organic frameworks (HOFs): from design to potential applications. *Chem. Eng. J*. **2020**, *399*, 125873.

18. P. Li, et al., Solvent dependent structures of hydrogen-bonded organic frameworks of 2,6-diaminopurine. *Cryst. Growth Des*. **2014**, *14*, 3634.

19. D. J. Duchamp, et al., The crystal structure of trimesic acid (benzene-l,3,5-triearboxylic acid). *Acta Crystallogr*. **1969**, *25*, 5.

20. K. Kobayashi, et al., Two-dimensional hexagonal hydrogen-bonded network withtriangle-like large cavities: hexakis(4-carboxyphenyl)benzene. *Tetrahedron Letters*, **2000**, *4*, 89.

21. C. A. Zentner, et al., High surface area and Z' in a thermally stable 8-fold polycatenated hydrogen-bonded framework. *Chem. Commun*. **2015**, *51*, 11642.

22. T.-U. Yoon. et al., Efficient separation of C2 hydrocarbons in a permanently porous hydrogen-bonded organic framework, *Chem. Commun*. **2018**, *54*, 9360.

23. S. Nandi, et al., A permanently porous single molecule H-bonded organic framework for selective CO_2 capture. *Chem. Commun.* **2016**, *52*, 7249.

24. I. Hisaki, et al., A series of layered assemblies of hydrogen-bonded, hexagonal networks of C_3-symmetric π-conjugated molecules: a potential motif of porous organic materials. *J. Am. Chem. Soc*. **2016**, *138*, 6617.

25. I. Hisaki, et al., Precise elucidations of stacking manners of hydrogen-bonded two-dimensional organic frameworks composed of X-shaped π-conjugated systems. *CrystEngComm*, **2017**, *19*, 4892.

26. F. Hu, et al., An ultrastable and easily regenerated hydrogen-bonded organic molecular framework with permanent porosity. *Angew. Chem. Int. Ed.* **2017**, *56*, 2101.

27. Q. Yin, et al., An ultra-robust and crystalline redeemable hydrogen-bonded organic framework for synergistic chemo-photodynamic therapy. *Angew. Chem. Int. Ed.* **2018**, *57*, 7691.

28. P. H. Li, et al., Interpenetration isomerism in triptycene-based hydrogen-bonded organic frameworks. *Angew. Chem. Int. Ed*. **2019**, *58*, 1664.

29. B. Wang, et al., A microporous hydrogen-bonded organic framework for highly efficient turn-up fluorescent sensing of aniline, *J. Am. Chem. Soc.* **2020**. *142*, 12478.

30. M. Simard, et al., Use of hydrogen bonds to control molecular aggregation. self-assembly of three-dimensional networks with large chambers. *J. Am. Chem. Soc*. **1991**, *113*, 4696.

31. X. Wang, et al., Molecular tectonics. three-dimensional organic networks with zeolitic properties. *J. Am. Chem. Soc*. **1994**, *116*, 12119.

32. W. Yang, et al., Exceptional thermal stability in a supramolecular organic framework: porosity and gas storage. *J. Am. Chem. Soc*. **2010**, *132*, 14457.

33. P. Sozzani, et al., Methane and carbon dioxide storage in a porous van der Waals crystal. *Angew. Chem. Int. Ed*. **2005**, *44*, 1816.

34. H. L. Wang, et al., A flexible microporous hydrogen-bonded organicframework for gas sorption and separation. *J. Am. Chem. Soc*. **2015**, *137*, 9963.

35. H. L. Wang, et al., Two solvent-induced porous hydrogen-bonded organic frameworks: solvent effects on structures and functionalities. *Chem. Commun*. **2017**, *53*, 11150.

36. W. B. Yang, et al., Exceptional thermal stability in a supramolecular organic framework: porosity and gas storage. *J. Am. Chem. Soc*. **2010**, *132*, 14457.

37. W. J. L, et al., Nitrogen- and iodine-doped microporous carbon derived from a hydrogen-bonded organic framework: an efficient metal-free electrocatalyst for the oxygen reduction reaction. *J. Mater. Chem. A*, **2019**, *7*, 9587.

38. L. L. T, et al., Pillar[5]arene-based supramolecular organic frameworks for highly selective CO_2-capture at ambient conditions. *Adv. Mater*. **2014**, *26*, 7027.

39. G. R. Desiraju, Supramolecular synthons in crystal engineering—a new organic synthesis. *Angew. Chem., Int. Ed.* **1995**, *34*, 2311.

40. S. Ebenezer, et al., Design of a series of isostructural Co-crystals with aminopyrimidines: isostructurality through Chloro/Methyl exchange and studies on supramolecular architectures. *Cryst. Growth. Des*. **2011**, *11(8)*, 3579.

41. K. C. Perez, et al., A robust binary supramolecular organic framework (SOF) with high CO_2 adsorption and selectivity. *J. Am. Chem. Soc*. **2014**, *136(37)*, 12828.

42. M. Mastalerz, et al., Rational construction of an extrinsic porous molecular crystal with an extraordinary high specific surface area. *Angew. Chem. Int. Ed*. **2012**, *51(21)*, 5252.

43. X. Z. Luo, et al., A microporous hydrogen-bonded organicframework: exceptional stability and highly selective adsorption of gas and liquid. *J. Am. Chem. Soc*. **2013**, *135(32)*, 11684.

44. I. Hisaki, et al, Acid responsive hydrogen-bonded organic frameworks. *J. Am. Chem. Soc*. **2019**, *141*, 2111.

45. B. Wang, et al., A novel mesoporous hydrogen-bonded organic framework with high porosity and stability. *Chem. Commun*. **2020**, *56*, 66.

46. K. Ma, et al., Ultrastable mesoporous hydrogen-bonded organic framework-based fiber composites toward mustard gas detoxification. *Cell Reports Physical Science* **2020**, *1*, 100024.

47. D.B. Paul, Polycyclic aromatic hydrocarbons. *Environ Forensics.* **1964**, *15*, 313.

48. P. O. Dral, et al., Doped polycyclic aromatic hydrocarbons as building blocks for nanoelectronics: A Theoretical Study. *J. Org. Chem*. **2013**, *78*, 1894.

49. R. Tang, et al., Efficient approach to electron-deficient 1,2,7,8-tetraazaperylene derivatives. *Org. Lett*. **2014**, *16*, 4726.

50. C. Bazzini, et al., Synthesis and characterization of some aza[5]helicenes. *Eur. J. Org. Chem*. **2005**, *2005*, 1247.

51. S. Arai, et al., Synthesis of azonia derivatives of benzoperylene and benzocoronene by photocyclization. *Chem. Soc. Jpn*. **1991**, *64*, 1996.

52. J. Fortage, et al., Expanded pyridiniums: bis-cyclization of branched pyridiniums into their fused polycyclic and positively charged derivatives—assessing the impact of pericondensation on structural, electrochemical, electronic, and photophysical features. *Chem. Eur. J*. **2010**, *16*, 11047.

53. S. Arai, et al., Synthesis of polycyclic azonia-aromatic compounds by photo-induced intramolecular quaternization: Azonia derivatives of benzo[c]phenanthrene, [5]helicene and [6]helicene. *J. Chem. Soc*., **1998**, *1*, 1561.

54. A. C. Benniston, et al., Charge transfer properties of a donor–acceptor dyad based on an expanded acridinium cation. *RSC Adv*. **2013**, *3*, 4995.

55. V. Coropceanu, et al., Charge transport in organic semiconductors. *Chem. Rev*. **2007**, *107*, 926.

56. N. J. Demarais, et al., Gas-phase reactions of polycyclic aromatic hydrocarbon cations. *Astrophys. J*, **2014**, *784*, 25.

57. U. H. F. Bunz, N-Heteroacenes. *Chem. Eur. J.* **2009**, *15*, 6780.

58. G. J. Richards, et al., Amphiprotism-coupled near-infrared emission in extended pyrazinacenes containing seven linearly fused pyrazine units. *J. Am. Chem. Soc.* **2019**, *141*, 19570.

59. U. H. F. Bunz, Freudenberg, *J. Acc. Chem. Res*. **2019**, *52*, 1575.

60. K. Oki, et al., Synthesis and isolation of antiaromatic expanded azacoronene via intramolecular vilsmeier-type reaction. *J. Am. Chem. Soc*. **2019**, *141*, 16255.

61. M. Saito, et al., Figuration of bowl-shaped π-conjugated molecules: properties and functions. *Mater. Chem. Front.* **2018**, *2*, 635.

62. H. Yokoi, et al., Nitrogen-embedded buckybowl and its assembly with C_{60}. *Nat. Commun.* **2015**, *6*, 8215.

63. W. Wu, et al., π-Conjugated molecules with fused rings for organic field-effect ransistors: design, synthesis and applications, *Chem. Soc. Rev*. **2010**, *39*, 1489.

64. I. Georgiou, et al., Versatile self-adapting boronic acids for H-bond recognition: from discrete to polymeric supramolecules. *J. Am. Chem. Soc*. **2017**, *139*, 2710.

65. Y. Lin, et al., Small molecule semiconductors for high-efficiency organic photovoltaics. *Chem. Soc. Rev*. **2012**, *41*, 4245.

66. H. Imahori, et al., Large π-aromatic molecules as potential sensitizers for highly efficient dye-sensitized solar cells. *Acc. Chem. Res*. **2009**, *42*, 1809.

67. S. R. Forrest, The path to ubiquitous and low-cost organic electronic appliances on plastic, *Nature*, **2004**, *428*, 911.

68. J. G. Veinot, et al., Toward the ideal organic light-emitting diode. The versatility and utility of interfacial tailoring by cross-linked siloxane interlayers. *Acc. Chem. Res*. **2005**, *38*, 632.

69. J. E. Anthony, Functionalized Acenes and Heteroacenes for Organic Electronics. *Chem. Rev*. **2006**, *106*, 5028.

Chapter 2

Positional Effects of Annelated Pyrazine Rings on Structure and Stability of Hydrogen-Bonded Frameworks of Hexaazatrinaphthylene Derivatives

Abstract

A porous hydrogen-bonded organic framework (HOF) composed of N-hetero π-conjugated molecules (Nπ-HOF) is a promising candidate for multi-functional porous materials. However, such HOFs are still limited and only handful examples were reported. In this study, we investigated positional effects of annelated pyrazine-rings on structure and stability of Nπ-HOFs to establish design principle of Nπ-HOFs. A new isomer of hexaazatrinaphthylene (**CPBTQ**) was synthesized and subjected to Nπ-HOF construction, activation, evaluation of stability and permanent porosity. Comparison between two kinds of Nπ-HOF composed of isomers (**CPBTQ** and **CPHATN**) possessing three pyrazine rings annelated at the different positions indicates that the positional difference of the pyrazine rings strongly effects on conformation of the peripheral phenylene groups, which then lead to different structure and stability of the Nπ-HOFs. The Nπ-HOF composed of **CPBTQ (CPBTQ-1a)** are revealed to exhibit the Brunauer-Emmett-Teller (BET) surface area of 471 $m^2 g^{-1}$ and show reversible HCl responsiveness thanks to the basic pyrazine rings annulated to the triphenylene core. We believe that the present results can contribute not only for construction of multifunctional porous materials but also for chemistry on heteroaromatic compounds.

2-1. Introduction

Nitrogen (N)-containing relatives of polycyclic aromatic hydrocarbons (aza-PAHs) have recently attracted much attention regarding application for organic semiconducting materials, sensors, and so on. These include linear azaacenes,[1–4] star-shaped azatriphenylene,[5] discotic azabenzocoronene,[6,7] and bowl-shaped aza-PAHs[8] such as azacorannulene[9] and azasumanene.[10] Incorporation of N atoms into the π-conjugated systems is capable of fine-tuning electronic states of the systems,[11–14] capturing and sensing cationic species,[15,16] making metal complexes,[17–21] and improving molecular packing in crystalline states through C–H···N interactions[22] or dative bonds[23] to achieve effective charge-transport properties. To date, systematic studies on relationship among numbers and positions of the N atoms in the system,

molecular properties, aggregate structures, and solid-state properties were conducted from theoretical and experimental aspects. Bunz, Dreuw, Himmel, and co-workers reported spectroscopic precise analyses of tetracene analogues with different numbers of N atoms in solid noble-gas matrices.[24] Day and co-workers reported organic semiconduction properties of pentacene analogues with five or seven N atoms based on the predicted crystal structures, energy evaluation, and calculated charge carrier mobility.[25] Theoretical calculation on reorganization energies were also reported.[26] Isoda, Tadokoro, and co-workers demonstrated redox properties of azaacene-based in liquid crystalline states.[27] Bonifazi and co-workers conducted systematic crystallization of aza-PAHs and boronic acids via hydrogen-bonding to yield various co-crystals.[28] However, effects of N atoms in aza-PAHs on their molecular arrangements in hydrogen-bonded organic frameworks (HOFs) with permanent porosity have not fully been understood, although the chemistry of such porous molecular crystals have been intensively investigated recently.

HOFs are porous molecular crystals particularly constructed through intermolecular hydrogen bonds. Because of their high crystallinity, easy recrystallization process, and development of a design strategy based on multiplicity and/or directionality of hydrogen bonds, various HOFs have been constructed and their properties investigated as a new class of porous frameworks.[29–35] In connection with HOFs, we previously demonstrated that C_3-symmetric π-conjugated hydrocarbons, such as a triphenylene derivative **Tp**, possessing six carboxyphenyl groups in their periphery (Chart 2.1) form a hydrogen-bonded hexagonal network (H-HexNet) and that the H-HexNet stacks without interpenetration to yield the corresponding layered HOFs.[36–38] More recently, Chen and co-workers reported a HOF based on C_3- or C_6-symmetric benzene derivatives with carboxy groups.[39,40] Interestingly, when the triphenylene moiety of **Tp** was replaced by hexaazatriphenylene (HAT), the resulting derivative **CPHAT** formed no layered 2D framework but a three-dimensional (3D) rigid framework with permanent porosity.[41,42] In the 3D framework, the HAT moiety is deformed into a propeller-shaped conformation by packing forces. Because of the

conformation, the six peripheral carboxyphenyl groups alternately direct upward and downward to form a 3D H-bonded network. These results are crucially provided by introduction of pyrazine rings into the π-conjugated core. Subsequently, we synthesized its larger analogue, carboxyphenyl-substituted hexaazatrinaphthylene derivative (**CPHATN**).[43] **CPHATN** was revealed to form a very stable porous layered framework based on the 2D H-HexNet, which is importantly responsive to HCl vapor or solution by changing its color from yellow to brown due to protonation of the pyrazine rings. That is, to our knowledge, the first example for proof-of-concept of stimuli-responsive HOFs.

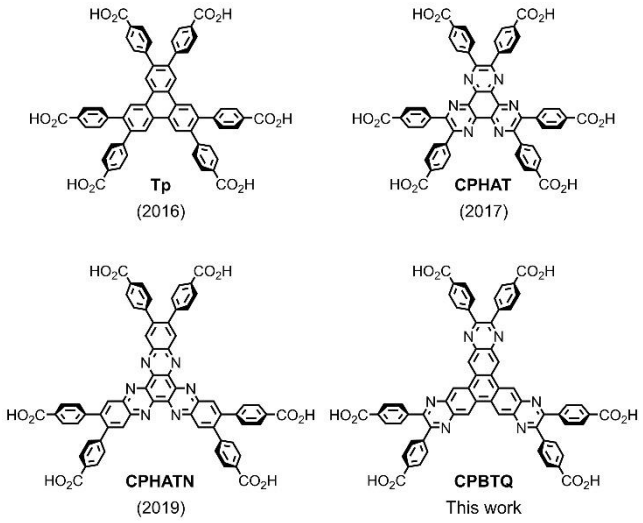

Chart 2.1 C_3-symmetric π-conjugated molecules (C_3PI) without and with incorporated pyrazine rings as a building blocks to construct porous hydrogen-bonded organic frameworks.

Keeping this in mind, we became interested in a H-bonded assembly structure of carboxyphenyl-substituted benzotriquinoxaline derivative **CPBTQ**. **CPBTQ** possess three pyrazine rings annelated in different position from **CPHATN**. Therefore, comparison of the assembly structures of these two regioisomers can provide positional effects of the N-hetero rings on molecular arrangements and properties.

In this chapter, synthesis and characterization of **CPBTQ**, construction and structural determination of its HOF, an evaluation of porosity and stability of the activated HOF, acid responsiveness, and effects of the N atoms in **CPBTQ** on structure and property of the HOF are described. Interestingly, **CPBTQ** forms a H-HexNet-based

HOF with a stacking manner of H-HexNet sheets different from that of **CPHATN**. The H-HexNet involves dissociated and pertly H-bonded dimers, in addition to fully H-bonded carboxy dimer (Figure 2.1). Moreover, it is revealed that the position of the pyrazine rings strongly effects on conformation of the peripheral phenylene groups, which then makes the structure, particularly H-bonding patterns, and property of the HOF different from that of **CPHATN**. We believe that the present results can contribute not only to the construction of new functional N-hetero π-conjugated molecule based HOFs (Nπ-HOFs), but also for chemistry on heteroaromatic compounds.

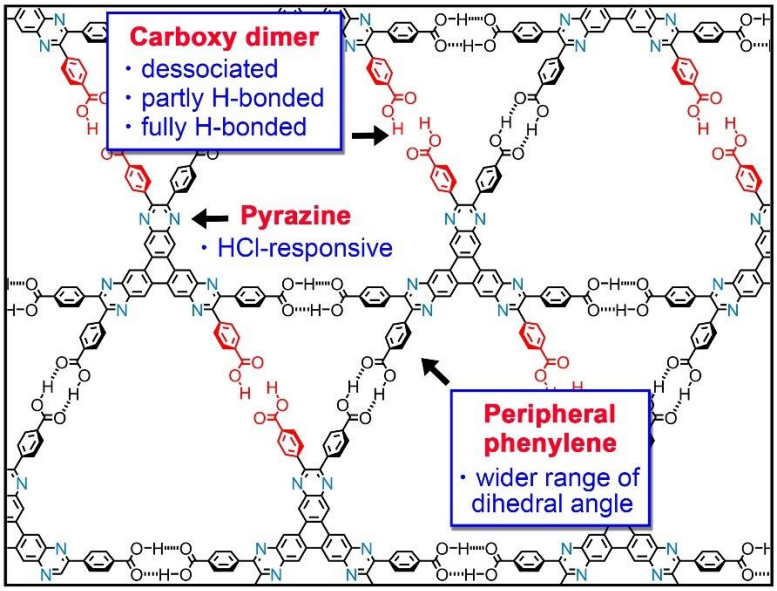

Figure 2.1 Schematic representation of hydrogen-bonded hexagonal network (H-HexNet) of **CPBTQ** and its features.

2-2. Results and Discussion

2-2-1. Synthesis and crystallization of CPBTQ.

2,3,6,7,10,11-Hexaaminotriphenylene hydrochloride salt, which was synthesized from the corresponding hexabromotriphenylene derivative according to the literature,[44] was treated by benzil derivative **1** in acetic acid to give ester derivative **2** (Scheme 2.1). **CPBTQ** was subsequently prepared by hydrolysis of **2**. **CPBTQ** was characterized by ^{1}H and ^{13}C NMR spectroscopy, HR-MS, and crystallographic analysis. The solvated

framework **CPBTQ-1(MeBz)** with a H-HexNet motif was obtained as needle-shaped orange crystals by slow evaporation of a solution of **CPBTQ** dissolved in *N*,*N*-dimethylacetamide (DMA) and methyl benzoate (MeBz) at 120 °C for 3 days. We also attempted to obtain a crystal of **CPBTQ** with the same solvent system (i.e., N-methylpyrrolidone and 1,2,4-trichlorobenzene) as in the case of **CPHATN**. However, no crystal was obtained.

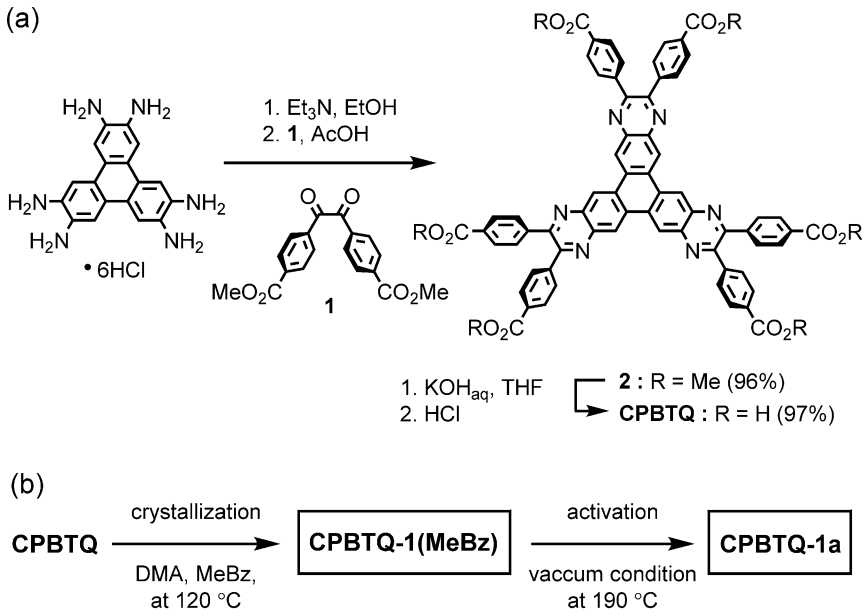

Scheme 2.1 (a) Synthesis and (b) crystallization of **CPBTQ**

2-2-2. Crystal structure of CPBTQ-1(MeBz).

CPBTQ crystallized into the space group of $P3_212$ (no.153) to give the solvated H-HexNet framework, **CPBTQ-1(MeBz)**, as shown in Figure 2.2 and Table 2.1. The crystal consists of four symmetrically-independent molecules of **CPBTQ** (A, B, C, and D), two of which possess C_2-symmetric axis (A and D). Since C_2-symmetric axis lies on the center of carboxy dimer, the hydrogen atoms are expediently attached on both the oxygen atoms of the carboxy group, as shown in Figure 2.3. The BTQ cores are slightly deformed due to the packing force in solid state: the root-mean-square deviation (RMSD) of the cores ranges from 0.06 to 0.19 Å (Table 2.2). **CPBTQ** molecules (A–D) are stacked along the *c* axis in a three-fold helical manner, and each of them respectively forms a perfect or quasi H-HexNet sheet. In contrast with the previously

reported HOF **CPHATN-1(124TCB)**, H-HexNets of **CPBTQ-1(MeBz)** involve a dissociated dimer (dd) and defective H-bonded dimers such as an open dimer (od) and truncated chain (tc), in addition to perfectly H-bonded dimer of the carboxy groups, as shown in Figures 2.2b and 2.4. These defective H-bonded dimers has open-end hydroxy groups, which are probably trapped by solvent molecules through H-bonds[36] although most of solvent molecules were not able to be solved crystallographically due to sever disorder. It is noteworthy that anisotropic displacement of the peripheral carboxyphenyl groups is much more significant than that of the BTQ core moiety: averaged U_{iso} values for cores A, B, C, and D range from 0.053 to 0.062, while those of phenylene moieties and carboxy groups range from 0.080 to 0.11, and from 0.123 to 0.143, respectively (Table 2.2). Particularly, the groups with defectively H-bonded or dissociated dimers are severely disordered (Figure 2.5). H-HexNet frameworks stacked nearly in an eclipsed manner between layers B and C. In the cases of layers A-B and C-D, on the other hand, the H-HexNet layers stack in an inverted fashion, resulting less overlap of the frameworks. The defective H-bonded dimers and highly disordered atoms with larger U_{iso} exist in these less-overlapped regions. The imperfect H-bonded network formation in **CPBTQ-1(MeBz)** effects on stability of the framework, as will be described later. The framework has two kinds of three-fold helical channels (I and II) along the crystallographic *c* axis (Figure 2.6). In the channels, MeBz molecules are accommodated thought they are highly disordered, and therefore, most of them are not able to characterized crystallographically (Figure 2.7). Channel I has a narrow width of 5 Å and unlevel surface. Channel II has a more complicated shape, like a shish-kebab structure, with a narrow bottle neck (7 Å) and wide discotic spaces (20 Å). The ratio of total potential solvent area volume is calculated to be 36% by PLATON software with probe radius of 1.2 Å (cell volume: 34267.5 $Å^3$, void volume per cell: 12418 $Å^3$).

Table 2.1 Crystal data of **CPBTQ-1(MeBz)**, as well as previously reported **CPHATN-1(124TCB)**.

	CPBTQ-1(MeBz)	**CPHATN-1(124TCB)**
Formula	$2(C_{66}H_{36}N_6O_{12})$, $2(C_{33}H_{18}N_3O_6)$, $C_8H_8O_2$	$(C_{66}H_{36}N_6O_{12})$
Formula weight	3451.17	1105.04
Crystalline system	*trigonal*	*triclinic*
Space group	$P3_212$ (no.153)	*P*-1 (no.2)
a [Å]	26.3357(3)	7.27754(17)
b [Å]	26.3357(3)	20.8039(4)
c [Å]	57.0508(14)	21.7135(4)
α [°]	90	76.5118(17)
β [°]	90	89.6714(17)
γ [°]	120	86.3993(18)
V [Å^3]	34267.5(10)	3190.33(12)
Z / Z'	6 / 4	2 / 1
Number of reflection (obs./uniq.)	232956 / 52578	27298/ 12287
R1 ($I > 2.0\sigma(I)$)	0.0910	0.0808
Rw (all)	0.3104	0.2490
T [K]	100	213
CCDC No.	1976117	1877481 [43]

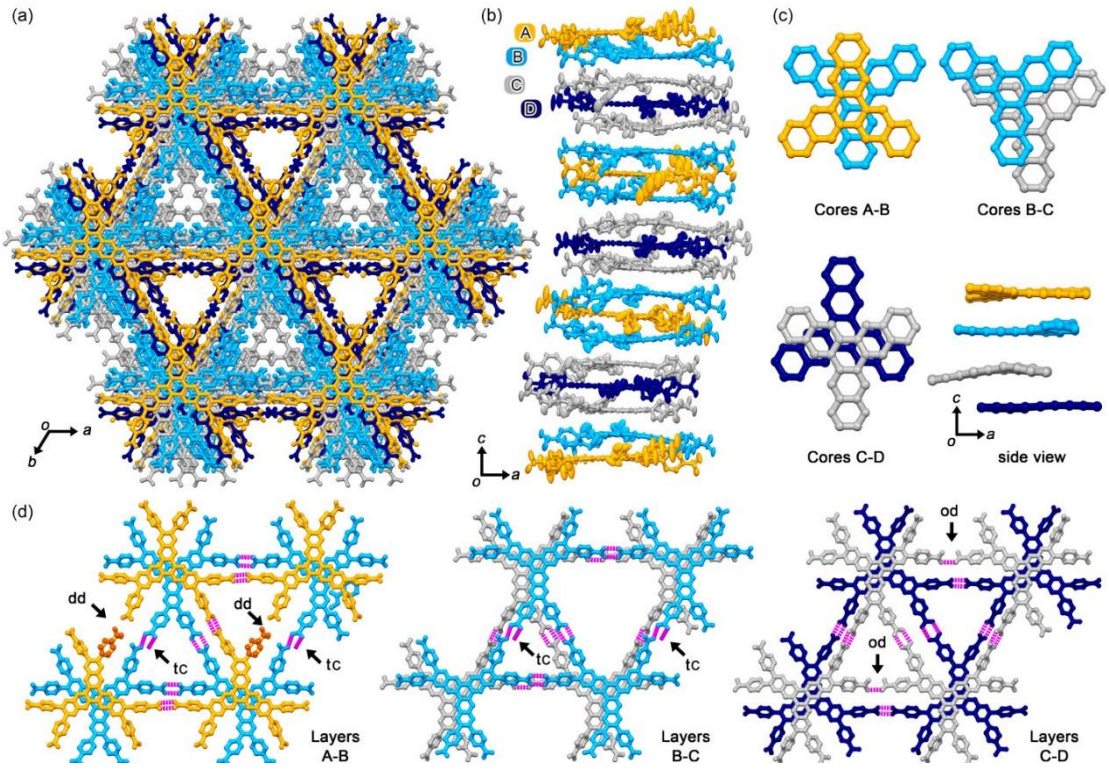

Figure 2.2 Crystal structure of **CPBTQ-1(MeBz)**. (a) Packing diagram viewed down from the *c* axis. (b) Side view of stacked molecules in the unit cell drawn by displacement anisotropic ellipsoids with 50% probability, where four symmetrically-independent molecules (A, B, C, and D) are colored by yellow, cyan, gray, and dark blue, respectively. A and D have C_2-axis within the molecules. (c) Relative positions of the stacked BTQ cores. (d) Stacking motifs of the adjacent layeres A-B, B-C, and C-D. Dash lines in magenta denote H-bonds. Orange spheres in layer A denote the other part of the carboxyphenyl groups disordered in two positions. dd: dissociated dimer, tc: truncated H-bonded chain, od: open dimer.

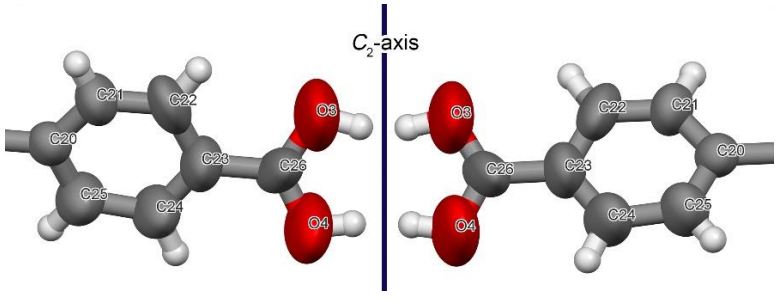

Figure 2.3 An example of carboxy dimer with the C_2-symmetric axis, which causes disorder of hydrogen atoms.

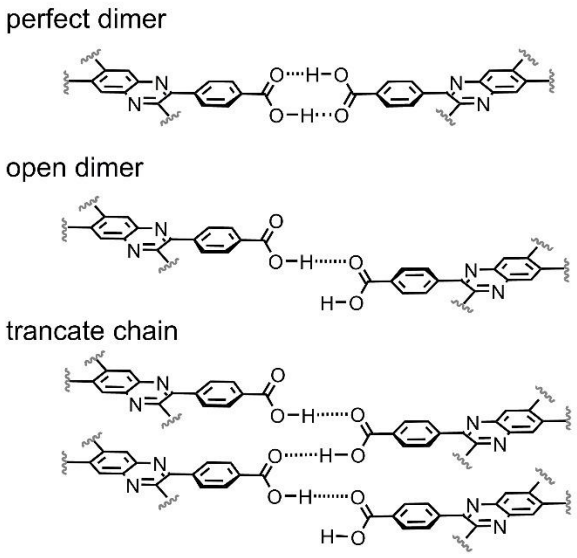

Figure 2.4 H-bonding patterns of carboxy groups observed in a crystal structure of **CPBTQ-1(MeBz)**.

Table 2.2 Structural displacement parameters of **CPBTQ** molecules A, B, C, and D.

	A[a]	B	C	D
RMSD of BTQ core[b]	0.10	0.18	0.19	0.06
U_{iso}(BTQ core)[c]	0.062	0.053	0.054	0.050
U_{iso}(phenylene)[c]	0.107	0.084	0.080	0.080
U_{iso}(carboxy)[c]	0.143	0.128	0.123	0.132

[a] Values for one of the symmetrically-independent three carboxyphenyl groups are not included due to its significantly disordered structure, which is refined with structural restrain.

[b] Root mean square deviation (RMSD) of BTQ moiety.

[c] Averaged values of U_{iso} are applied.

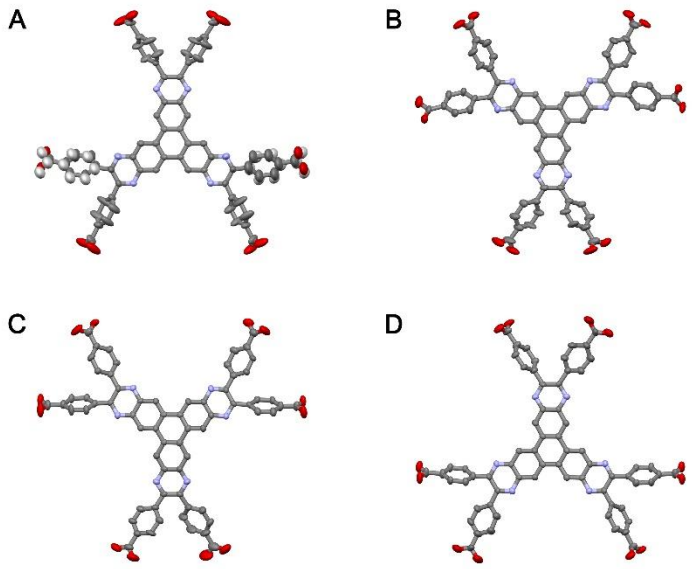

Figure 2.5 Anisotropic displacement ellipsoid plots of the molecules A, B, C, and D with 50% probability.

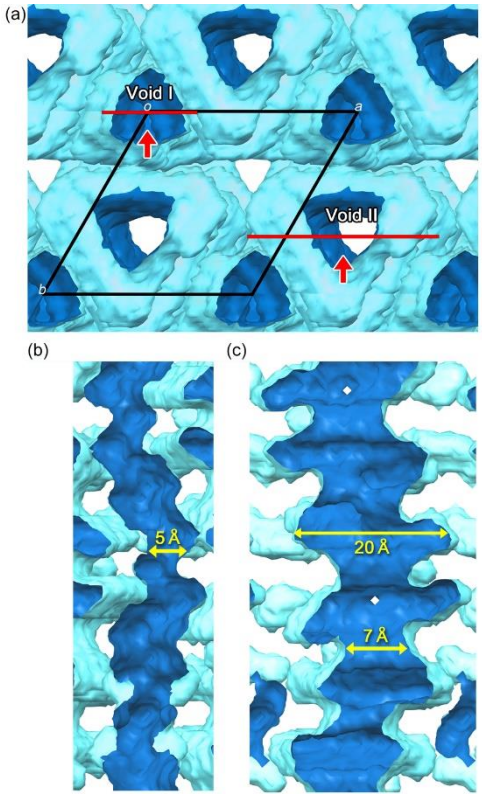

Figure 2.6 Visualized surfaces of the void. (a) Top view of the voids. (b) Cross-section of the channel I. (c) Cross section of the channel II. The cross-section images were prepared by cutting on the red lines and viewing from a direction along red arrows.

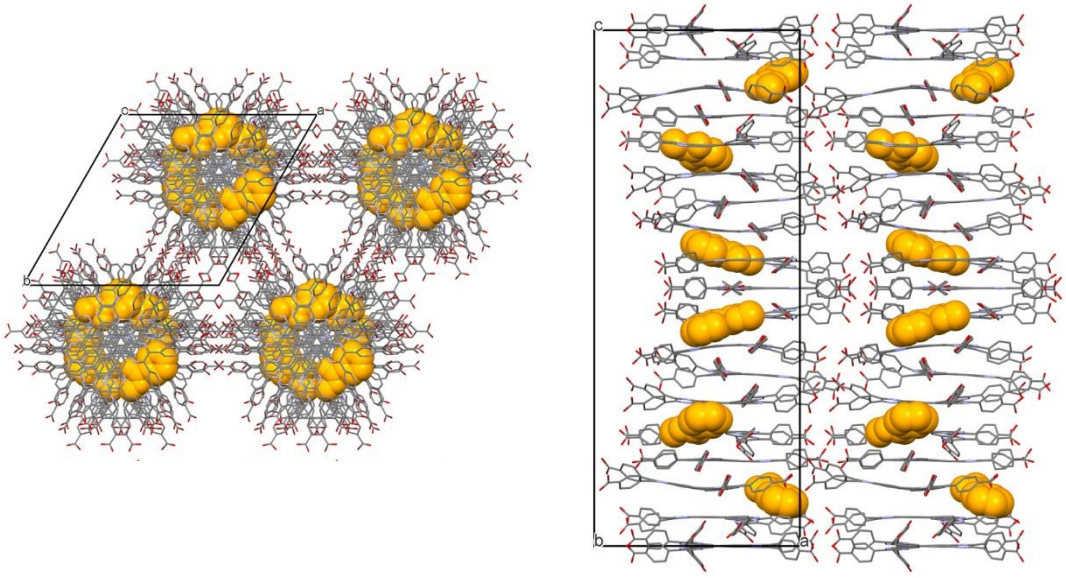

Figure 2.7 Packing diagram of **CPBTQ-1(MeBz)** with guest molecules (MeBz). Symmetrically independent one molecule of MeBz was solved crystallographically.

As previously reported, **CPHATN**, which is an isomer of **CPBTQ**, is crystallized into *P*-1 space group with *Z*' = 1. The structural differences between molecules **CPHATN** and **CPBTQ** is location of the pyrazine rings as shown in Chart 1. This difference, however, caused crucial differences on their molecular packing in crystalline states. These differences can be explained from conformation of the peripheral phenylene moieties. Figure 2.8 shows distribution of dihedral angle (ϕ) of biphenyl derivatives with *ortho*-substituents and of 2-phenyl-3-substituted pyridine derivatives, where the substituent R is a phenyl group or an ortho-, meta-, or para-substituted phenyl group, surveyed by Mogul, which is a knowledge-based library of molecular geometry derived from the Cambridge Structural Database.[45,46] The distribution of the dihedral angle in the phenyl-pyridine systems slightly shifted into smaller angle region for ϕ <90° and into larger angle region for ϕ >90° in compared with the phenyl-benzene systems due to less steric hindrance at the *ortho*-position (i.e. C–H vs. N). These results indicate that phenyl-pyridine systems have larger degree of freedom regarding rotational conformations. Indeed, the ϕ values observed in HOFs and Nπ-HOFs composed of C_3PIs **Tp**, **CPHAT**, **CPHATN**, and **CPBTQ** show the same tendency (Table 2.3). HOFs **Tp-1**, **-2**, **-3**, **-4**, and **CPHATN-1a** exhibit the angle

ϕ ranging from 43.7 to 72.8°. On the other hand, that of HOFs **CPHAT-1a** and the present **CPBTQ-1(MeBz)** ranges from 27.9 to 65.6°. The high degree of freedom in the conformation of the peripheral phenylene groups, in the case of **CPBTQ**, results in increase of versatility of molecular packing pattern, to yield the framework with high *Z*' values and partly defected H-bonding network. Additionally, in the crystal structure of **CPBTQ-1(MeBz)**, interlayer CH···N interactions form between the N atoms in the BTQ core and aromatic proton of the phenylene groups of **CPBTQ** located in the next stacked layer: [C(197)–H···N(11): H···N distance: 2.62 Å, C–H–N angle: 157.7°. C(164)–H···N(16): H···N distance: 2.58 Å, C–H–N angle: 164.5°] (Figure 2.9). Because of these interlayer C–H···N contacts, the involved phenylene rings have more twisted conformation with larger values of ϕ (ϕ = 65.6° and 49.4°). In the case of **CPHATN**, on the other hand, the N atoms in the core are difficult to make interlayer C–H···N interactions due to steric hindrances.

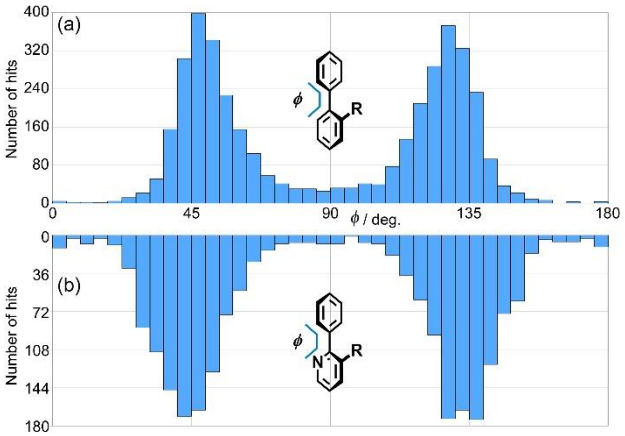

Figure 2.8. Dihedral angle distribution of (a) phenyl-benzene and (b) phenyl-pyridine systems possessing substituents at the *ortho*-position of the phenyl group.

Table 2.3 Dihedral angles ϕ in Nπ-HOFs **CPBTQ-1(MeBz)** and the related crystals.

crystal	ϕ [a] [°]
Tp-1, **-2**, **-3**, and **-4**	49.8–72.8 (56.2)[b]
CPHATN-1a	43.7–67.6 (52.8)[b]
CPHAT-1a (124TCB)	27.9
CPBTQ-1(MeBz)	
(A)	34.9–65.6 (49.9)[b]
(B)	38.3–49.4 (45.5)[b]
(C)	33.3–56.4 (42.6)[b]
(D)	38.2–57.6 (48.9)[b]

a Ranges of ϕ

b Values in the parentheses are averaged angle of ϕ.

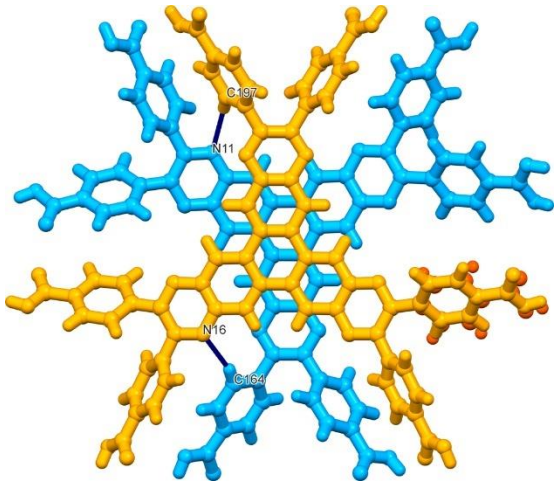

Figure 2.9 CH···N contacts in **CPBTQ-1(MeBz)**. The contacts are observed between molecules A and B. C(197)–H···N(11): H···N distance: 2.62 Å, C–H–N angle: 157.7°. C(164)–H···N(16): H···N distance: 2.58 Å, C–H–N angle: 164.5°

2-2-3. Thermal behaviors.

Thermo gravimetric (TG) analysis of as-formed crystalline bulk of **CPBTQ-1(MeBz)** shows two weight loss processes, (Figure 2.10a) indicating that the MeBz molecules are located at least two different positions through different intermolecular interactions. Indeed, crystallographic analyses were capable of solving one symmetrically independent MeBz molecule, which was stacked at the corner of the void, while the other MeBz molecules were not solved due to severe disorder, as shown in Figure 2.7. Consequently, solvent molecules inside the framework were completely removed at around 240 °C under ambient pressure. To reveal the structural changes of **CPBTQ-1(MeBz)** during desolvation by heating, powder X-ray diffraction (PXRD) patterns of crystalline bulk were recorded as gradually heated upto 360 °C (Figure 2.10b). Although initial intensity of the diffraction peaks are weak due to sever disorder of solvent molecules inside voids,[38] peaks at 3.92° as well as ca. 6.8° and 7.8° gradually appeared, and grew up to 210 °C by heating. The resultant pattern is in good agreement with the original pattern of **CPBTQ-1(MeBz)**, indicating that the desolvated material retains its original framework. At higher temperature than 210 °C, however, the peaks became broader and weaker, indicating that crystallinity of the bulk was gradually lost. These results are consistent with the complicated crystal structure of **CPBTQ-1(MeBz)** containing as many as four symmetrically-independent molecules and a defective H-boned network. With these results in mind, activation of the material was accomplished by heating at 190 °C for 48 h under a vacum condition, giving the corresponding desolvated materials **CPBTQ-1a**. Complete desolvation and crystallinity of the activated materials were confirmed by ^{1}H NMR spectra of solutions dissolved in dueterated DMSO and PXRD patterns, respectively.

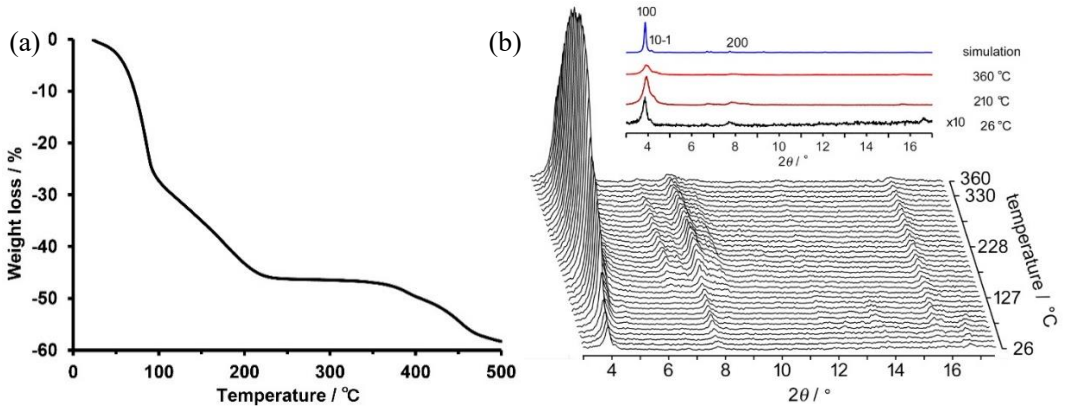

Figure 2.10 (a) TG analysis of **CPBTQ-1(MeBz)** crystalline bulk. (b) Variable temperature (VT) PXRD patterns of crystalline bulk of as-formed **CPBTQ-1**. Temperature was increased at the rate of 1 °C min^{-1}. PXRD patterns were recorded from 3° to 18° of 2θ with the scan rate of 3°min^{-1}. Therefore, each scan has a temperature gradient of 5 °C.

2-2-4. Evaluation of permanent porosity.

CPBTQ-1a shows type-I or quasi-type-I isotherms for N_2, CO_2, H_2, and O_2 sorption at low temperature. The uptakes are 125 $cm^3\ g^{-1}$ for N_2 at 101.5 kPa, 147.7 $cm^3\ g^{-1}$ for O_2 at 20.9 kPa, 135 $cm^3\ g^{-1}$ for CO_2 at 100.4 kPa, and 57.5 $cm^3\ g^{-1}$ for H_2 at 101.7 kPa. (Figure 2.11). The calculated BET surface area and pore volume based on the CO_2 sorption isotherm are 471 $m^2\ g^{-1}$ and 0.3721 $cm^3\ g^{-1}$, respectively (Figure 2.12). Pore size distribution of **CPBTQ-1a** calculated by the Non Localized Density Functional Theory (NLDFT) analysis shows two peaks at 0.7 nm and 1.1 nm (Figure 2.13), supporting the complex shape of the void channels in **CPBTQ-1a** as shown in Figure 2.6. It is noteworthy that N_2 sorption processes of **CPBTQ-1a** undertook much more slowly compared with the case of **CPHATN-1a**.[44] This result is also supported by the crystal structure of **CPBTQ-1(MeBz)** possessing narrower bottle neck of the 1D channels.

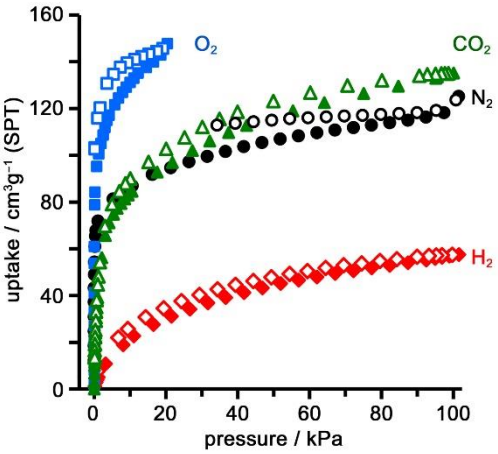

Figure 2.11 Gas sorption isotherms of **CPBTQ-1a** at low temperature. Nitrogen (black circle) at 77K, carbon dioxide (green triangle) at 195 K, oxygen (blue squre) at 77K, and hydrogen (red diamond) at 77K. Solid symbol: adsorption. Open symbol: desorption.

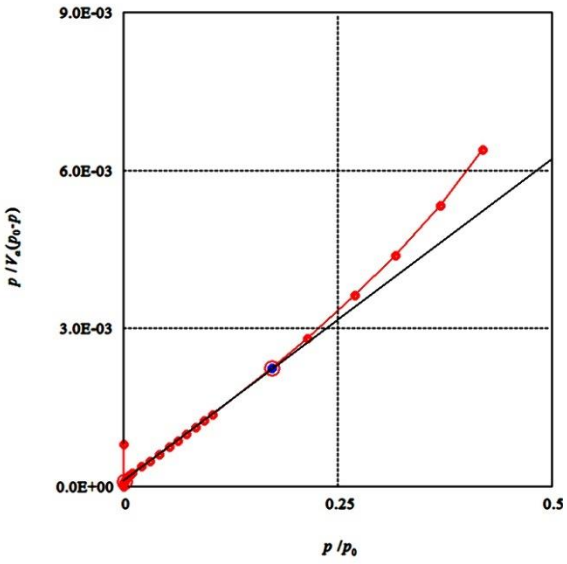

BET range limit	p/p_0 = 0.1729
Maximum V_a (p_0-p) value	7780.1
Vm [cm^3(STP) g^{-1}]	81.14
AS(BET) [m^2 g^{-1}]	471
C	109.72
Total pore volume (p/p_0=0.988) [cm^3 g^{-1}]	0.372
Averaged pore size [nm]	3.16

Figure 2.12 BET plot of **CPBTQ-1a** based on CO_2 absorption isotherm at 195 K.

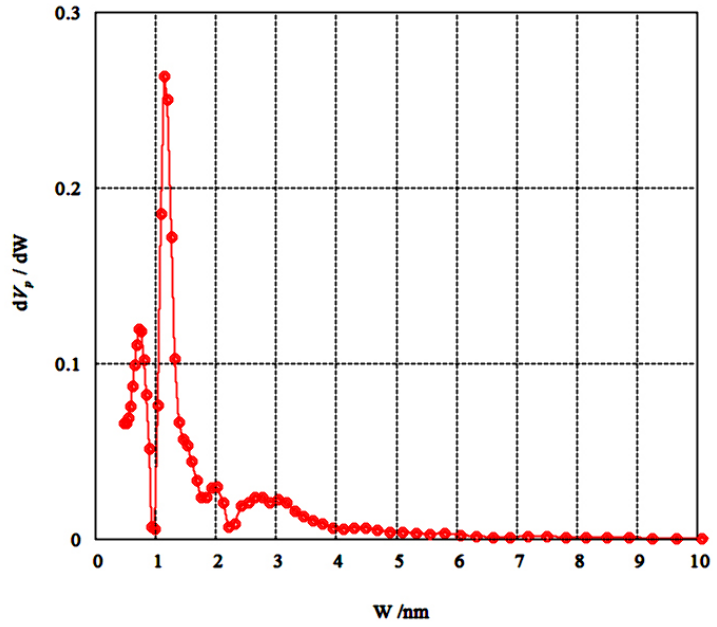

Figure 2.13 Pore size distribution of **CPBTQ-1a** calculated by the NLDFT method. The calculation was performed based on N_2 absorption isotherm at 77 K.

2-2-5. Struture durability toward common solvents.

To disclose structural durability of the frameworks toward common solvents, crystalline powder of **CPBTQ-1a** was immersed into hot solvents [chloroform (60 °C), toluene (100 °C), ethanol (60 °C), and water (100°C)] for 24 h, filtered, and subjected to PXRD measurement (Figure 2.14). The original pattern was also retained and the peak intensity was recovered after heating, except for the case of water and concentrated HCl, in which recovery of the peak intensity was prevented. These results indicate that **CPBTQ-1a** is stable toward less poloar organic solvent but is not stable suficieently toward highly polar solvents, which is in contrast to the case of **CPHATN-1a**.

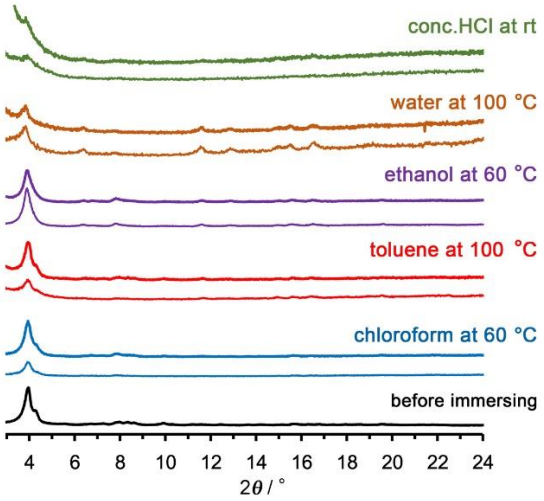

Figure 2.14 PXRD patterns of crystalline bulk of **CPBTQ-1a** before and after immersed into hot solvents and ambient conc. HCl for 24 h. Bottom lines: wet materials obtained just after filteration. Top lines: dried materials obtained after heating the filtered samples at 150 °C for 1h to remove the solvents.

2-2-6. Acid-induced Color changes.

Since **CPBTQ** has three pyrazine rings annelated to triphenylene core, the corresponding HOF **CPBTQ-1a** exhibits HCl responsivness, as in the cases of **CPHATN-1a**[43] and **CBPHAT-1a**.[47] As shown in Figure 2.15a, the yellow-brown crystalline bulks of **CPBTQ-1a** immideately turned into redish brown by adding a drop of concentrated HCl aqueous solution. In the solid-state absorption spectrum of **CPBTQ-1a** (Figure 2.15b), an absorpion shoulder at aroud 550–600 nm is observed after adding HCl. Subsequence heating of the brown bulks resulted in recovery of the original color due to removal of HCl. To obtain structural information of **CPBTQ-1a** upon exposure to HCl, PXRD patterns of the crystalline bulk were recorded before and after added a drop of conc. HCl, and after removeal of HCl by heating for 30 min at 150 °C as shown in Figure 2.15c. The PXRD patterns were once disappered by adding a HCl drop. The original pattern was then recovered slightly by heating, implying that addition of HCl to the framework may perturbe the crystal structure through rearrangement or exchanges of H-bonding. This observation is also in contrast to the case for **CPHATN-1a** with a rigid framework.

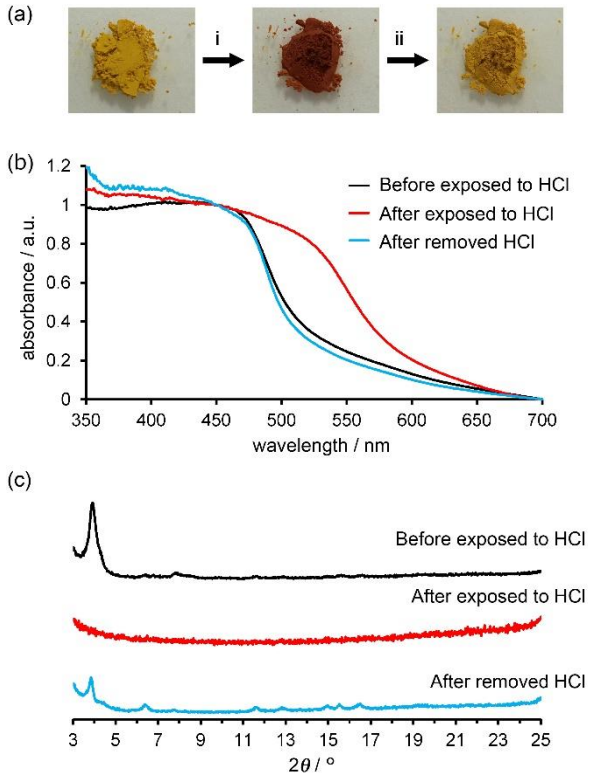

Figure 2.15 HCl responsiveness of **CPBTQ-1a**. (a) Color changes of crystalline bulk upon exposing to HCl. Conditions: (i) adding a drop of conc. HCl on the materials, (ii) heating at 150 °C for 30 min. Changes on (b) absorption spectra and (c) PXRD patterns upon exposing to HCl and subsequent removing of HCl.

2-3. Conclusion

In this study, a porous hydrogen-bonded organic framework (HOF) composed of N-hetero π-conjugated molecules (NπHOF) was constructed from a carboxyphenyl-substituted benzotriquinoxaline derivative (**CPBTQ**). The resultant solvated framework **CPBTQ-1**(**MeBz**) consists of layered 2D hexagonal network sheets, which was precisely revealed by single-crystal X-ray diffraction analysis. In comparison with a previously reported Nπ-HOF composed of the isomeric hexaazatrinaphthylene derivative (**CPHATN**) possessing pyrazine rings in different positions, the present framework has a complicated and defective H-bonded network structure. We thoroughly studied the positional effects of the pyrazine rings on the structure and revealed that the positional difference strongly affects the conformation of the

peripheral phenylene groups. The dihedral angles of the peripheral phenylene rings (ϕ) can range more widely in the case of **CPBTQ** (33.3−65.6°) than in **CPHATN** (43.7-67.6°) due to less steric hindrance at the *ortho* positions. The permanent porosity, thermal and chemical stabilities, and reversible HCl responsiveness of the activated Nπ-HOF **CPBTQ-1a** were also evaluated. We believe that the present results can contribute not only to the construction of new functional Nπ-HOFs but also to the chemistry of heteroaromatic compounds.

2-4. Experimental Section

General. All reagents and solvents were used as received from commercial suppliers. ^{1}H and ^{13}C NMR spectra were measured by JEOL 400 YH (400 MHz) spectrometer. Residual proton and carbon of deuterated solvents were used as internal standards for the measurements (for ^{1}H NMR, $CDCl_3$, δ = 7.26 ppm; DMDO-d_6, δ = 2.49 ppm: for ^{13}C NMR, $CDCl_3$, δ = 77.00 ppm; DMSO-d_6, δ = 39.50 ppm). Mass spectrum data were obtained from a autoflex III Bruker. Thermo gravimetric (TG) analysis were performed on Rigaku TG8120 under an N_2 purge (100 mL min^{-1}) at a heating rate of 5 Kmin^{-1}. Powder X-ray diffraction (PXRD) data were collected on a Rigaku Ultima-IV (40 kV, 44 mA) using graphite-monochromatized Cu-*Kα* radiation (λ = 1.54187 Å) at room temperature. A scan rate is 2.0 ° min^{-1}.

Single crystal X-ray measurement and analysis. Diffraction data of **CPBTQ-1** was collected on a CCD (MX225HE, Rayonix) with the synchrotron radiation (λ = 0.8500 Å) monochromated by the fixed exit Si (111) double crystal. The cell refinements were performed with a software CrysAlisPro.[48] SHELXT[49] was used for the structure solution of the crystals. All calculations were performed with the observed reflections [I > 2σ(I)] with the program CrystalStructure crystallographic software packages, except for refinement which was performed by SHELXL.[50] All non-hydrogen atoms were refined with anisotropic displacement parameters, and hydrogen atoms were placed in idealized positions and refined as rigid atoms with the relative

isotropic displacement parameters. SQUEEZE function equipped in the PLATON softeware[51,52] was used to remove severely disordered solvent molecules in voids.

Variable temperature (VT) PXRD measurement. Crystalline bulk of **CPBTQ-1** placed on an aluminum substrate was subjected to VT-PXRD measurement under the air atmosphere. PXRD data were collected on a Rigaku Ultima-IV using graphite-monochromatized Cu-Kα radiation (λ = 1.54056 Å) with a temperature control unit. Temperature of the sample was increased from room temperature to 633 K with a rate of 1 K/min. During temperature increasing, XRD patterns ranged from 2° to 17° was repeatedly recorded with a scan rate of 3 ° min^{-1}. Therefore, each PXRD scan has a temperature width of 5 K.

Sorption/desorption experiment. Activation of **CPBTQ-1(MeBz)** was performed under vacuum condition (0.2 kPa) for 48h at 463 K to give **CPBTQ-1a** for sorption experiments. Gas sorption measurements were performed on BELSORP-max (BEL, Japan). The adsorption isotherms of N_2, O_2, CO_2, and H_2 were corrected at 77K, 77 K, 195 K and 77 K, respectively.

Methyl ester 2. To a mixture of 2,3,6,7,10,11-hexaaminotriphenylene HCl salt[44] (747 mg, 1.39 mmol) in dry EtOH (100 mL) was added dropwise triethylamine (1.0 g). The reaction mixture was stirred for 10 min. To the reaction mixture was added benzyl derivative **1** (1.54 g, 4.72 mmol) and acetic acid (2 mL), and the mixture was stirred for 24 h under reflux condition. The dark green suspension turned into a brown one. After cooled to room temperature, the precipitate was collected by centrifuge, washed with EtOH and THF, and dried in vacuo to give **2** (1.59 g, 96%) as an orange solid. Mp. >300 °C. ^{1}H NMR (400 MHz, $CDCl_3$) δ 9.12 (s, 6H), 8.03 (d, J = 8.0 Hz, 12H), 7.65 (d, J = 8.4 Hz, 12H), 3.99 (s, 18H) ppm. ^{13}C NMR (100 MHz, $CDCl_3$) δ 166.5, 153.5, 142.6, 140.4, 131.8, 130.8, 130.0, 129.6, 124.9, 52.4 ppm. HR-MS (MALDI) *m/z* calc. for $[M]^-$ $C_{72}H_{48}N_6O_{12}$: 1188.3372; found: 1188.3330.

CPBTQ. Ester **2** (1.08 g, 0.908 mmol) and KOH (1.00 g, 17.8 mmol) in 1,4-dioxane (70 mL) and water (130 mL) was stirred for 48 h under reflux condition. The

reaction mixture was passed through a filter paper and the filtrate was acidized with 2M HCl. The resulting precipitate was corrected by centrifuge, washed with water, EtOH, and THF, and dried in vacuo to give CPBTQ (974 mg, 97%) as a dark orange solid. Mp. >300 °C. ^{1}H NMR (400 MHz, DMSO-d_6, 70 °C) δ 8.08 (s, 6H), 7.81 (d, J = 8 Hz, 12H), 7.30 (d, J = 7.6 Hz, 12H) ppm. ^{13}C NMR (100 MHz, DMSO-d_6, 25 °C) δ 166.75, 152.24, 141.75, 139.51, 134.04, 130.84, 129.77, 128.75, 124.87 ppm. HR-MS (MALDI) *m/z* calc. for $[M]^-$ $C_{66}H_{36}N_6O_{12}$: 1104.2391; found: 1104.2407.

References

1. G. J. Richards, J. P. Hill, N. K. Subbaiyan, F. D'Souza, P. A. Karr, J. Elsegood, S. J. Teat, T. Mori, K. Ariga, Pyrazinacenes: Aza Analogues of Acenes. *J. Org. Chem.* **2009**, *74*, 8914.

2. U. H. F. Bunz, N-Heteroacenes. *Chem. Eur. J.* **2009**, *15*, 6780.

3. G. J. Richards, A. Cador, S. Yamada, A. Middleton, W. A. Webre, J. Labuta, P. A. Karr, K. Ariga, F. D'Souza, S. Kahlal, J.-F. Halet, J. P. Hill, Amphiprotism-coupled near-infrared emission in extended pyrazinacenes containing seven linearly fused pyrazine units. *J. Am. Chem. Soc.* **2019**, *141*, 19570.

4. U. H. F. Bunz, Freudenberg, J. *Acc. Chem. Res*. **2019**, *52*, 1575.

5. J. L. Segura, R. Juárez, M. Ramos, C. Seoane, Hexaazatriphenylene (HAT) derivatives: from synthesis to molecular design, self-organization and device applications. *Chem. Soc. Rev.* **2015**, *44*, 6850.

6. M. Takase, V. Enkelmann, D. Sebastiani, M. Baumgarten, K. Müllen, Annularly fused hexapyrrolohexaazacoronenes: An extendedp system with multiple interior nitrogen atoms displays stable oxidation states. *Angew. Chem. Int. Ed.* **2007**, *46*, 5524.

7. K. Oki, M. Takase, S. Mori, H. Uno, Synthesis and isolation of antiaromatic expanded azacoronene via intramolecular vilsmeier-type reaction. *J. Am. Chem. Soc*. **2019**, *141*, 16255.

8. M. Saito, H. Shinokubo, H. Sakurai, Figuration of bowl-shaped π-conjugated molecules: properties and functions. *Mater. Chem. Front.* **2018**, *2*, 635.

9. H. Yokoi, Y. Hiraoka, S. Hiroto, D. Sakamaki, S. Seki, H. Shinokubo, Nitrogen-embedded buckybowl and its assembly with C_{60}. *Nat. Commun.* **2015**, *6*, 8215.

10. O. Tan, S. Higashibayashi, S. Karanjit, H. Hidehiro Sakurai, Enantioselective synthesis of a chiral nitrogen-doped buckybowl. *Nat. Commun.* **2012**, *3*, 891.

11. R. Scipioni, M. Boero, G. J. Richards, J. P. Hill, T. Ohno, T. Mori, K. Ariga, Tautomerism in reduced Pyrazinacenes. *J. Chem. Theory Comput.* **2010**, *6*, 517.

12. Z. He, R. Mao, D. Liu, Q. Miao, Highly electron-deficient hexaazapentacenes and their dihydro precursors, *Org. Lett*., **2012**, *14*, 4190.

13. J. Fleischhauer, S. Zahn, R. Beckert, U.-W. Grummt, U.-W. Birckner, H. Gçrls, A way to stable, highly emissive fluorubine dyes: Tuning the electronic properties of azaderivatives of pentacene by introducing substituted pyrazines, *Chem. Eur. J.* **2012**, 18, 4549.

14. A. N. Lakshminarayana, A. Ogn, C. Chi, Modification of acenes for n-channel OFET materials. *J. Mater. Chem. C.* **2018**, *6*, 3551.

15. B. Nie, T.-G. Zhan, T.-Y. Zhou, Z.-Y. Xian, G.-F. Jiang, X. Zhao, Self-assembly of chiral propeller-like supermolecules with unusual "sergeants-and-soldiers" and "majority-rules" effects. *Chem. Asian J.* **2014**, *9*, 754.

16. J. Li, S. Chen, P. Zhang, Z. Wang, G. Long, R. Ganguly, Y. Li, Q. Zhang, A colorimetric and fluorimetric chemodosimeter for copper ion based on the conversion of dihydropyrazine to pyrazine. *Chem. Asian J*. **2016**, *11*, 136.

17. V. J. Catalano, W. E. Larson, M. M. Olmstead, H. B. Gray, Mononuclear and binuclear palladium(II)/rhenium(I) complexes containing a sterically hindered trinucleating Ligand: 2,3,8,9,14,15-Hexamethyl-5,6,11,12,17,18-hexaazatrinaphthalene (hhtn) *Inorg. Chem*. **1994**, *33*, 4502.

18. I. M. Piglosiewicz, R. Beckhaus, W. Saak, D. Haase, Dehydroaromatization of quinoxalines: one-step syntheses of trinuclear 1,6,7,12,13,18-hexaazatrinaphthylene titanium complexes. *J. Am. Chem. Soc*. **2005**, *127*, 14190.

19. S. Roy, B. Sarkar, C. Duboc, J. Fiedler, O. Sarper, F. Lissner, S. M. Mobin, G. K. Lahiri, W. Kaim, Heterohexanuclear (Cu_3Fe_3) complexes of substituted hexaazatrinaphthylene (HATN) ligands: twofold BF_4^- association in the solid and stepwise oxidation (3e) or reduction (2e) to spectroelectrochemically characterized species. *Chem. Eur. J*. **2009**, *15*, 6932.

20. M. G. Fraser, C. A. Clark, R. Horvath, S. J. Lind, A. G. Blackman, X.-Z. Sun, M. W. George, K. C. Gordon, Complete family of mono-, bi-, and trinuclear $Re(I)(CO)_3Cl$ complexes of the bridging polypyridyl ligand 2,3,8,9,14,15-hexamethyl-5,6,11,12,17,18-hexaazatrinapthalene: syn/anti isomer separation, characterization, and photophysics. *Inorg. Chem*. **2011**, *50*, 6093.

21. X.-H. Bu, K. Biradha, T. Yamaguchi, M. Nishimura, T. Ito, K. Tanaka, M. Shionoya, A novel polymeric AgI complex consisting of two three-dimensional networks which are enantiometric and interpenetrating. *Chem. Commun*. **2000**, 1953–1954.

22. Winkler, M.; Houk, K. N., Nitrogen-rich oligoacenes: Candidates for n-channel organic semiconductors. *J. Am. Chem. Soc.* **2007**, 129, 1805.

23. M. Tadokoro, S. Yasuzuka, M. Nakamura, et al, A high-conductive crystal containing a copper (I) coordination polymer bridged by the organic acceptor TANC, *Angew. Chem. Int. Ed.*, **2006**, *45*, 5144.

24. J. Thusek, M. Hoffmann, O. Hebner, O. Tverskoy, U. H. F. Bunz, A. Dreuw, H.-J. Himmel, Low-energy electronic excitations of N-substituted heteroacene molecules: matrix isolation spectroscopy in concert with quantum-chemical calculations, *Chem. Eur. J.* **2019**, *25*, 15147.

25. J. E. Campbell, J. Yang, G. M. Day, Predicted energy–structure–function maps for the evaluation of small molecule organic semiconductors. *J. Mater. Chem. C* **2017**, 5, 7574.

26. H.-Y. Chen, I. Chao, Toward the rational design of functionalized pentacenes: reduction of the impact of functionalization on the reorganization energy. *ChemPhysChem* **2006**, *7*, 2003.

27. Isoda, K.; Matsuzaka, M.; Sugaya, T.; Yasuda, T.; Tadokoro, M., Synthesis and electrochromic behavior of a multi-electron redox-active N-heteroheptacenequinone. *Org. Biomol. Chem.* **2019**, *17*, 7884.

28. I. Georgiou, S. Kervyn, A. Rossignon, F. De Leo, J. Wouters, G. Bruylants, D. Bonifazi, Versatile self-adapting boronic acids for H-bond recognition: from discrete to polymeric supramolecules. *J. Am. Chem. Soc.* **2017**, *139*, 2710.

29. J. Lu, R. Cao, Porous organic molecular frameworks with extrinsic porosity: a platform for carbon storage and separation. *Angew. Chem. Int. Ed.* **2016**, *55*, 9474.

30. A. I. Cooper, Porous molecular solids and liquids. *ACS Cent. Sci*. **2017**, *3*, 544.

31. Y.-F. Han, Y.-X. Yuan, H.-B. Wang, Porous hydrogen-bonded organic frameworks. *Molecules* **2017**, *22*, 266.

32. J. Luo, J.-W. Wang, J.-H. Zhang, S. Lai, D.-C. Zhong, Hydrogen-bonded organic frameworks: design, structures and potential applications. *CrystEngComm* **2018**, *20*, 5884.

33. R.-B. Lin, Y. He, P. Ki, H. Wang, W. Zhou, B. Chen, Multifunctional porous hydrogen-bonded organic framework materials. *Chem. Soc Rev.* **2019**, *48*, 1362.

34. I. Hisaki, X. Chen, K. Takahashi, T. Nakamura, Designing hydrogen-bonded organic frameworks (HOFs) with permanent porosity. *Angew. Chem. Int. Ed*. **2019**, *58*, 11160.

35. Positional effects of the carboxy groups on frameworks are studied, see; a) T. Takeda, M. Ozawa, T. Akutagawa, Jumping crystal of a hydrogen-bonded organic framework induced by the collective molecular motion of a twisted π system. *Angew. Chem. Int. Ed.* **2019**, *58*, 10345. b) T. Takeda, M. Ozawa, T. Akutagawa,

Versatile hydrogen-bonded assemblies of twisted tetra[3,4]thienylene tetracarboxylic acid with Selective solvent sorption. *Cryst. Growth Des.* **2019**, *19*, 4784.

36. I. Hisaki, S. Nakagawa, N. Tohnai, M. Miyata, A C_3-symmetric macrocycle-based, hydrogen-bonded, multiporous hexagonal network as a motif of porous molecular crystals. *Angew. Chem. Int. Ed.* **2015**, *54*, 3008.

37. I. Hisaki, N. Ikenaka, N. Tohnai, M. Miyata, Polymorphs of layered assemblies of hydrogen-bonded hexagonal networks caused by conforma-tional frustration. *Chem. Commun*. **2016**, *52*, 300.

38. I. Hisaki, S. Nakagawa, N. Ikenaka, Y. Imamura, et al, A series of layered assemblies of hydrogen-bonded, hexagonal networks of C_3-symmetric π-conjugated molecules: a potential motif of porous organic materials. *J. Am. Chem. Soc*. **2016**, *138*, 6617.

39. W. Yang, W. Zhou, B. A. Chen, flexible microporous hydrogen-bonded organic framework. *Cryst. Growth Des*. 2019, *19*, 5184.

40. X. Zhang, L. Li, J.-X. Wang, H.-M. Wen, R. Krishna, H. Wu, W. Zhou, Z.-N. Chen, B. Li, G. Qian, B. Chen, Selective ethane/ ethylene separation in a robust microporous hydrogen-bonded organic framework. J. Am. Chem. Soc. 2020, 142, 633.

41. I. Hisaki, N. Ikenaka, E. Gomez, B. Cohen, N. Tohnai, A. Douhal, Hexaazatriphenylene-based hydrogen-bonded organic framework with permanent porosity and single-crystallinity. *Chem. Eur. J.* **2017**, *23*, 11611.

42. I. Hisaki, Y. Suzuki, E. Gomez, B. Cohen, N. Tohnai, A. Douhal, Docking strategy to construct thermostable, single-crystalline, hydrogen-bonded organic framework with high surface area. *Angew. Chem. Int. Ed*. **2018**, *57*, 12650.

43. I. Hisaki, Y. Suzuki, E. Gomez, Q. Ji, N. Tohnai, T. Nakamura, A. Douhal, Acid Responsive Hydrogen-bonded Organic Framework. *J. Am. Chem. Soc*. **2019**, *141*, 2111.

44. A. Lebkücher, C. Wagner, O. Hübner, E. Kaifer, H.-J. Himmel, Trinuclear complexes and coordination polymers of redox-active guanidino-functionalized aromatic (GFA) Compounds with a triphenylene core. *Inorg. Chem.* **2014**, *53*, 9876.

45. I. J. Bruno, J. C. Cole, M. Kessler, J. Luo,et al, Retrieval of crystallographically-derived molecular geometry information. *J. Chem. Inf. Comput. Sci*., **2004**, *44*, 2133.

46. S. J. Cottrell, T. S. G. Olsson, R. Taylor, J. C. Cole, J. W. Liebeschuetz, Validating and understanding ring conformations using small molecule crystallographic data. *J. Chem. Inf. Model*. **2012**, *52*, 956.

47. E. Gomez, Y. Suzuki, I. Hisaki, M. Moreno, Douhal, A. Spectroscopy and dynamics of a HOF and its molecular units: remarkable vapors acid sensing. *J. Chem. Mater. C* **2019**, 7, 10818.

48. Rigaku Oxford Diffraction (2015), Software CrysAlisPro 1.171.38.41o. Rigaku Corporation, Tokyo, Japan.

49. G. M. Sheldrick, *Acta Crystallogr. A* **2015**, *71*, 3.

50. G. M. Sheldrick, *Acta Crystallogr. Sect. C* **2015**, *71*, 3.

51. P. van der Sluis, Spek, A. L. *Acta Crystallogr. Sect. A* **1990**, *46*, 194.

52. A. L. Spek, *Acta Crystallogr. Sect. D* **2009**, *65*, 148.

Chapter 3

A Hydrogen-Bonded Organic Framework Based on Pyrazinopyrazine

Abstract

Hydrogen-bonded organic frameworks (HOFs) composed of highly N-content π-conjugated molecules are expected to show multi-functionality. In this chapter, I studied on a hydrogen-bonded framework based on pyradinopyradine (PP), which is one of the simplest and the most essential structural motifs of highly N-content polycyclic aromatic hydrocarbons. Herein, I describe synthesis of a PP-based building block molecule with four carboxyphenyl groups (**CP-PP**), spectroscopic and electronic properties of **CP-PP** and its ester precursor, structures of **CP-PP** based HOFs, and thermal behaviors of the HOFs. Interestingly, the initial framework with H-bonded rhombic 2D network rapidly undergoes three step structural transformation into other frameworks, including a semi-opening framework with small void, through rearrangement of H-bonds. These results contribute to solid-state chemistry on porous molecular crystalline materials.

3-1. Introduction

Nitrogen-containing polycyclic aromatic hydrocarbons (N-PAHs) have attracted significant attention as they have valuable characteristics including good electron acceptors, increased stability, luminescent properties, and attractive interactions with cationic species such as proton and metal ions. In particular, the introduction of pyrazine into π-conjugated systems is a typical way of modifying and enhancing the useful properties, where pyrazine acts as the electron withdrawing part to induce intramolecular charge transfer[1,2]. Pyrazinopyrazine (PP) is one of the simplest and the most essential umits of highly N-content acene (Chart 3.1a). Expanded and highly-expanded heteracene possessing PP units were investigated for long time in terms of electronic properties tuning[3-7] and sensing or complexation with cationic species.[8-12] For example, Pyradinoquinoxaline was reported by Armand and coworkers to be formed a redox system in the aqueous organic medium.[13] Tadokoro, Isoda, and coworkers reported that tetraazatetracene (TANC) and tetraazapentacene (BTANC) show electron acceptors functioning as novel *n*-type semiconductors with weaker FET

activity.[14] Bonifazi and coworkers also constructed solid-state supramolecular structures based on TANC and boronic acids through strong H-bonding.[15] Richards and coworkers reported dipyrazinopyrazine indicate it is expected to be good candidates as materials for organic thin film transistors due to the substantial electron deficiency.[16] Bunz and coworkers systematically synthesized pyrazinodiquixaline derivative and its analogues to reveal nitrogen atoms introduced into the acene skeleton give persistent disubstituted heteropentacenes, which are stable even when stored for longer periods of time.[17] More recently, Gary J. Richards successfully synthesized and characterized highly N-content acene analogues tetradecaazadihydroheptacene (N_{14}Hp).[18] However, HOFs based on highly N-content heteroacene possessing annelated-pyrazine units have not been developed yet, and therefore, we have been interested in constructing pyrazinebased HOFs with permanent porosity.

HOFs are porous molecular crystalline materials, in which molecules are connected through well-designed directional hydrogen bonding, allowing high crystallinity, programmed self-assembly, and reusability. Because of their attractive features such as high crystallinity, flexibility, and easy recrystallization process to obtain, various HOFs have been constructed and investigated as a new class of porous frameworks,[19-23] suitable not only for the storage and separation of gas and organic molecules, but for organic electronic devices and sensors.[24-28] Particularly, pyrazine-based HOFs are expected to show multi-functionality. Annelation of pyrazine ring to π-conjugated cores can fine-tune frontier orbital levels, which enables to control optoelectronic properties of the frameworks. Furthermore, incorporated N atoms can interact and/or coordinate with cations species such as metal cations and proton to achieve external stimuli-responsive frameworks. Indeed, we previously reported that HOFs based on hexaazatrinaphthylene derivatives with carboxyphenyl groups show HCl responsiveness by changing color from yellow to redish-brown and by quenching fluorescence.[29,30]

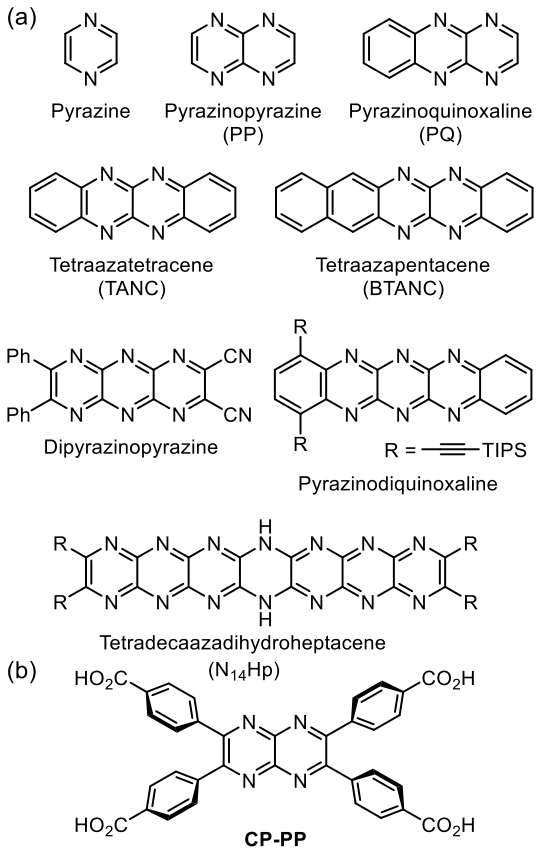

Chart 3.1. (a) Examples of heteroacenes composed of annelated pyrazinopyrazine. (b) Building block molecule **CP-PP** composed of PP core and carboxyphenyl groups.

In this chapter, I designed a 2D-networked HOF (**CP-PP-1**) built on a carboxyphenyl-substituted pyrazinopyraine derivative as a building block, as shown in Chart 1b. It is surprising that no HOF based on PP has reported so far, although PP is one of the most essential structural motif of N-hetero acenes. Synthesis and spectroscopy of **CP-PP** and its ester precursor and crystal structures, thermal behavior, and porosity evaluation of HOFs composed of **CP-PP** are presented. Interestingly, solvent included as-formed HOF **CP-PP-1** changes the framework to **CP-PP-2** upon solvent release. In more details, the initial rhombic 2D network rapidly undergoes three step structural transformation by rearrangement of H-bonds into other frameworks including **CP-PP-2**. These behaviors are in contrast to previously reported HOFs composed of *C*3-symmetric molecules.[31] The present study provides insight to design new functional Nπ-HOFs and contribute to solid-state chemistry on porous molecular crystalline materials.

3-2. Results and Discussion

3-2-1. Synthesis and spectroscopy

CP-PP was synthesized as shown in Scheme 3.1. 1,2,5-Thiadiazole-3,4-diamine (**1**) and dimethyl 4,4'-oxalyldibenzoate (**2**) were synthesized according to literatures.[32,33] Condensation reaction of **1** and **2** gave thidiazolopyrazine derivative **3**, which were subsequently reduced by $SnCl_2$ and HCl to yield pyrazinediamine derivative **4**. Condensation reaction of **4** and **2**, followed by hydrolysis of the resultant pyrazinopyrazine derivative **5** gave **CP-PP**. Pyrazinopyrazine derivatives **5** and **CP-PP** were fully characterized by ^1H and ^{13}C NMR spectroscopy and HR-MS (see, Experimental Section).

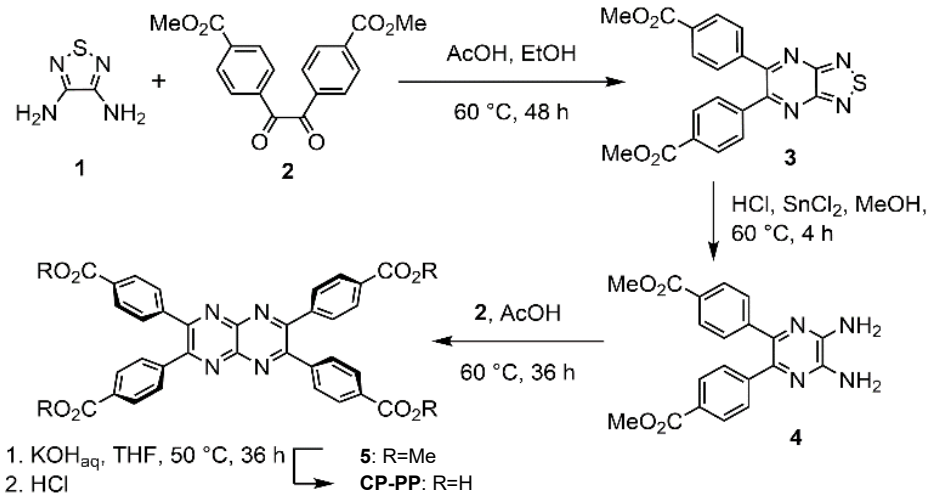

Scheme 3.1 Synthesis of **CP-PP**.

The optical properties of ester derivative **5** and **CP-PP** in solution are investigated by employing UV-vis absorption and steady-state fluorescence spectroscopy (Figure 3.1). The absorption spectrum of ester derivative **5** in $CHCl_3$ shows the absorption maxima at 402 nm. And the UV-vis spectrum of **CP-PP** in DMSO exhibits the maximum absorption prominent peaks at 405 nm. While the distinguish absorption band centered at 402 nm (broad absorption band from 350 nm tailing to 470 nm) can be ascribed as n-π^* transition coming from nitrogen-containing inside the aromatic domains. Photoluminescence spectra of ester derivative **5** excited at 400 nm, has a

broaden band at 518 nm, while that of **CP-PP** does relatively sharp band at 465 nm together with a shoulder at ca. 520 nm. The observed prominent difference in the wavelength is presumably caused by formation of molecular aggregation in a $CHCl_3$ solution of **5** even at a concentration of 5.0×10^{-5} M, which can be supported by the solid-state fluorescence spectrum of **CP-PP-1(DCB)** that shows band at the similar wavelength at 539 nm.

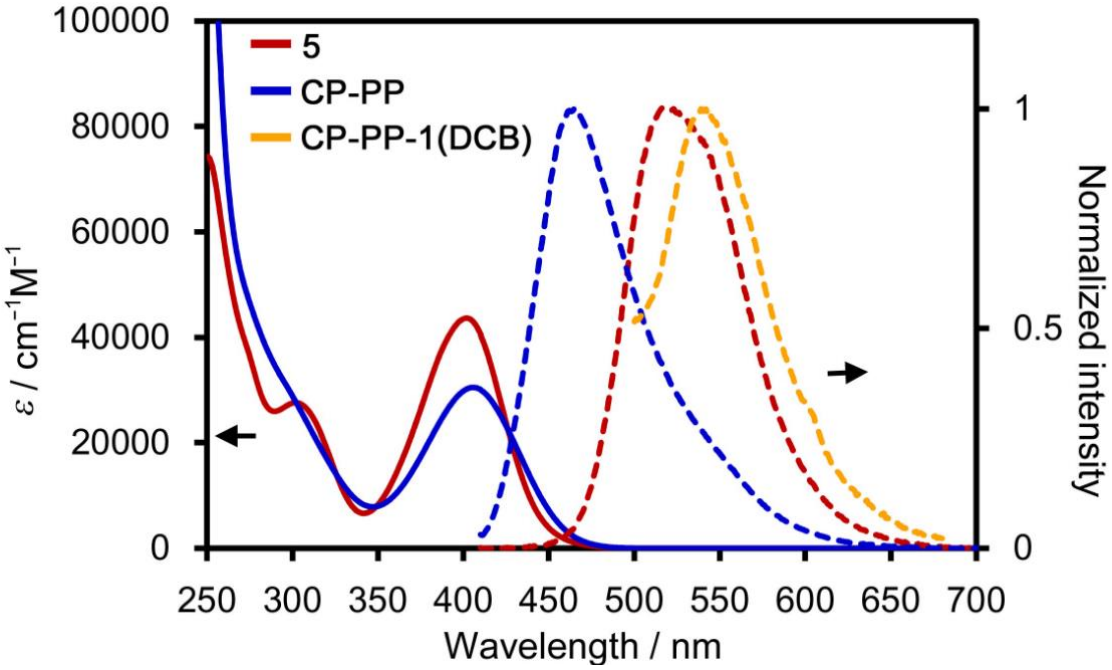

Figure 3.1 UV-vis absorption and fluorescence emission spectra of **CP-PP** (blue) and its methyl ester derivative **5** (red) in a solution of DMSO and $CHCl_3$ at a concentration of 5.0×10^{-5} M, respectively, together with solid state fluorescence spectrum of **CP-PP-1(DCB)** (orange).

The redox properties of ester derivative **5** were evaluated by cyclic voltammetry in CH_2Cl_2 solutions of 0.1 M Bu_4NBF_4. The cyclic voltammogram of **5** shows two reversible redox peaks in the negative region (Figure 3.2). Two consecutive peaks due to two-step two-electron reduction waves at $E_{1/2}^1 = -0.75$ eV and $E_{1/2}^2 = -1.40$ eV versus SCE were observed, indicating the formation of the radical anion and dianion for the PP moiety. These reduction potentials are slightly higher compared with the pristine PP because of the peripheral four methoxycarbonylphenyl groups,[35] while are much lower compared with TANC because of no benzene rings annelated to the PP core.[14] A comparison of the calculated highest occupied molecular orbital (HOMO) and

lowest unoccupied molecular orbital (LUMO) levels of **CP-PP** with the electronic properties of **5** and its naphthalene analogue is shown in Figure 3.3. The calculation was performed by DFT at the B3LYP/6-31(d) level, which is typical calculation method. And the DFT calculations revealed that the LUMO was dependent only upon the core framework. LUMO level of **CP-PP** is lower than that of the naphthalene analogue, whereas the LUMO level is almost the same between **CP-PP** and its methyl ester derivative.

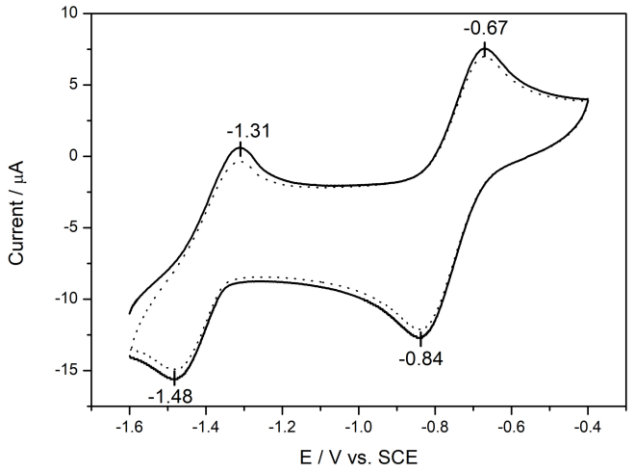

Figure 3.2 Cyclic voltammograms of **5** at 297 K in CH_2Cl_2 containing 0.1 M Bu_4NBF_4 as a supporting electrolyte (scan rate 0.5 V s^{-1}, Pt electrodes). The second cycles are shown by dashed lines.

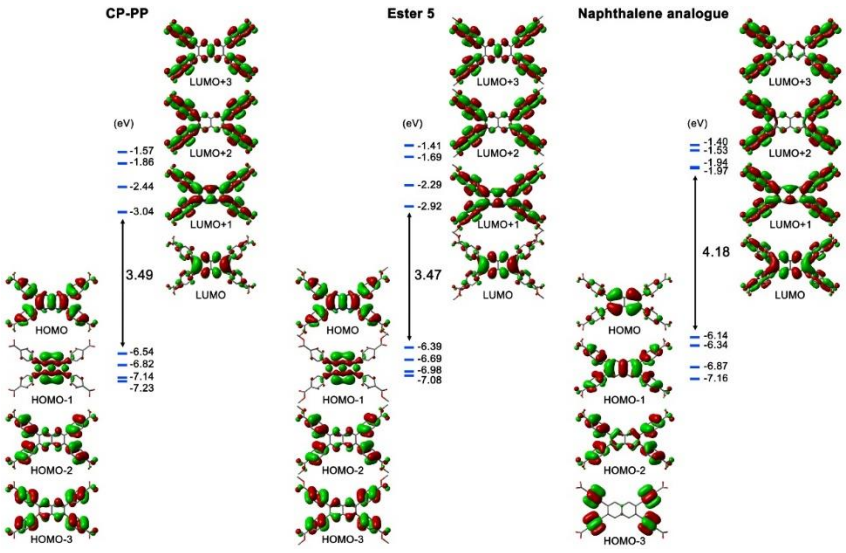

Figure 3.3 Selected molecular orbitals and energy levels of **CP-PP**, Ester **5** and Naphthalene

analogue calculated at the B3LYP/6-31G(d) level of theory.

3-2-2. Crystallography

The crystallization of **CP-PP** was conducted by slow evaporation of a mixed solution of *N*,*N*-dimethylformide (DMF) and *ortho*-dichlorobenzene (DCB) at 80 °C for 3 days to yield solvated HOF **CP-PP-1(DCB)** as needle-shaped orange crystals. The crystallization was also conducted under the same condition except for use of 1,2,4-trichlorobenzene (TCB) instead of DCB, resulting concomitant formation of two kinds of crystals, (1) rhombic framework **CP-PP-1(TCB)** and (2) semi-opening framework with smaller void **CP-PP-2(TCB)**. (Table 3.1)

Table 3.1 Crystal data of the obtained frameworks.

Identification code	**CP-PP-1 (DCB)**	**CP-PP-1 (TCB)**	**CP-PP-2 (TCB)**	**CP-PP-3(TCB)**
Empirical formula	$C_{34}H_{20}N_4$. $3(C_6H_4Cl_2)$	$C_{52}H_{24}Cl_9N_4O_8$	$C_{40}H_{23}Cl_3N_4O_8$	$C_{34}H_{24}N_4O_{10}$
Formula weight	1053.52	1150.91	793.97	648.57
Temperature/K	223	223	223	223
Crystal system	Triclinic	Triclinic	Triclinic	Triclinic
Space group	*P*-1	*P*-1	*P*-1	*P*-1
a (Å)	6.3370(3)	11.6824(3)	6.0673(4)	6.2470(2)
b (Å)	11.2577(5)	12.8824(3)	12.0949(11)	11.7392(4)
c (Å)	17.7097(8)	18.6905(3)	12.3301(7)	11.9977(3)
α (°)	74.135(4)	103.6816(15)	85.133(6)	89.645(3)
β (°)	80.270(4)	101.8187(17)	79.388(5)	84.404(2)
γ (°)	78.129(4)	108.764(2)	78.290(6)	78.070(2)
Z	1	2	1	1
V (Å^3)	1180.73(10)	2464.21(9)	869.78(11)	856.65(5)
ρ_{calc} / g cm^{-3}	1.482	1.551	1.516	1.257
μ / mm^{-1}	3.833	5.180	2.927	0.794
F(000)	538.0	1161	406	336
Crystal size/mm^3	0.038×0.061×0.049	0.177×0.113×0.059	0.234×0.066×0.057	0.192×0.039×0.031
Radiation	1.54184	1.54184	1.54184	1.54184
2θ max /°	67.495	74.23	69.618	72.757
Goodness-of-	1.060	1.181	1.025	1.063

fit on F^2				
Final R indexes [I>=2σ (I)]	R_1 = 0.0712, wR_2 = 0.2157	R_1 = 0.1091, wR_2 = 0.3305	R_1 = 0.0608, wR_2 = 0.1901	R_1 = 0.0515, wR_2 = 0.1610
CCDC Nos.	2078212	2080626	2080627	2080628

CP-PP-1(DCB) belongs to the triclinic system with space group *P*-1 (Figure 3.4). The molecule of **CP-PP** has an inversion center (C_i). The twisted angle of the two kinds of phenylene group and the PP core are 21.2° and 55.9°. The peripheral carboxy groups of **CP-PP** forms a dimer through self-complementary H-bonding with O•••O distance of 2.620–2.622 Å to give a rhombic networked structure. A rhombic void has a dimension of 18.1 Å × 30.3 Å. The adjacent layers are overlapped due to π-π stacking interactions between the PP and the phenylene group with the dihedral angle of 21.2° and between the phenylene group and the carboxy dimer. The rhombic networked sheets are stacked in an inclined AA pattern, with an interplanar distance of 3.36 Å. In addition to the π/π stacking, interlayer C–H•••N interactions between the nitrogen atom of PP and the aromatic hydrogen atom of the phenylene group form a dihedral angle of 55.9°.

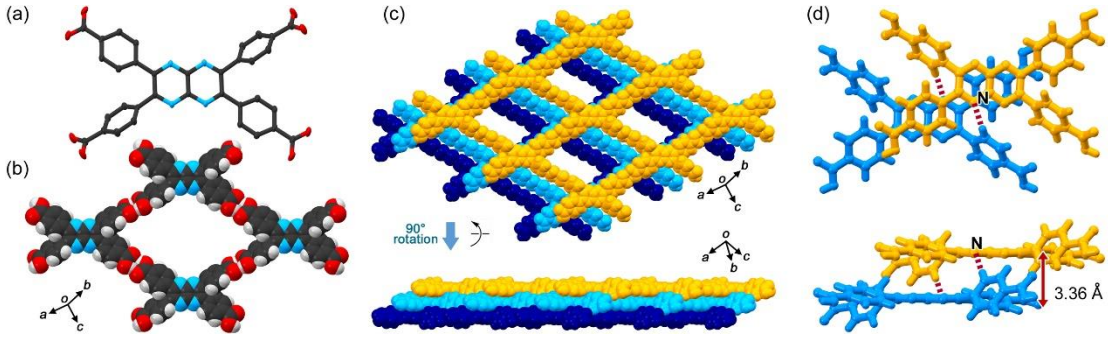

Figure 3. Crystal structure of **CP-PP-1(DCB)**: (a) Molecular structure drawn with anisotropic displacement ellipsoids with 50% provability. (b) Hydrogen-bonded network motif composed of four molecules. (c) Selected layered structure stacked with an inclined AA pattern. (d) Orientation of two adjacent molecules.

CP-PP-1(TCB) also belongs to triclinic system with space group *P*-1. The crystal structure is shown in Figure 3.5a. The framework is closely similar with that of **CP-PP-1(DCB)**, except for subtle structural differences such as lower molecule symmetry

with no symmetric center. The twisted angle of four phenylene groups and the PP core are 59.8°, 23.1°, 18.6°, and 59.8°. The peripheral carboxy groups of **CP-PP** forms a dimer through self-complementary H-bonding with O•••O distance of 2.609–2.624 Å to give a rhombic networked structure (Figure 3.5b). The adjacent rhombic networked sheets are stacked in an inclined AA pattern (Figure 3.5c), with an interplanar distance of 3.42 Å (Figure 3.5d).

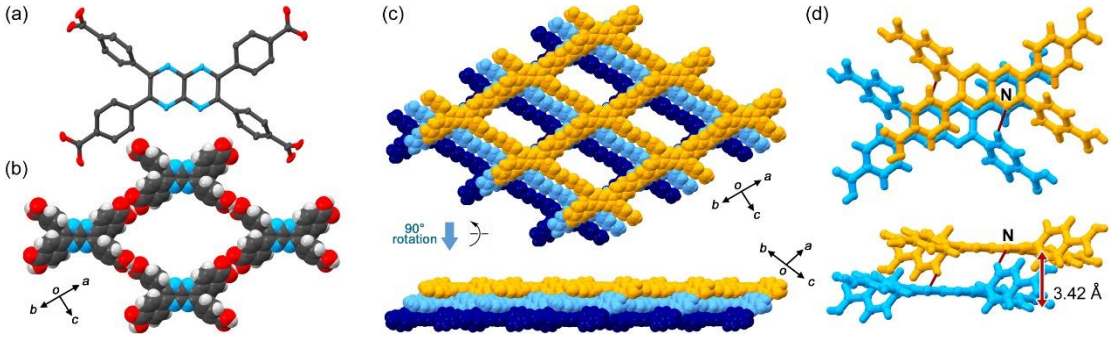

Figure 3.5 Crystal structure of **CP-PP-1(TCB)**: (a) Molecular structure drawn with anisotropic displacement ellipsoids with 50% provability. (b) Hydrogen-bonded network motif composed of four molecules. (c) Selected layered structure stacked with an inclined AA pattern. (d) Orientation of two adjacent molecules. The crystal structure is closely similar with that of **CP-PP-1(DCB)**, while subtle differences such as symmetry of the molecule of CP-PP, the dihedral angle between the PP core and peripheral phenylene rings, N•••C-H interactions are observed.

It is noteworthy that solvent molecules (i.e. DCB and TCB) have different alignments in the channels of **CP-PP-1(DCB)** and **CP-PP-1(TCB)** crystals. In the case of **CP-PP-1(DCB)**, one dimensional (1D) channels are formed along the *a* axis, in which DCB molecules align in three lines with herring-bone arrangements with a host-guest ratio of 1 : 3 (Figure 3.6a). The neighboring DCB molecules contact with a dihedral angle of 45.8° in the channel. Interactions between the DCB molecule and CP-PP framework are (i) Cl•••π interaction between Cl atom of DCB and carboxy part (ii) C–H•••N interactions between the nitrogen atom of PP and the aromatic hydrogen atom of DCB and (iii) C–H•••π interactions (Figure 3.6b).

In the case of **CP-PP-1(TCB)**, One dimensional channels are formed along the *a* axis, in which TCB molecules align in two lines with slip-stacked columnar arrangements with a host-guest ratio of 1 : 3 (Figure 3.6c). Each column is composed of crystallographically independent three kinds of TCB molecules with interplanar distances of ca. 3.5–3.6 Å. Interactions between the TCB molecule and CP-PP framework are (i) Cl•••N interactions between the chlorine atoms and nitrogen atom of PP, (ii) Cl•••π interactions between the chlorine atoms and the peripheral phenylene ring, and (iii) Cl•••π interactions between the chlorine atoms and the carboxy part (Figure 3.6d).

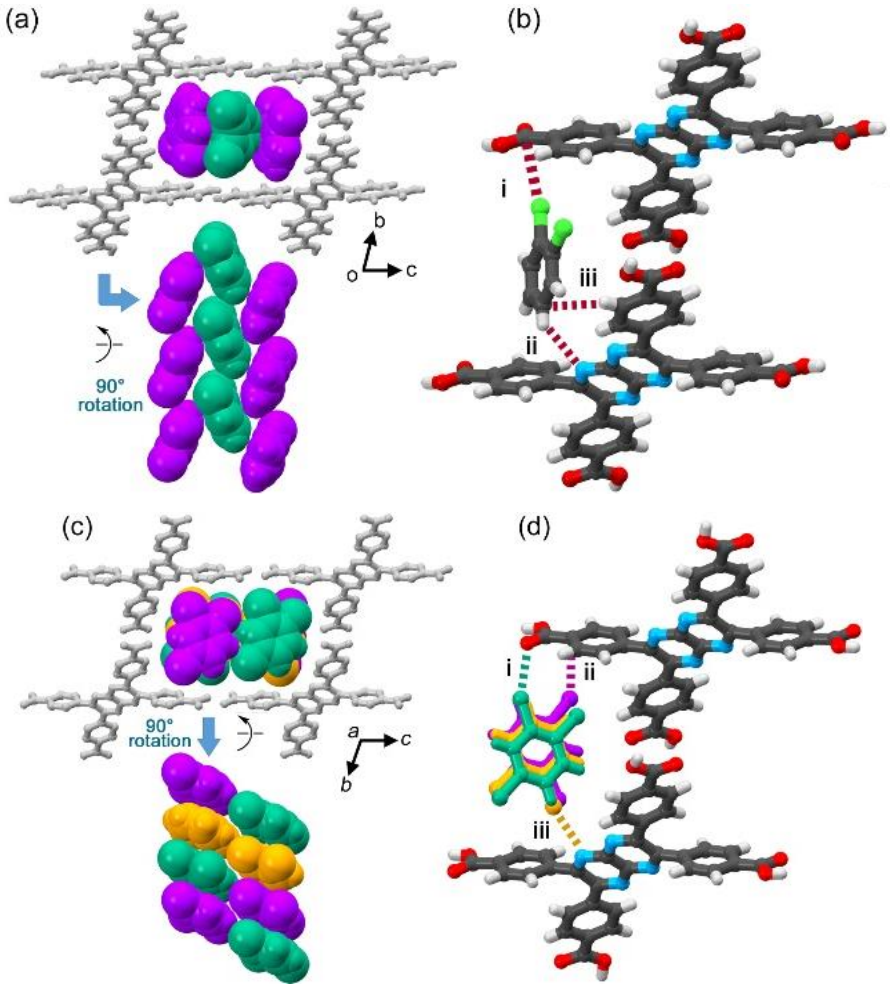

Figure. 3.6 Solvent molecules inside the channels of (a,b) **CP-PP-1(DCB)** and (c,d) **CP-PP-1(TCB)**. (a) Packed DCB molecules in **CP-PP-1(DCB)**, where molecules colored light green are located at the inversion centers, and therefore, disordered in two positions, one of which are omitted for clarity. (b) Intermolecular interactions between the DCB molecule and the framework: i) Cl•••π,

ii) C–H•••N, and iii) C–H•••π interactions. (c) Packed TCB molecules in **CP-PP-1(TCB)**, where crystallographically independent three molecules are colored by purple, orange, and green. (d) Intermolecular interactions between the TCB molecules and the framework: i) Cl•••π, ii) Cl•••π, and iii) Cl•••N interactions.

A crystal structure of **CP-PP-2(TCB)** is shown in Figure 3.7. The molecule has a *C*i-symmetric center and the twisted angles of the peripheral phenylene group and the PP core are 21.8° and 59.3°. **CP-PP** crystallized into space group *P*-1. The resultant framework is completely different from that of **CP-PP-1(TCB)** and **CP-PP-1(DCB)**. Two of four carboxy groups of **CP-PP** with the smaller twisted angle form a dimer through self-complementary H-bonding with O•••O distance of 2.63 Å to yield one-dimensional network. The other two carboxy groups with the larger twisted angle, on the other hand, form intermolecular H-bonds with the nitrogen atom of PP core with O•••N distance of 2.94 Å. The resultant squire voids have dimension of 15.2 Å × 10.6 Å smaller than that of **PP-1(TCB)** and **CP-PP-1(DCB)**. The void accommodates TCB molecules with a 1 : 1 host/guest ratio though Cl•••O and Cl•••π interactions.

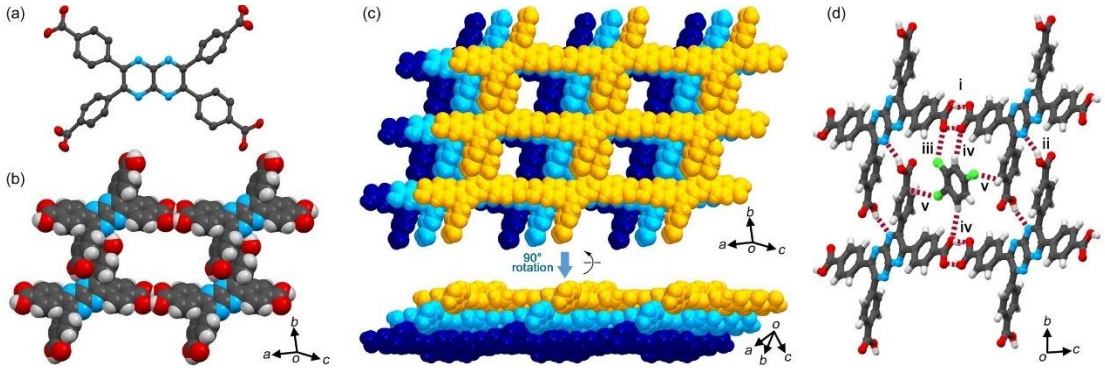

Figure 3.7 Crystal structure of **CP-PP-2(TCB)** possessing semi-opening framework. (a) Molecular structure drawn with anisotropic displacement ellipsoids with 50% provability. (b) Hydrogen-bonded network motif composed of four molecules. (c) Selected layered structure stacked with an inclined AA pattern. (d) Intermolecular interactions among the frameworks and a TCB molecule: i) typical H-bonded dimer, ii) H-bond between carboxy and pyrazine groups, iii) Cl•••O, iv) C–H•••O, and v) Cl•••π interactions.

Structural comparison among the rhombic frameworks [i.g. **CP-PP-1(DCB)** and **CP-PP-1(TCB)**], and the semi-opening framework [i.g. **CP-PP-2(TCB)**] discloses that both frameworks have the common network motif (Figure 3.8). In the motif, **CP-PP** forms self-complementary H-bonds between the diagonal peripheral carboxyphenyl groups with the smaller twisted angle to give a 1D ribbon. The ribbon is slip-stacked to give a sheet. In the case of framework **CP-PP-1**, the sheet is connected by another self-complementary H-bonds between the carboxyphenyl groups. In the case of framework **CP-PP-2**, the sheet is connected by hetero H-bonds between the carboxy group and the N atom of the PP core.

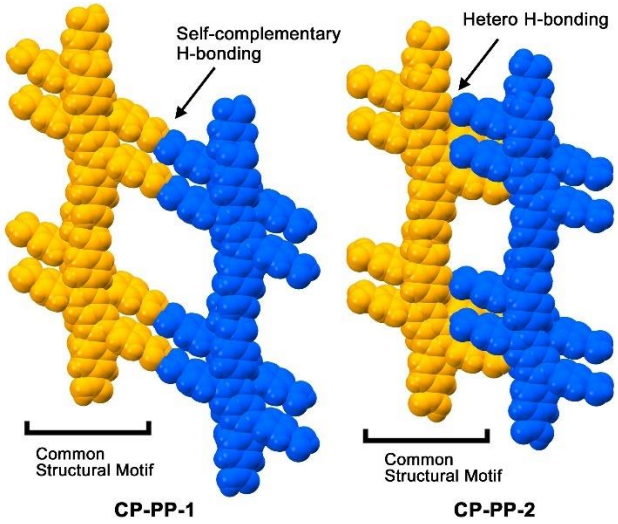

Figure 3.8 Structural comparison between the framework **CP-PP-1(DCB)** and **CP-PP-2(TCB)**.

3-2-2. Thermal analysis

Since a pure crystalline bulk of either **CP-PP-1(TCB)** or **CP-PP-2(TCB)** were not obtained despite great effort, we performed property evaluation only for a bulk sample of **CP-PP-1(DCB)** as shown in the latter part. In order to investigate thermal behavior of the framework, crystalline bulk of as-formed **CP-PP-1(DCB)** was subjected to thermogravimetric (TG) analysis (Figure 3.9a). TG curve indicates that molecules of DCB are released in two steps. In the first step up to 125 °C, two third of DCB molecules are released. In the second step up to 253 °C, the other DCB molecules are released. Total weight loss of 41.1% corresponds to the host/guest ratio of 1 : 3,

which consists of crystallographic results. Further heating leads to weight loss beyond 400 °C, which indicates the onset of decomposition. In order to obtain more information about the structural changes of **CP-PP-1(DCB)** upon heating, variable temperature powder X-ray diffraction (VT-PXRD) patterns were recorded on as-formed crystalline bulks from room temperature to 327 °C (Figure 3.9b). The initial patterns are quickly decayed up to 60 °C and new peaks, such as that at $2\theta = 7.3°$ appears and the intensity of the peaks gradually increased up to ca. 150 °C, indicating structural transition into the second phase. The PXRD pattern of the second phase slightly shifted into the wide angle region in the range of 150–170 °C, indicating subtle structural changes to give the third phase. The third phase then undertakes further structural changes at around 300 °C to give the fourth phase. The observed changes on PXRD patterns are in consistent with the results of TG analysis.

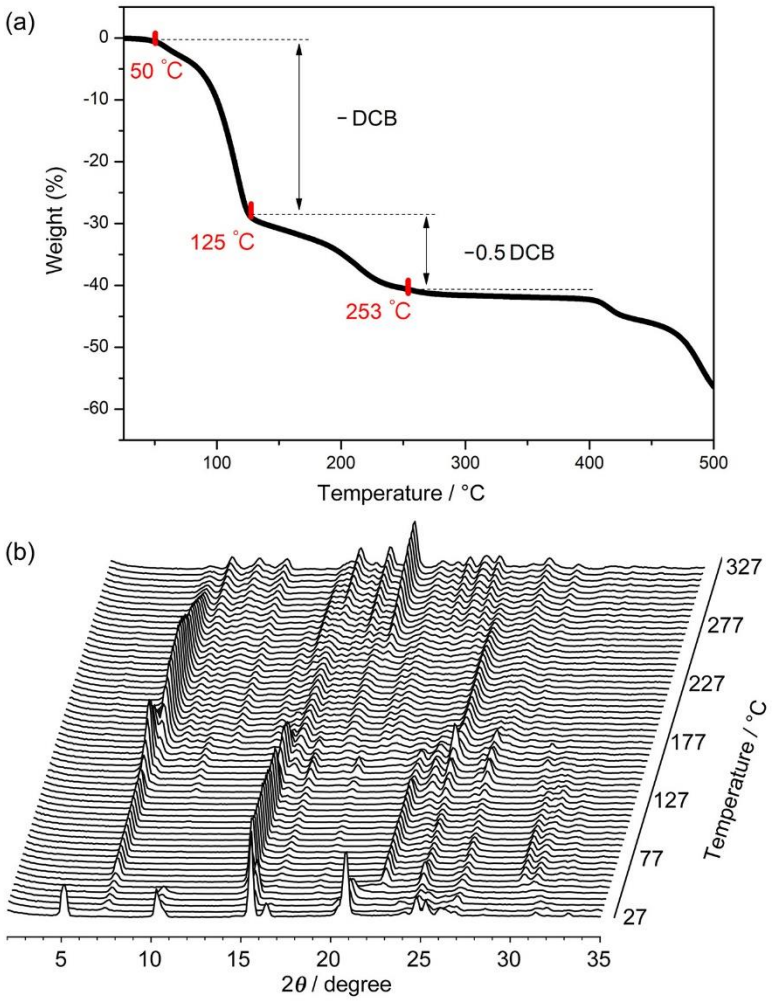

Figure 3.9 Thermal analyses of as-formed **CP-PP-1(DCB)**. (a) TG curve. (b) VT-PXRD patterns.

Several PXRD patterns characteristic for each phases are shown in Figure 3.10, together with the simulated patterns of **CP-PP-1(DBC)** with the rhombic framework and **CP-PP-2(TCB)** with the semi-opening framework. The initial pattern of **CP-PP-1(DBC)** is in good agreement with the simulated pattern of **CP-PP-1(DBC)** at room temperature. At 42 °C, a new peak at 7.3° appears, indicating that the part of the original framework began to change as solvent molecules were lost. Interestingly, the pattern at 142 °C, which is typical for the second phase, is almost matches the simulated pattern of **CP-PP-2(TBC)**, indicating that the semi-opening framework similar to the structure of **CP-PP-2(TBC)** was formed by removal of the two third of solvent molecules. The pattern at 242 °C, typical for the third phase, has the similar profile with the second phase, indicating the similar structure with slightly shorten crystallographic periodicity. The peaks for the fourth phase became more numerous and complex.

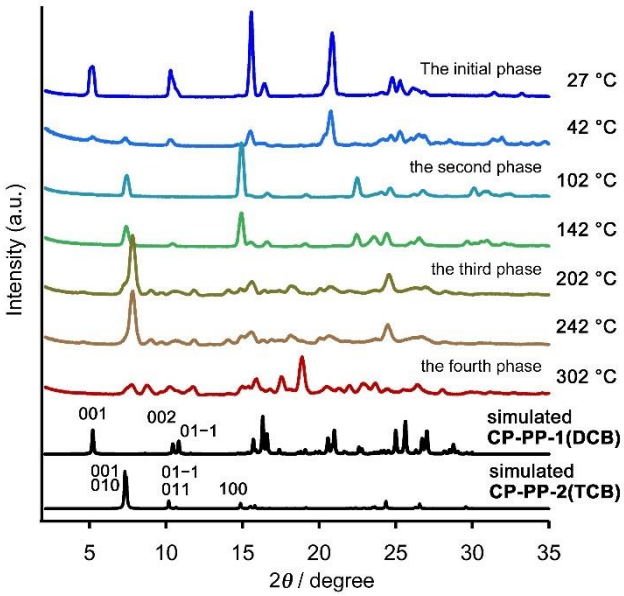

Figure 3.10 Characteristic PXRD patterns observed in the heating process of **CP-PP-1(DBC)** crystalline bulk. Simulated patterns of **CP-PP-1(DCB)** and **CP-PP-2(TCB)** are shown at the bottom as a reference. These patterns were generated by Mercury software based on the SXRD data.

3-2-3. Porosity evaluation.

Activation of **CP-PP-1(DCB)** was performed by heating the crystals at 150 °C for 22 hours under vacuum condition. Complete removal of the solvent from pores of the crystals was evident from the weight loss of 40.5%. The activated HOF (**CP-PP-1a)** exhibits broad PXRD patterns with several peaks, for example, at 2θ = 7.5°, 8.7°, 10.3°, 11.8°, and 15.4°, To speculate the structure of **CP-PP-1a**, the PXRD pattern was compared with the simulated patterns of **CP-PP-2(TCB)** and **CP-PP-3(TCB)**, where **CP-PP-3(TCB)** has closely similar framework with **CP-PP2(TCB)**, except for empty void and existence of water molecule H-bonded with the carboxy group, and the crystals was accidentally found in samples obtained when a mixture of **CP-PP-1(TCB)** and **CP-PP-2(TCB)** was heated at 150 °C under vacuum condition (for the details, see Figures 3.11, 3.12). The comparison indicates that the activated HOF **CP-PP-1a** partially contains semi-opening framework with small void spaces, as well as other non-identifiable crystalline phases. Indeed, porosity of **CP-PP-1a** is not so significant: The total uptake is 74.0 $cm^3\ g^{-1}$ at p/p_0 = 1.00 and SA_{BET} was calculated to be 114 $m^2\ g^{-1}$ based on the CO_2 sorption isotherm. It is noteworthy that **CP-PP-1a** shows a stepped sorption profile with hysteric behavior at p/p_0 = 0.81, which is a typical IV profile (Figure 3.13). It is generally recognized that there are two reasons for this hysteresis. One is for capillary condensation taking place in mesopores[34], and the other is for framework flexibility and the existence of molecular gates, which are reported in flexible porous materials such as MOF and HOF.[35,36] Moreover, **CP-PP-1a** adsorbed CO_2, but didn't adsorb N_2. This result indicated that **CP-PP-1a** showed gas adsorption selectivity for CO_2.

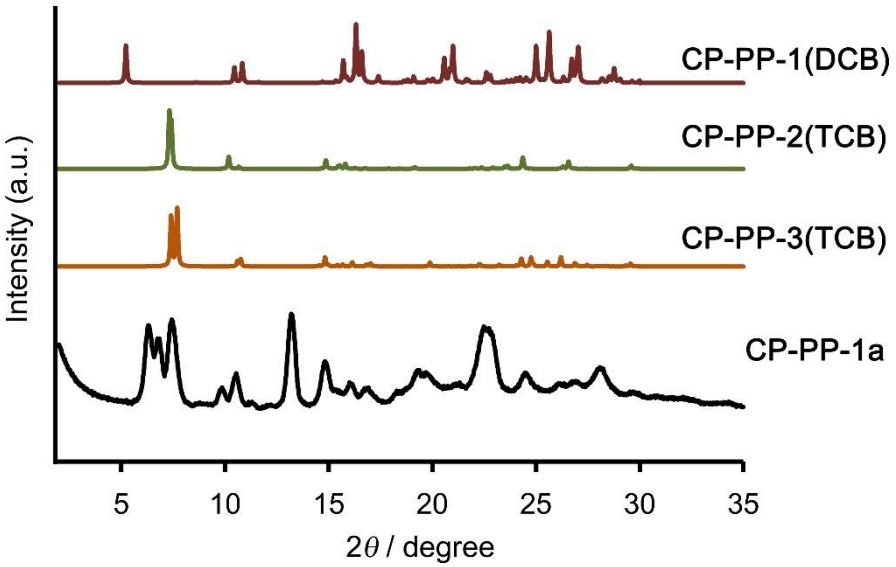

Figure 3.11 A PXRD pattern of activated HOF **CP-PP-1a**, together with simulated patterns of **CP-PP-1(DCB)**, **CP-PP-2(TCB)**, and **CP-PP-3(TCB)**.

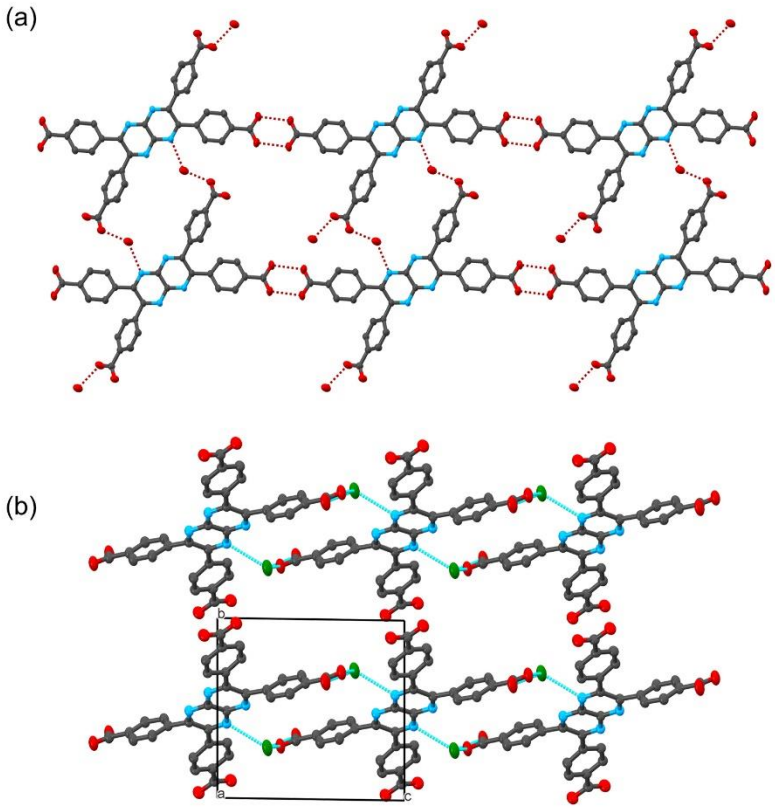

Figure 3.12. Crystal structure of **CP-PP-3(TCB)**. (a) A layer structure composed of **CP-PP** and water molecules connected through H-bonds. The water molecules also form H-bonds with **CP-PP** molecules of the neighboring layers. (b) Packing diagram viewed down from the *a* axis. The water molecules are colored green for clarity.

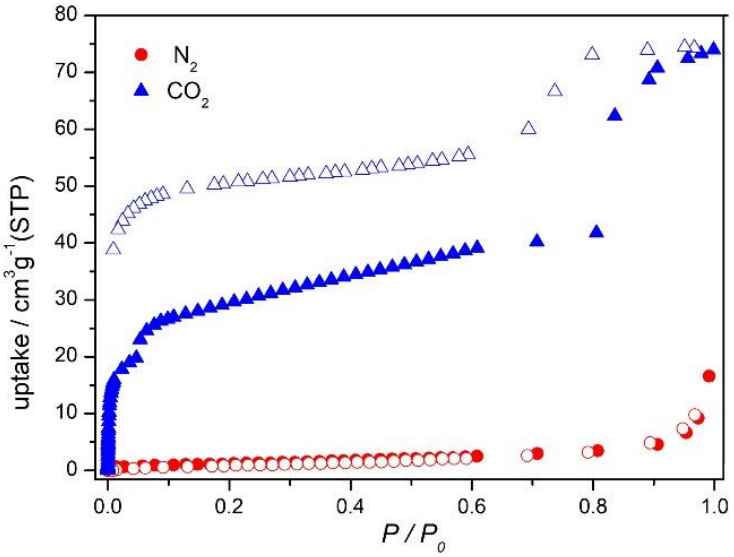

Figure 3.13 N_2 (77 K, red) and CO_2 (195 K, blue) sorption isotherms of **CP-PP-1a**. Solid symbols, sorption; open symbols, desorption.

3-3. Conclusion

In summary, I have successfully synthesized novel hydrogen-bonded organic frameworks (HOFs) composed of highly N-content π-conjugated molecule, a pyrazinopyrazine derivative with carboxyphenyl groups (**CP-PP**). Single crystalline X-ray diffraction analysis precisely revealed that the solvated framework **CP-PP-1(DCB)** has the layered structure of two-dimensional rhombic network sheets. Interestingly, the initial rhombic 2D network rapidly undergoes three step structural transformation by rearrangement of H-bonds into other frameworks, one of which was revealed to have a semi-opening framework with small void. These results contribute to solid-state chemistry on porous molecular crystalline materials.

3-4. Experimental Section

General. All reagents and solvents were used as received from commercial suppliers and used as received without further purification. Analytical thin layer chromatography (TLC) was carried out on aluminum sheets coated with silica gel (Kieselgel $60F_{254}$, Merck). Column chromatographic purifications were performed

using silica gel (63-200 μm, Merck and 64-210 μm, Wakosil®). Melting points were determined on a Yanaco micro melting point apparatus. IR spectrum data were obtained from Thermo Scientific Nicolet 6700 FTIR spectrometer. ^{1}H and ^{13}C NMR spectra were measured by AV 400 MHz JEOL ECX-400 NMR spectrometers. Residual proton and carbon of deuterated solvents were used as internal standards for the measurements (for ^{1}H NMR, $CDCl_3$, δ = 7.26 ppm; DMSO-D6, δ = 2.5 ppm: for ^{13}CNMR, $CDCl_3$, δ = 77.16 ppm; DMSO-D6, δ = 39.52 ppm)[37]. Mass spectrum data were obtained from Thermo Scientific Exactive mass spectrometers with ESI and APCI ionization methods. Thermo gravimetric (TG) analysis were performed on Rigaku Thermo Plus TG8120 under an N_2 purge (100 mL/min) at a heating rate of 5 °C min^{-1}. Powder X-ray diffraction (PXRD) data were collected on a Rigaku RINT2100 (40 kV, 40 mA) using graphite-monochromatized $Cu_{K\alpha}$ radiation (λ = 1.54187 Å) at room temperature and a scan rate is 2.0 °/min.

Crystallography. Single crystalline X-ray diffraction data was collected by Rigaku MicroMax-007HF diffractometer with a Pilatus 200 K detector and $Cu_{K\alpha}$ radiation (λ = 1.54184 Å). Analytical and multi-scan absorption corrections were applied to the reflection data. A single crystal was mounted on MicroMounts™ tip (MiTeGen) with Paratone® 8277 (Hampton Research). Data collection, cell refinement, and data reduction were carried out with Crysalis^{PRO} (Rigaku Oxford Diffraction, 2017). The initial structure was solved by using SHELXT,[38] and structural refinement was performed by using full-matrix least-squares techniques on F^2 using OLEX^2 package.[39] Anisotropic refinement was applied to all atoms except for hydrogens. These data are provided free of charge in The Cambridge Crystallographic Data Centre.

Sorption/desorption experiment. Activation of **PP-1(DCB)** was performed under vacuum condition (0.2 kPa) for 22 h at 423 K to give **CP-PP-1a** for sorption experiments. Gas sorption measurements were performed on BELSORP-max (BEL, Japan). The adsorption isotherms of N_2 and CO_2 were corrected at 77 K and 195 K, respectively.

UV/vis spectrum and Cyclic Voltammetry experiment. UV/vis spectrum was recorded on a Hitachi U-2910 and on a JASCO-V770 spectrophotometers for a solution. Fluorescence and excitation spectra in a solution and solid state were measured on a Hitachi F-7000 spectrofluorometer. Differential pulse voltammetry was conducted on a BAS ALS-600A in dry CH2Cl2 containing 0.1 M Bu4NBF4 as a supporting electrolyte. Pt electrodes were used as the working and counter electrodes. The working disk electrode was polished using a water suspension of aluminum oxide (0.05 μmol) before use.

Dimethyl 4,4'-([1,2,5]thiadiazolo[3,4-b]pyrazine-5,6-diyl)dibenzoate (3). A three-neck flask equipped with magnetic stirrer, mixture of compound **1** (232 mg, 2.00 mmol) and compound **2** (650 mg, 1.99 mmol) with ethanol (15.0 mL) was stirred, then added acetic acid (15.0 mL) under the protection of N_2 for 48 h at 80 °C. After the reaction solvent was removed in a rotary evaporator, then dried in vacuo. The product was purified by column chromatography (silica gel, $CHCl_3$) to yield **3** (512 mg, 1.26 mmol, 63%) as a yellow solid.

Mp. > 300 °C. ^{1}H NMR (400 MHz, $CDCl_3$): δ 8.03 (d, 4H, J = 8.5 Hz), 7.61 (d, 4H, J = 8.6 Hz), 3.94 (s, 6H) ppm. ^{13}C NMR (100 MHz, $CDCl_3$): δ 166.7, 157.8, 153.7, 141.8, 132.0, 130.6, 130.1, 52.8 ppm. HR-MS (ESI) calc. for $C_{20}H_{14}N_4O_4SNa$ $[M]^+$ 429.0622; found 429.0628.

Dimethyl 4,4'-(5,6-diaminopyrazine-2,3-diyl)dibenzoate (4). Mixture of compound **3** (134 mg, 0.330 mmol) and tin(II) chloride (313 mg, 1.65 mmol) in 37% hydrochloric acid (10.0 mL) and methanol (10.0 mL) was stirred and heated at 60 °C for 4 h. After being cooled to room temperature, the solution was basified with sodium carbonate at pH 8–9 and then extracted by AcOEt, washed with water and brine solution, and dried over anhydrous $MgSO_4$ to yield **4** (94 mg, 0.25 mmol, 75%) as a light yellow solid.

Mp. 240 °C. ^{1}H NMR (400 MHz, $CDCl_3$): δ 7.92 (d, 4H), 7.40 (d, 4H, J = 8.1 Hz), 4.46 (s, 4H), 3.90 (d, 6H, J = 7.2 Hz) ppm. HR-MS (ESI) calc. for $C_{20}H_{18}N_4O_4$ $[M]^+$

378.1319; found 378.1328.

Tetramethyl 4,4',4'',4'''-(pyrazino[2,3-b]pyrazine-2,3,6,7-tetrayl)tetrabenzoate (5). Mixture of compound **4** (87 mg, 0.23 mmol) and compound **2** (76 mg, 0.23 mmol) with ethanol (6.0 mL) and acetic acid (6.0 mL) under the protection of N_2 for 48 h at 80 °C. After the reaction solvent was removed in a rotary evaporator, and wash by water, then dried in vacuo. The product was purified by column chromatography (silica gel, $CHCl_3$: Methanol = 20 : 1) to yield **5** (69.1 mg, 0.10 mmol, 45%) as a bright yellow solid.

Mp. 246 °C. ^{1}H NMR (400 MHz, $CDCl_3$): δ 8.04 (d, 8H, J = 8.5 Hz), 7.72 (d, 8H), 3.94 (s, 12H) ppm. ^{13}C NMR (100 MHz, $CDCl_3$): δ 166.2, 156.8, 142.7, 141.2, 131.4, 130.2, 129.6, 52.3 ppm. HR-MS (ESI) calc. for $C_{38}H_{28}N_4O_8Na$ $[M]^+$ 691.1805; found 691.1799.

4,4',4'',4'''-(pyrazino[2,3-b]pyrazine-2,3,6,7-tetrayl)tetrabenzoic acid (CP-PP).

A reaction mixture of **5** (56 mg, 0.084 mmol) in THF (5.0 mL) and 5%-KOH aqueous solution (5.0 mL) was stirred for 24 h at 60 °C. After cooled to room temperature, 37% HCl was added into the reaction mixture until precipitate was not formed anymore. The precipitate was collected by centrifugation, washed with water and ethanol, then dried in vacuo to yield **CP-PP** (39 mg, 76%) as yellow powder.

Mp. > 300 °C. ^{1}H NMR (400 MHz, DMSO-d_6): δ 7.99 (d, 4H, J = 8.5 Hz), 7.73 (d, 4H, J = 8.5 Hz) ppm. ^{13}C NMR (100 MHz, DMSO- d_6): δ 166.6, 156.1, 142.2, 141.3, 131.5, 130.1, 129.0 ppm. HR-MS (ESI) calc. for $C_{34}H_{19}N_4O_8$ $[M]^-$ 611.1281; found 611.1208.

References

1. U. H. F. Bunz, The larger N-heteroacenes. *Pure Appl. Chem*. **2010**, *82*, 953.

2. P. Meti, H. H. Park, Y. D. Gong, Recent developments in pyrazine functionalized π-conjugated materials for optoelectronic applications. *J. Mater. Chem. C*. **2020**, *8*, 352.

3. T. Kato, T. Yamabe, Electron-phonon interactions in the monoanions of polycyanodienes. *J. Phys. Chem. A*. **2004**, *108*, 11223.

4. R. Scipioni, M. Boero, G. J. Richards, J. P. Hill, T. Ohno, T. Mori, K. Ariga, Tautomerism in reduced Pyrazinacenes. *J. Chem. Theory Comput.* **2010**, *6*, 517.

5. Z. He, R. Mao, D. Liu, Q. Miao, Highly electron-deficient hexaazapentacenes and their dihydro precursors. *Org. Lett*. *14*. **2012**, *14*, 4190.

6. J. Fleischhauer, S. Zahn, R. Beckert, U.-W. Grummt, E. Birckner, H. Gçrls, A way to stable, highly emissive fluorubine dyes: Tuning the electronic properties of azaderivatives of pentacene by introducing substituted pyrazines. *Chem. Eur. J.* **2012**, 18, 4549.

7. A. N. Lakshminarayana, A. Ogn, C. Chi, Modification of acenes for n-channel OFET materials. *J. Mater. Chem. C.* **2018**, *6*, 3551.

8. J. Li, S. Chen, P. Zhang, Z. Wang, G. Long, R. Ganguly, Y. Li, Q. Zhang, A colorimetric and fluorimetric chemodosimeter for copper ion based on the conversion of dihydropyrazine to pyrazine. *Chem. Asian J*. **2016**, *11*, 136.

9. I. M. Piglosiewicz, R. Beckhaus, W. Saak, D. Haase, Dehydroaromatization of quinoxalines: one-step syntheses of trinuclear 1,6,7,12,13,18-hexaazatrinaphthylene titanium complexes. *J. Am. Chem. Soc*. **2005**, *127*, 14190.

10. B. Nie, T.-G. Zhan, T.-Y. Zhou, Z.-Y. G.-F. Xian, Jiang, X. Zhao, Self-assembly of chiral propeller-like supermolecules with unusual "sergeants-and-soldiers" and

"majorityrules" effects. *Chem. Asian J.* **2014**, *9*, 754.

11. S. Roy, B. Sarkar, C. Duboc, J. Fiedler, O. Sarper, F. Lissner, S. M. Mobin, G. K. Lahiri, W. Kaim, Heterohexanuclear (Cu_3Fe_3) complexes of substituted hexaazatrinaphthylene (HATN) ligands: twofold BF_4^- association in the solid and stepwise oxidation (3e) or reduction (2e) to spectroelectrochemically characterized species. *Chem. Eur. J*. **2009**, *15*, 6932.

12. M. G. Fraser, C. A. Clark, R. Horvath, et al, Complete family of mono-, bi-, and trinuclear $Re(I)(CO)_3Cl$ complexes of the bridging polypyridyl ligand 2,3,8,9,14,15-hexamethyl-5,6,11,12,17,18-hexaazatrinapthalene: syn/anti isomer separation, characterization, and photophysics. *Inorg. Chem*. **2011**, *50*, 6093.

13. J. Armand, L. Boulares, K. Cheki, C. Belle, Chemical and electrochemical reduction of pyrazino[2,3-b]quinoxalines. *Can. J. Chem.* **1981**. *59*. 3237.

14. K. Isoda, M. Nakamura, T. Tatenuma, H. Ogata, T. Sugaya, M. Tadokoro, Synthesis and characterization of electron-accepting nonsubstituted tetraazaacene derivatives. *Chem. Lett.* **2012**, *41*, 937.

15. I. Georgiou, S. Kervyn, A. Rossignon, F. De Leo, J. Wouters, G. Bruylants, D. Bonifazi, Versatile self-adapting boronic acids for H-bond recognition: from discrete to polymeric supramolecules. *J. Am. Chem. Soc.* **2017**, *139*, 2710.

16. G. J. Richards, J. P. Hill, N. K. Subbaiyan, F. D'Souza, P. A. Karr, M. R. J. Elsegood, S. J. Teat, T. Mori, K. Ariga, Pyrazinacenes: aza analogues of acenes. *J. Org. Chem.* **2009**, *74*, 8914.

17. U. H. F. Bunz, J. Freudenberg, N-heteroacenes and N-heteroarenes as N-nanocarbon Segments. *Acc. Chem. Res*. **2019**, *52*, 1575.

18. G. J. Richards, A. Cador, S. Yamada, et al, Amphiprotism-coupled nearinfrared emission in extended pyrazinacenes containing seven linearly fused pyrazine units. *J. Am. Chem. Soc.* **2019**, *141*, 19570.

19. J. Lu, R. Cao, Porous organic molecular frameworks with extrinsic porosity: a platform for carbon storage and separation. *Angew. Chem. Int. Ed.* **2016**, *55*, 9474.

20. J. Luo, J.-W. Wang, J.-H. Zhang, S. Lai, D.-C. Zhong, Hydrogen-bonded organic frameworks: design, structures and potential applications. *CrystEngComm.* **2018**, *20*, 5884.

21. I. Hisaki, X. Chen, K. Takahashi, T. Nakamura, Designing hydrogen-bonded organic frameworks (HOFs) with permanent porosity. *Angew. Chem. Int. Ed*. **2019**, *58*, 11160.

22. P. Tholen, C. A. Peeples, R. Schaper, et al, Semiconductive microporous hydrogen-bonded organophosphonic acid frameworks. *Nat. Commun*. **2020**, *11*, 3180.

23. B. Wang, R. B. Lin, Z. J. Zhang, S. C. Xiang, B. L. Chen, Hydrogen-bonded organic frameworks as a tunable platform for functional materials. *J. Am. Chem. Soc.* **2020**, *142*, 14399.

24. X. Crispin, J. Cornil, R. Friedlein, et al, Electronic delocalization in discotic liquid crystals: a joint experimental and theoretical study. *J. Am. Chem. Soc*. **2004**, *126*, 11889.

25. D. Zhao, Z. Zhu, M.-Y. Kuo, C.-C. Chueh, A. K.-Y. Jen, Hexaazatrinaphthylene derivatives: efficient electron-transporting materials with tunable energy levels for inverted perovskite solar cells. *Angew. Chem. Int. Ed*. **2016**, *55*, 8999.

26. M. Lehmann, G. Kestemont, R. G. Aspe, et al, High charge-carrier mobility in pi-deficient discotic mesogens: design and structure-property relationship. *Chem. Eur. J.* **2005**, *11*, 3349.

27. W. Yang, F. Yang, T.-L. Hu, S. C. King, H. Wang, H. Wu, W. Zhou, J.-R. Li, H. D. Arman, B. Chen, Microporous diaminotriazine-decorated porphyrin-based hydrogen-bonded organic framework: permanent porosity and proton conduction. *Cryst. Growth Des*. **2016**, *16 (10)*, 5831.

28. A. Karmakar, R. Illathvalappil, B. Anothumakkool, A. Sen, P. Samanta, A. V. Desai, S. Kurungot, Hydrogen-bonded organic frameworks (HOFs): a new class of porous crystalline proton-conducting materials. *Angew. Chem. Int. Ed.* **2016**, *55*, 10667.

29. I. Hisaki, Y. Suzuki, E. Gomez, Q. Ji, N. Tohnai, T. Nakamura, A. Douhal, Acid responsive hydrogen-bonded organic framework. *J. Am. Chem. Soc*. **2019**, *141*, 2111.

30. I. Hisaki, Q. Ji, K. Takahashi, N. Tohnai, T. Nakamura, Positional effects of annelated pyrazine rings on structure and stability of hydrogen-bonded frameworks of hexaazatrinaphthylene derivatives. *Cryst. Growth Des.* **2020**, *20*, 3190.

31. I. Hisaki, S. Nakagawa, N. Ikenaka, et al, A series of layered assemblies of hydrogenbonded, hexagonal networks of C_3-symmetric π-conjugated molecules: a potential motif of porous organic materials. *J. Am. Chem. Soc*. **2016**, *138*, 6617.

32. A. P. Komin, M. Carmack, The chemistry of 1,2,5-thiadiazoles V. Synthesis of 3,4-diamino-1,2,5-thiadiazole and [1,2,5] thiadiazolo[3,4-*b*]pyrazines. *J. Heterocyclic Chem*. **1976**, *13*, 13.

33. (a) P. T. K. Nguyen, H. T. D. Nguyen, H. Q. Pham, et al., Synthesis and selective CO_2 capture properties of a series of hexatopic linker-based metal-organic frameworks. *Inorg. Chem.* **2015**, *54*, 10065. (b) L. Zhang, K. C. Lo, W. K. Chan, A new route to the synthesis of near-infrared absorbing pyrazinopyrazine bridged dyes with intramolecular charge transfer character. *Chem. Commun*. **2014**, *50*, 4245.

34. S. F. Mason, The electronic spectra of N-heteroaromatic systems. Part IX. *J. Chem. Soc.* **1962**, 493.

35. R. B. Araujo, A. Banerjee, P. Panigrahi, L. Yang, M. Strømme, et al., Ahuja R. Designing strategies to tune reduction potential of organic molecules for sustainable high capacity battery application. *J. Mater. Chem. A.* **2017**, *5*, 4430.

36. S. Henke, A. Schneemann, A. Wutscher, R. Fischer, Directing the breathing

behavior of pillared-layered metal-organic frameworks via a systematic library of functionalized linkers bearing flexible substituents. A., *J. Am. Chem. Soc*. **2012**, *134*, 9464.

37. Y. B. He, S. C. Xiang, B. L. Chen, A microporous hydrogen-bonded organic framework for highly selective C_2H_2/C_2H_4 separation at ambient temperature. *J. Am. Chem. Soc*. **2011**, *133*, 14570.

38. G. R. Fulmer, A. J. Miller, N. H. Sherden, H. E. Gottlieb, A. Nudelman, B. M. Stoltz, J. E. Bercaw, K. I. Goldberg, NMR chemical shifts of trace impurities: common laboratory solvents, organics, and gases in deuterated solvents relevant to the organometallic Chemist. *Organometallics* **2010**, *29*, 2176.

39. G. M. Sheldrick, *SHELXT* -Integrated space-group and crystal-structure determination. *Acta Crystallogr. Sect. A Found. Adv.*, **2015**, *71*, 3.

40. O. V. Dolomanov, L. J. Bourhis, R. J. Gildea, J. A. K. Howard, H. Puschmann, OLEX2: A complete structure solution, refinement and analysis program. *J. Appl. Crystallogr*. **2009**, *42*, 339.

Chapter 4

General conclusion

Conclusions

The hydrogen-bonded organic frameworks have shown the advantages of high crystallinity, solution processability, easy healing and purification, due to the reversible and flexible nature of H-bonding connections. Although HOFs have the above advantages, the weak hydrogen bonding force and poor directional nature also restrict the development of HOFs materials. In this thesis, we started with the construction of multifunctional hydrogen-bonded organic framework with novel structures and excellent performance under the guidance of the basic theory of organic chemistry. Introducing nitrogen atoms into the core of π-conjugated systems gives the framework multiple active sites to achieve external stimuli-responsive frameworks. The research contents are mainly divided into two parts: one is the design and synthesis of a kind of hexagonal networked (HexNets) hydrogen-bonded organic framework and its structure was measured and part of the properties of the study; The second is a kind of rhombic networked (RhomNets) hydrogen-bonded organic framework, and their structures are characterized. The results are as follows:

1) Based on the previously reported **CPHATN**, and the introduction of the concept of Nitrogen atoms' s location isomerism, we designed and synthesized a new compound, **CPBTQ**. In comparison with a previously reported Nπ-HOF composed of the isomeric hexaazatrinaphthylene derivative (**CPHATN**) possessing pyrazine rings in different positions, the present framework has a complicated and defective H-bonded network structure. We thoroughly studied the positional effects of the pyrazine rings on the conformation of the peripheral phenylene groups, and the permanent porosity, thermal and chemical stabilities, and reversible HCl responsiveness of the activated Nπ-HOF **CPBTQ-1a**.

2) Based on the construction of highly N-content π-conjugated molecule, pyradinopyradine (**PP**), we have successfully synthesized a novel hydrogen-bonded organic framework and described synthesis of PP-based building block molecule with four carboxyphenyl groups (**CP-PP**), spectroscopic and electronic properties of **CP-PP**

and its ester precursor, structures of **CP-PP** based HOFs, and thermal behaviors of the HOFs.

List of publication

Chapter 2

Positional Effects of Annelated Pyrazine Rings on Structure and Stability of Hydrogen-bonded Frameworks of Hexaazatrinaphthylene Derivatives

Ichiro Hisaki, Qin Ji, Kiyonori Takahashi, Norimitsu Tohnai, Takayoshi Nakamura
Cryst. Growth Des. **2020**, 20, 3190–3198.

Chapter 3

A Hydrogen-Bonded Organic Framework Based on Pyrazinopyrazine

Qin Ji, Kiyonori Takahashi, Shin-ichiro Noro, Yusuke Ishigaki, Kenta Kokado, Takayoshi Nakamura, Ichiro Hisaki.

Cryst. Growth Des. in press.

Appendix

Appendix I: Chapter 2

I-1. NMR spectra of the compounds newly synthesized in this study

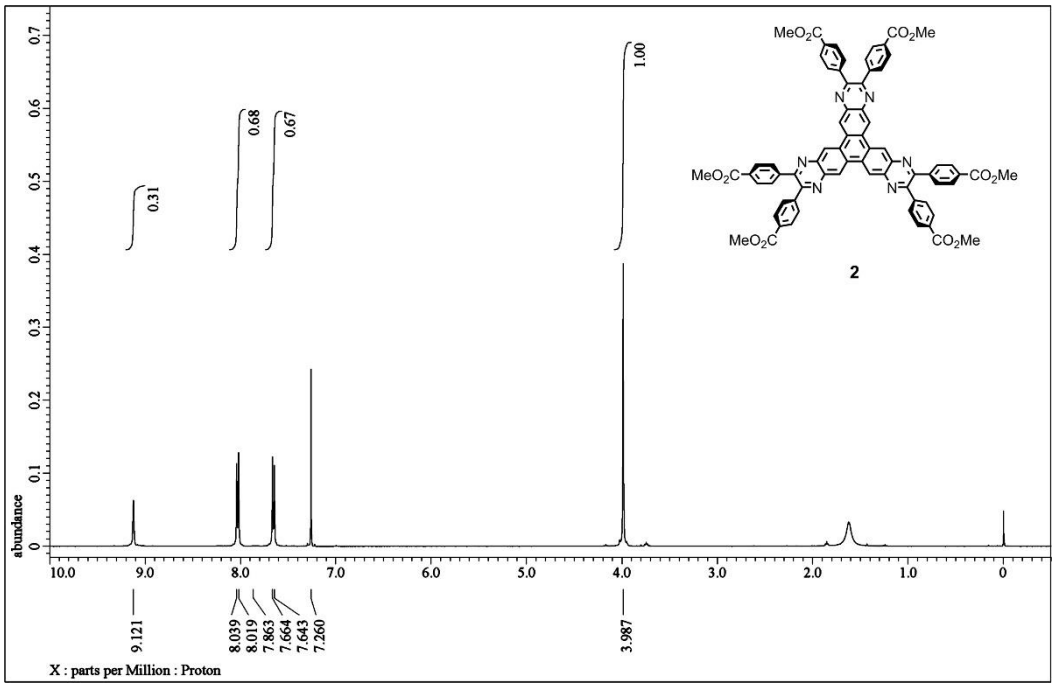

Figure 1. ^{1}H NMR (400 MHz, $CDCl_3$) spectrum of **2**.

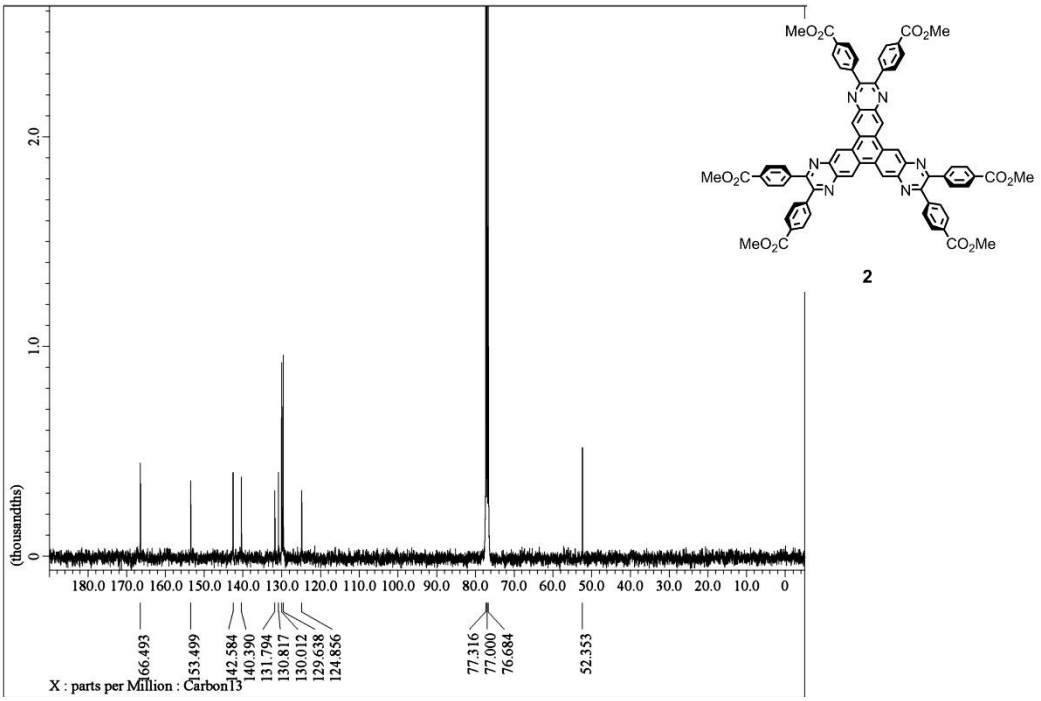

Figure 2. ^{13}C NMR (100 MHz, $CDCl_3$) spectrum of **2**.

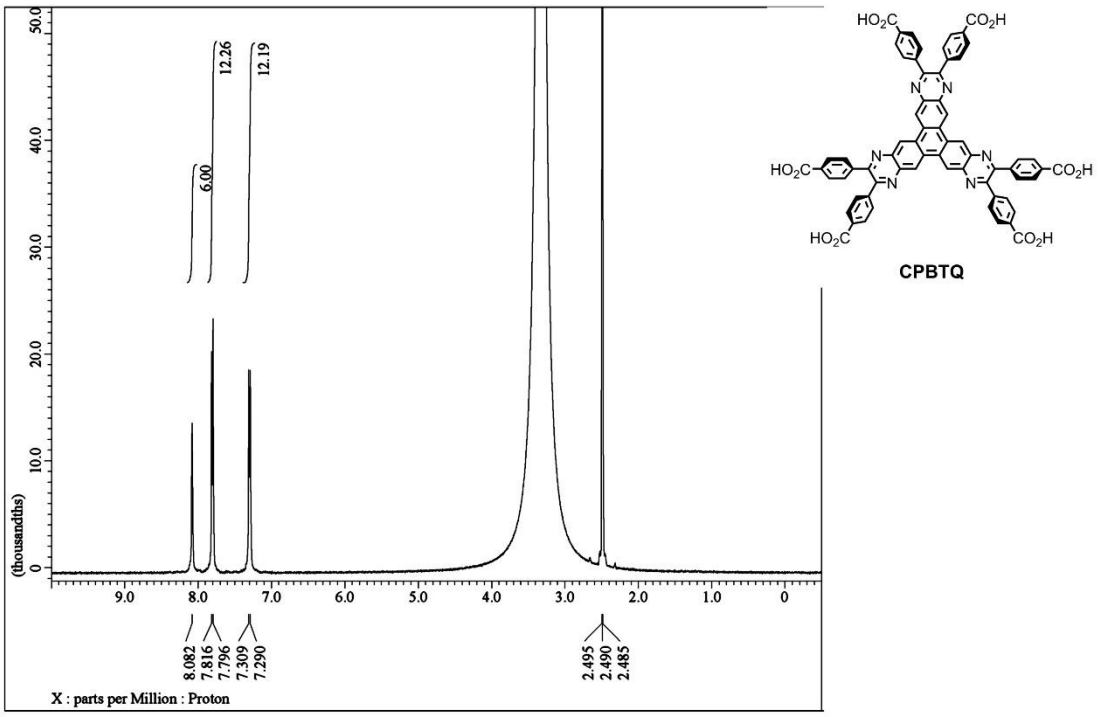

Figure 3. ^{1}H NMR (400 MHz, DMSO-d_6) spectrum of **CPBTQ**.

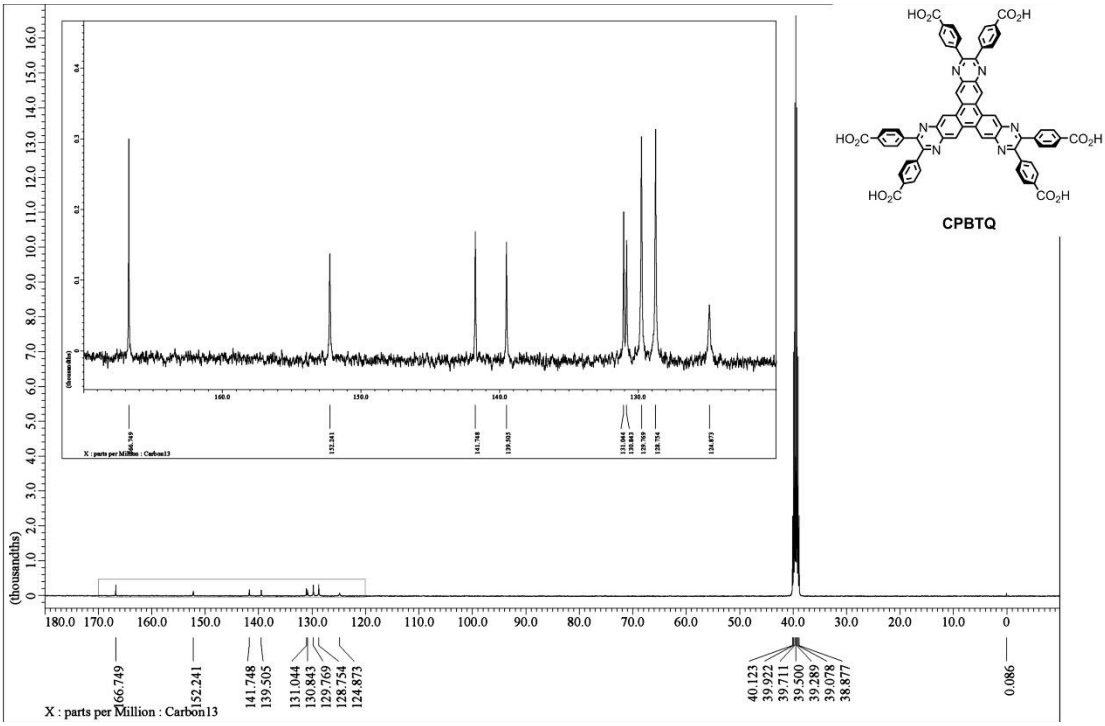

Figure 4. ^{13}C NMR (100 MHz, DMSO-d_6) spectrum of **CPBTQ**.

Appendix

Appendix II: Chapter 3

II-1. NMR spectra of the compounds newly synthesized in this study

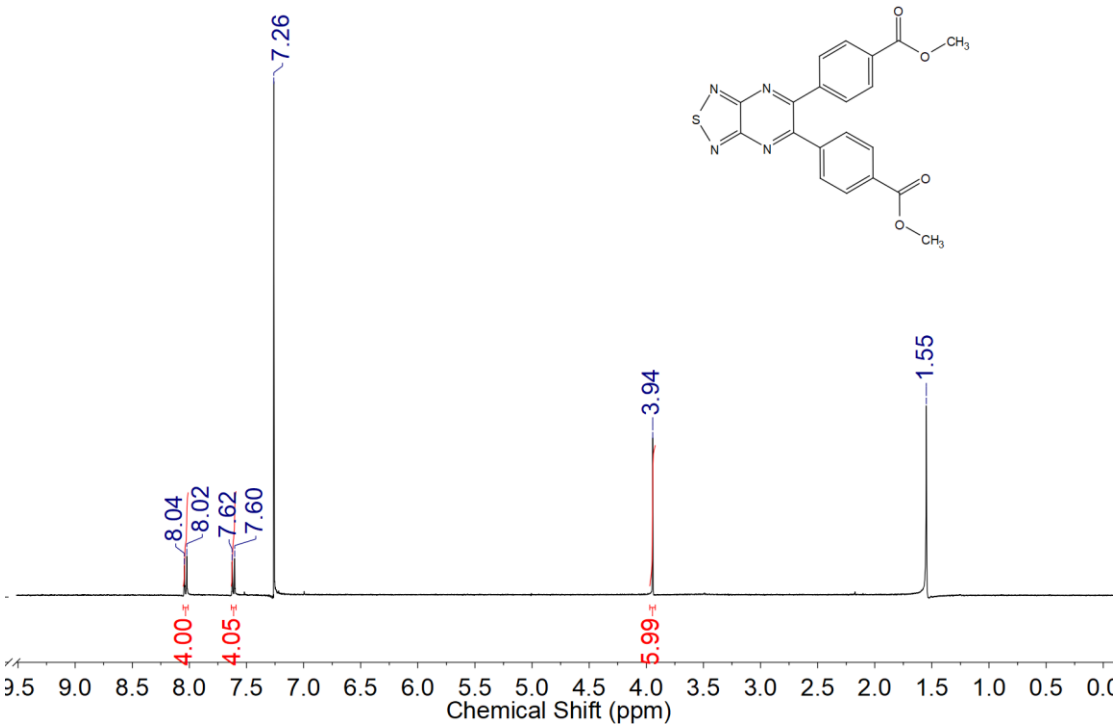

Figure II-1. ^{1}H NMR (400 MHz, $CDCl_3$) spectrum of **3**.

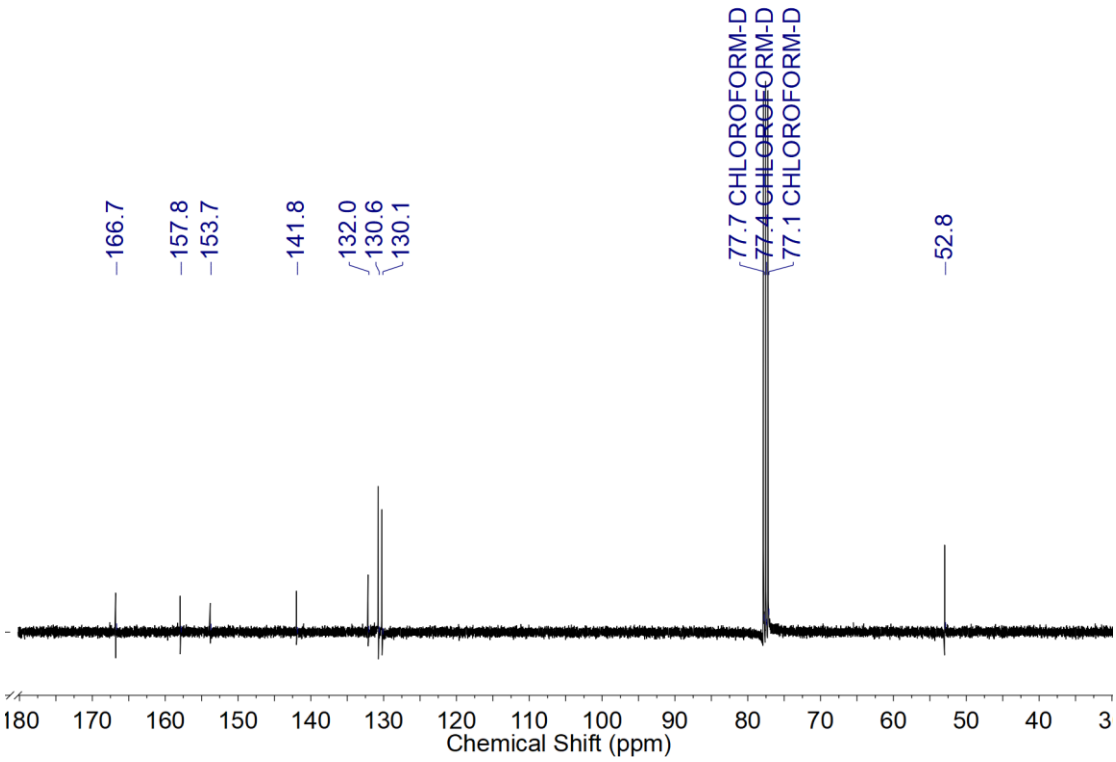

Figure II-2. ^{13}C NMR (400 MHz, $CDCl_3$) spectrum of **3**.

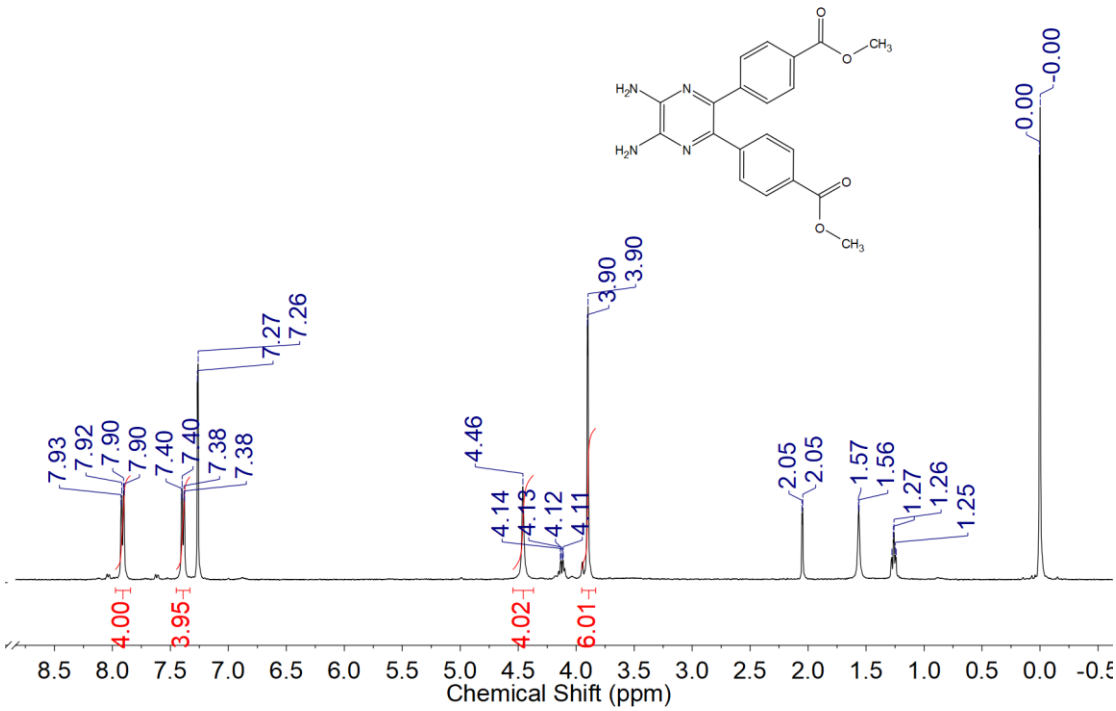

Figure II-3. ^{1}H NMR (400 MHz, $CDCl_3$) spectrum of **4**.

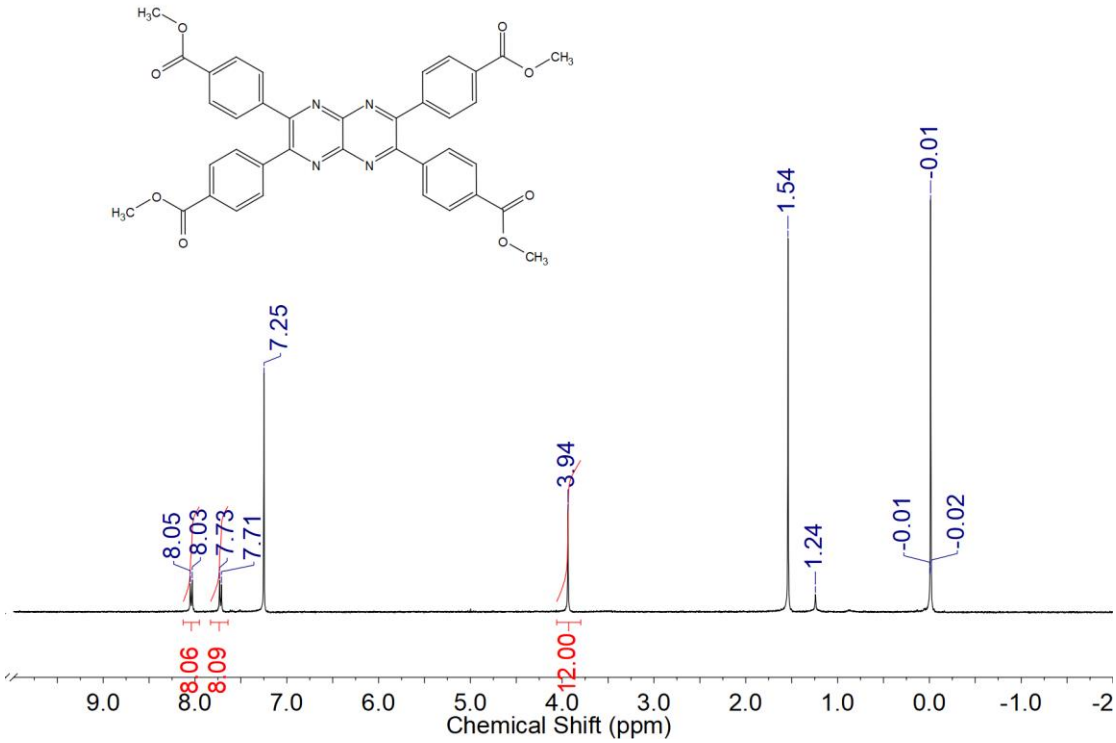

Figure II-4. ^{1}H NMR (400 MHz, $CDCl_3$) spectrum of **5**.

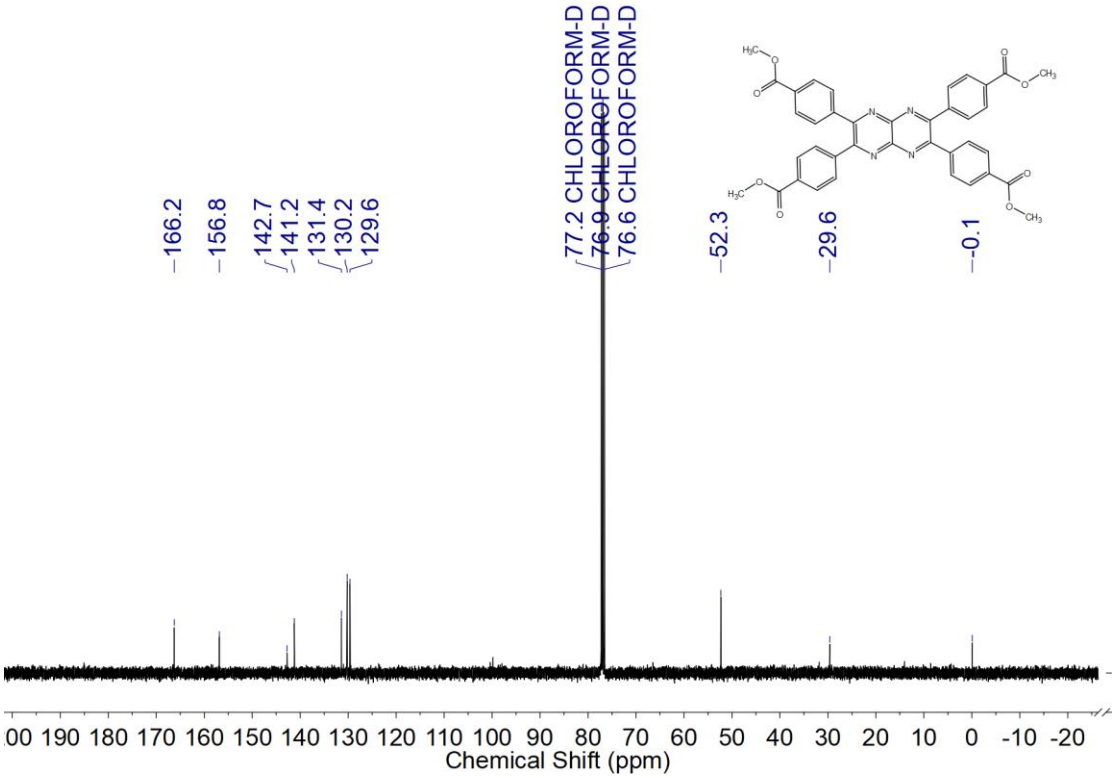

Figure II-5. ^{13}C NMR (400 MHz, $CDCl_3$) spectrum of **5**.

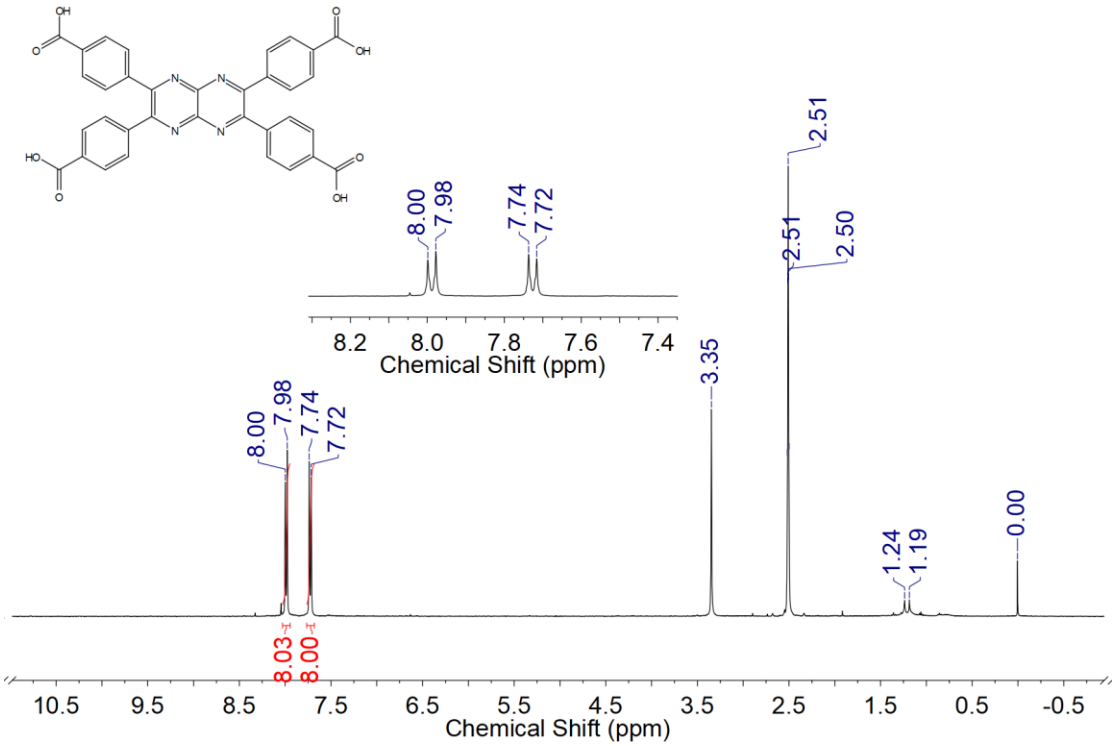

Figure II-6. ^{1}H NMR (400 MHz, $CDCl_3$) spectrum of **CP-PP**.

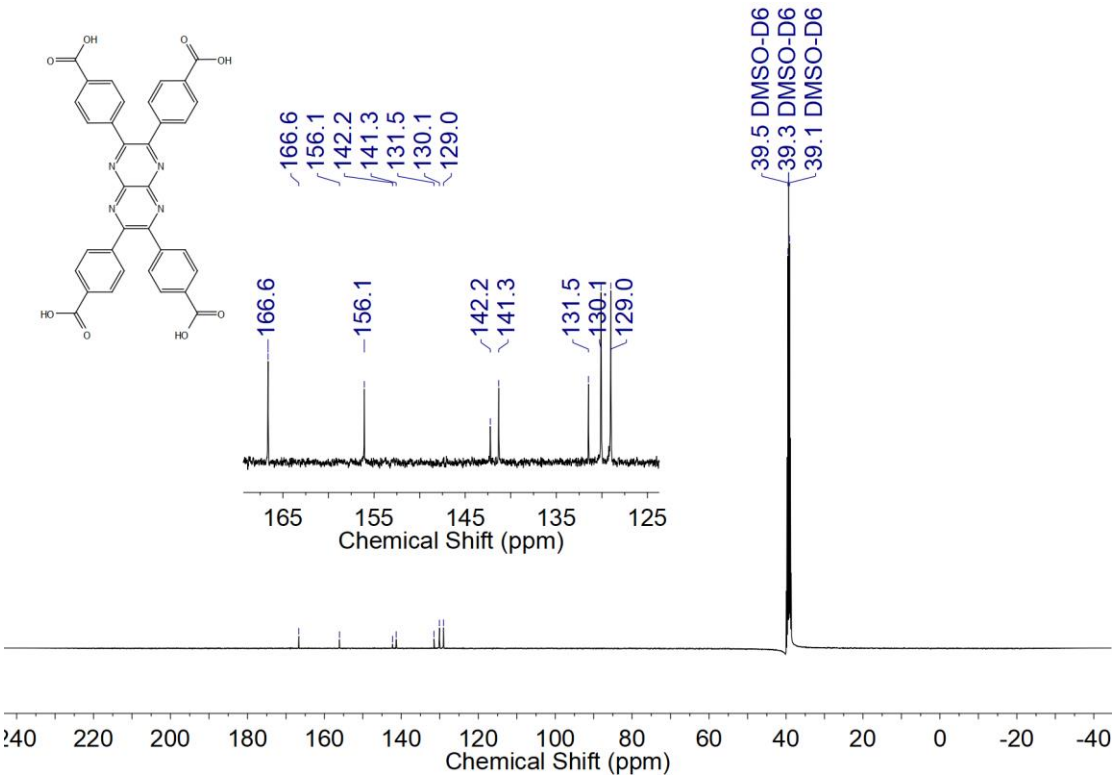

Figure II-7. ^{13}C NMR (400 MHz, $CDCl_3$) spectrum of **CP-PP**.

II-2. Theoretical calculation

Structural optimization and population analysis of **CP-PP**, ester derivative **5**, and naphthalene analogue were performed by DFT at the B3LYP/6-31(d) level.

Table II-1. Atomic coordinates of **CP-PP**

Center Number	Atomic Number	Atomic Type	Coordinates (Angstroms)		
			X	Y	Z
1	6	0	3.277593	0.161203	5.741615
2	6	0	1.567032	-0.002682	3.520940
3	6	0	3.54113	-0.758458	4.717135
4	6	0	2.163928	1.005498	5.644715
5	6	0	1.313161	0.920939	4.549134
6	6	0	2.698867	-0.829334	3.612824
7	1	0	4.406204	-1.408287	4.786334
8	1	0	1.98243	1.723497	6.437396
9	1	0	0.458444	1.585769	4.484026
10	1	0	2.91142	-1.520739	2.804473

11	6	0	0.724776	-0.06347	2.294452
12	7	0	-1.393145	0.19248	1.160184
13	6	0	0.699899	-0.118192	0.000000
14	6	0	-0.724776	0.06347	2.294452
15	6	0	-0.699899	0.118192	0.000000
16	7	0	1.393145	-0.19248	-1.160184
17	6	0	0.724776	-0.06347	-2.294452
18	6	0	-0.724776	0.06347	-2.294452
19	7	0	-1.393145	0.19248	-1.160184
20	6	0	-1.567032	0.002682	3.520940
21	6	0	-3.277593	-0.161203	5.741615
22	6	0	-1.313161	-0.920939	4.549134
23	6	0	-2.698867	0.829334	3.612824
24	6	0	-3.54113	0.758458	4.717135
25	6	0	-2.163928	-1.005498	5.644715
26	1	0	-0.458444	-1.585769	4.484026
27	1	0	-2.91142	1.520739	2.804473
28	1	0	-4.406204	1.408287	4.786334
29	1	0	-1.98243	-1.723497	6.437396
30	6	0	-1.567032	0.002682	-3.520940
31	6	0	-3.277593	-0.161203	-5.741615
32	6	0	-2.698867	0.829334	-3.612824
33	6	0	-1.313161	-0.920939	-4.549134
34	6	0	-2.163928	-1.005498	-5.644715
35	6	0	-3.54113	0.758458	-4.717135
36	1	0	-2.91142	1.520739	-2.804473
37	1	0	-0.458444	-1.585769	-4.484026
38	1	0	-1.98243	-1.723497	-6.437396
39	1	0	-4.406204	1.408287	-4.786334

40	6	0	1.567032	-0.002682	-3.520940
41	6	0	3.277593	0.161203	-5.741615
42	6	0	1.313161	0.920939	-4.549134
43	6	0	2.698867	-0.829334	-3.612824
44	6	0	3.54113	-0.758458	-4.717135
45	6	0	2.163928	1.005498	-5.644715
46	1	0	0.458444	1.585769	-4.484026
47	1	0	2.91142	-1.520739	-2.804473
48	1	0	4.406204	-1.408287	-4.786334
49	1	0	1.98243	1.723497	-6.437396
50	7	0	1.393145	-0.19248	1.160184
51	6	0	-4.146951	-0.288888	6.941640
52	8	0	-3.969674	-1.079919	7.846151
53	8	0	-5.187615	0.582856	6.938258
54	1	0	-5.681003	0.407619	7.760942
55	6	0	4.146951	0.288888	6.941640
56	8	0	3.969674	1.079919	7.846151
57	8	0	5.187615	-0.582856	6.938258
58	1	0	5.681003	-0.407619	7.760942
59	6	0	-4.146951	-0.288888	-6.941640
60	8	0	-3.969674	-1.079919	-7.846151
61	8	0	-5.187615	0.582856	-6.938258
62	1	0	-5.681003	0.407619	-7.760942
63	6	0	4.146951	0.288888	-6.941640
64	8	0	3.969674	1.079919	-7.846151
65	8	0	5.187615	-0.582856	-6.938258
66	1	0	5.681003	-0.407619	-7.760942

Table II-2. Atomic coordinates of **5**

Center Number	Atomic Number	Atomic Type	Coordinates (Angstroms)		
			X	Y	Z
1	6	0	3.275293	0.241332	5.742388
2	6	0	1.566795	0.035919	3.521037
3	6	0	3.561011	-0.669116	4.715579
4	6	0	2.139542	1.055698	5.646305
5	6	0	1.290122	0.950607	4.551142
6	6	0	2.720321	-0.760398	3.611673
7	1	0	4.442827	-1.295883	4.783690
8	1	0	1.939744	1.767569	6.440112
9	1	0	0.418001	1.592707	4.488037
10	1	0	2.950534	-1.444731	2.802070
11	6	0	0.726156	-0.045543	2.294706
12	7	0	-1.397331	0.158616	1.160242
13	6	0	0.702684	-0.101511	0.000000
14	6	0	-0.726156	0.045543	2.294706
15	6	0	-0.702684	0.101511	0.000000
16	7	0	1.397331	-0.158616	-1.160242
17	6	0	0.726156	-0.045543	-2.294706
18	6	0	-0.726156	0.045543	-2.294706
19	7	0	-1.397331	0.158616	-1.160242
20	6	0	-1.566795	-0.035919	3.521037
21	6	0	-3.275293	-0.241332	5.742388
22	6	0	-1.290122	-0.950607	4.551142
23	6	0	-2.720321	0.760398	3.611673
24	6	0	-3.561011	0.669116	4.715579
25	6	0	-2.139542	-1.055698	5.646305
26	1	0	-0.418001	-1.592707	4.488037
27	1	0	-2.950534	1.444731	2.802070
28	1	0	-4.442827	1.295883	4.783690
29	1	0	-1.939744	-1.767569	6.440112
30	6	0	-1.566795	-0.035919	-3.521037
31	6	0	-3.275293	-0.241332	-5.742388
32	6	0	-2.720321	0.760398	-3.611673
33	6	0	-1.290122	-0.950607	-4.551142
34	6	0	-2.139542	-1.055698	-5.646305
35	6	0	-3.561011	0.669116	-4.715579
36	1	0	-2.950534	1.444731	-2.802070
37	1	0	-0.418001	-1.592707	-4.488037
38	1	0	-1.939744	-1.767569	-6.440112
39	1	0	-4.442827	1.295883	-4.783690
40	6	0	1.566795	0.035919	-3.521037

Center Number	Atomic Number	Atomic Type	Coordinates (Angstroms)		
			X	Y	Z
41	6	0	3.275293	0.241332	-5.742388
42	6	0	1.290122	0.950607	-4.551142
43	6	0	2.720321	-0.760398	-3.611673
44	6	0	3.561011	-0.669116	-4.715579
45	6	0	2.139542	1.055698	-5.646305
46	1	0	0.418001	1.592707	-4.488037
47	1	0	2.950534	-1.444731	-2.802070
48	1	0	4.442827	-1.295883	-4.783690
49	1	0	1.939744	1.767569	-6.440112
50	7	0	1.397331	-0.158616	1.160242
51	6	0	-4.14189	-0.392864	6.946355
52	8	0	-3.935505	-1.183961	7.845635
53	8	0	-5.196019	0.454216	6.933235
54	6	0	4.14189	0.392864	6.946355
55	8	0	3.935505	1.183961	7.845635
56	8	0	5.196019	-0.454216	6.933235
57	6	0	-4.14189	-0.392864	-6.946355
58	8	0	-3.935505	-1.183961	-7.845635
59	8	0	-5.196019	0.454216	-6.933235
60	6	0	4.14189	0.392864	-6.946355
61	8	0	3.935505	1.183961	-7.845635
62	8	0	5.196019	-0.454216	-6.933235
63	6	0	6.072908	-0.357691	8.066400
64	1	0	6.502802	0.645148	8.134422
65	1	0	6.853373	-1.099662	7.895365
66	1	0	5.530592	-0.574529	8.990492
67	6	0	-6.072908	0.357691	8.066400
68	1	0	-6.502802	-0.645148	8.134422
69	1	0	-6.853373	1.099662	7.895365
70	1	0	-5.530592	0.574529	8.990492
71	6	0	-6.072908	0.357691	-8.066400
72	1	0	-5.530592	0.574529	-8.990492
73	1	0	-6.853373	1.099662	-7.895365
74	1	0	-6.502802	-0.645148	-8.134422
75	6	0	6.072908	-0.357691	-8.066400
76	1	0	5.530592	-0.574529	-8.990492
77	1	0	6.853373	-1.099662	-7.895365
78	1	0	6.502802	0.645148	-8.134422

Table II-3. Atomic coordinates of the naphthalene analogue.

Center Number	Atomic Number	Atomic Type	Coordinates (Angstroms)		
			X	Y	Z
1	6	0	3.170394	0.163102	5.991895
2	6	0	1.532866	0.022921	3.703454
3	6	0	3.382184	-0.83744	5.034826
4	6	0	2.138207	1.091934	5.800141
5	6	0	1.328961	1.020696	4.673376
6	6	0	2.572306	-0.901396	3.904334
7	1	0	4.175658	-1.562157	5.179905
8	1	0	1.98916	1.866137	6.545555
9	1	0	0.538451	1.750913	4.533076
10	1	0	2.734369	-1.686593	3.171187
11	6	0	0.719933	-0.024267	2.455363
12	6	0	0.711474	-0.039856	0.000000
13	6	0	-0.719933	0.024267	2.455363
14	6	0	-0.711474	0.039856	0.000000
15	6	0	0.719933	-0.024267	-2.455363
16	6	0	-0.719933	0.024267	-2.455363
17	6	0	-1.532866	-0.022921	3.703454
18	6	0	-3.170394	-0.163102	5.991895
19	6	0	-1.328961	-1.020696	4.673376
20	6	0	-2.572306	0.901396	3.904334
21	6	0	-3.382184	0.83744	5.034826
22	6	0	-2.138207	-1.091934	5.800141
23	1	0	-0.538451	-1.750913	4.533076
24	1	0	-2.734369	1.686593	3.171187
25	1	0	-4.175658	1.562157	5.179905
26	1	0	-1.98916	-1.866137	6.545555
27	6	0	-1.532866	-0.022921	-3.703454
28	6	0	-3.170394	-0.163102	-5.991895
29	6	0	-2.572306	0.901396	-3.904334
30	6	0	-1.328961	-1.020696	-4.673376
31	6	0	-2.138207	-1.091934	-5.800141
32	6	0	-3.382184	0.83744	-5.034826
33	1	0	-2.734369	1.686593	-3.171187
34	1	0	-0.538451	-1.750913	-4.533076
35	1	0	-1.98916	-1.866137	-6.545555
36	1	0	-4.175658	1.562157	-5.179905
37	6	0	1.532866	0.022921	-3.703454
38	6	0	3.170394	0.163102	-5.991895
39	6	0	1.328961	1.020696	-4.673376
40	6	0	2.572306	-0.901396	-3.904334

Center Number	Atomic Number	Atomic Type	Coordinates (Angstroms)		
			X	Y	Z
41	6	0	3.382184	-0.83744	-5.034826
42	6	0	2.138207	1.091934	-5.800141
43	1	0	0.538451	1.750913	-4.533076
44	1	0	2.734369	-1.686593	-3.171187
45	1	0	4.175658	-1.562157	-5.179905
46	1	0	1.98916	1.866137	-6.545555
47	6	0	-4.003515	-0.285662	7.215377
48	8	0	-3.866134	-1.139178	8.069109
49	8	0	-4.96622	0.669652	7.301578
50	6	0	4.003515	0.285662	7.215377
51	8	0	3.866134	1.139178	8.069109
52	8	0	4.96622	-0.669652	7.301578
53	6	0	-4.003515	-0.285662	-7.215377
54	8	0	-3.866134	-1.139178	-8.069109
55	8	0	-4.96622	0.669652	-7.301578
56	6	0	4.003515	0.285662	-7.215377
57	8	0	3.866134	1.139178	-8.069109
58	8	0	4.96622	-0.669652	-7.301578
59	6	0	1.389175	-0.063815	-1.243635
60	6	0	-1.389175	0.063815	-1.243635
61	6	0	1.389175	-0.063815	1.243635
62	6	0	-1.389175	0.063815	1.243635
63	1	0	5.440453	-0.488613	8.134024
64	1	0	-5.440453	0.488613	8.134024
65	1	0	5.440453	-0.488613	-8.134024
66	1	0	-5.440453	0.488613	-8.134024
67	1	0	2.476129	-0.074744	1.241152
68	1	0	2.476129	-0.074744	-1.241152
69	1	0	-2.476129	0.074744	-1.241152
70	1	0	-2.476129	0.074744	1.241152